Resonant inelastic X-ray scattering as a probe of exciton-phonon coupling

Andrey Geondzhian

Communauté
UNIVERSITÉ Grenoble Alpes

THÈSE

Pour obtenir le grade de

DOCTEUR DE LA COMMUNAUTE UNIVERSITE GRENOBLE ALPES

Spécialité : Physique de la Matière Condensée et du Rayonnement

Arrêté ministériel : 25 mai 2016

Présentée par

Andrey GEONDZHIAN

Thèse dirigée par **Dr. Nicholas BROOKES**
codirigée par **Dr. Keith GILMORE**

préparée au sein du laboratoire
European Synchrotron Radiation Facility (ESRF)
dans **l'École Doctorale Physique**

Resonant inelastic X-ray scattering as a probe of exciton-phonon coupling

Diffusion inélastique résonante de rayons X en tant que sonde du couplage exciton-phonon

Thèse soutenue publiquement le **11 décembre 2018**,
devant le jury composé de :

Monsieur Yves JOLY
Directeur de Recherche, Institut Néel,
CNRS et Université Grenoble Alpes, Président

Monsieur Andrea MARINI
Directeur de Recherche, Istituto di Struttura della Materia
of the National Research Council, Rapporteur

Monsieur Francesco SOTTILE
Ingénieur de Recherche, Laboratoire des Solides Irradiés,
École Polytechnique, Rapporteur

Monsieur Alexander FöHLISCH
Professeur, Institut für Physik und Astronomie Universität Potsdam,
Institute for Methods and Instrumentation in Synchrotron Radiation
Research, Helmholtz-Zentrum Berlin, Examinateur

Monsieur Valerio OLEVANO
Directeur de Recherche, Institut Néel,
CNRS et Université Grenoble Alpes, Examinateur

Monsieur Xavier BLASE
Directeur de Recherche, Institut Néel,
CNRS et Université Grenoble Alpes, Examinateur

Communauté
UNIVERSITÉ Grenoble Alpes

to my wife Lucy

Acknowledgements

First of all, I would like to acknowledge Dr. Keith Gilmore, my supervisor, for these three years of an exciting journey through the scientific world. I sincerely appreciate your patient and wise guidance. You gave me the right amount of scientific freedom which is essential for personal development, and at the same time, you were close enough so that I did not lose the way. You were supporting me through all these years and inspiring me by showing the example of an excellent scientist.

I thank my co-advisor Dr. Nicholas Brookes for arranging this project and collaboration.

Special thanks to Dr. Patrick Bruno for questions that always made me think deeply and Dr. Timothy Ziman for wisdom and great discussions.

I also would like to thank the European Synchrotron Radiation Facility for an opportunity to do this project.

Many thanks to my dear office mates Pablo Villar Arribi and Jordan Hervy for adventures, discussions and for friendship. With all respect, I thank Dr. Bruno Tomasello for conversations about spin systems and for riding the van. I sincerely thank Marija Krstulovic for all help during the time of writing the manuscript and the defence. I sincerely acknowledge all members of "Not Only Theory" meeting group for sharing scientific interests and for the great time.

I would like to thank my family for support and inspiration. Last but not least, I would like to express my gratitude to my wife. Thank you for understanding and for supporting me all the time. Thank you for our discussions and our dreams. Without you, this work would not have been possible.

Table of contents

Abstract

Phonons contribute to resonant inelastic X-ray scattering (RIXS) as a consequence of the coupling between electronic and lattice degrees of freedom. Unlike other techniques that are sensitive to electron-phonon interactions, RIXS can give access to momentum dependent coupling constants. Information about the dispersion of the electron-phonon interaction is highly desirable in the context of understanding anisotropic conventional and unconventional superconductivity [1, 2].

We considered the phonon contribution to RIXS from the theoretical point of view. In contrast to previous studies [3–5], we emphasize the role of the core-hole lattice coupling. Our model, with parameters obtained from first principles, shows that even in the case of a deep core-hole, RIXS probes exciton-phonon coupling rather than a direct electron-phonon coupling.

This difference leads to quantitative and qualitative deviations from the interpretation of the implied electron-phonon coupling from the standard view expressed in the literature. Thus, our objective is to develop a rigorous approach to quantify electron-phonon coupling within the context of RIXS measurements. The ability to accurately reproduce experimental results from first-principles calculations, without recourse to adjustable parameters, should be viewed as the ultimate test of a proper understanding of the phonon contribution to RIXS.

We start by considering only the core-hole–phonon interaction within the context of X-ray photoemission spectroscopy. We combine an ab initio calculation of the real-space response function with many-body Green's functions techniques to reproduce the vibrational side-bands in SiX_4 ($X = H, F$) molecules. The approach we developed is suitable for application to crystalline materials.

We next consider the phonon contribution to X-ray absorption spectra. Unlike the charged excitations generated by X-ray photoemission, X-ray absorption creates a neutral excitation that we approximate as a core-hole and an excited electron. We first solved the electronic part of the problem on the level of the Bethe-Salpeter equation and then dressed the resulting 2-particle excitonic quasiparticle with the exciton-phonon interactions using the cumulant ansatz. The viability of this methodology was tested by calculating the N K-edge XAS of the N_2 molecule and the O $K-$edge of acetone. The resulting vibronic spectra agreed favorably with experimental results.

Finally, we construct a hybrid formulation of the RIXS cross section that preserves explicit summation over a small number of final states, but replaces the summation over intermediate states, which might be enormously expensive, with a Green's function. We develop an expansion of the Green's function and derive both analytically exact (in the no-recoil limit) and approximate solutions. The formalism was again tested on the O $K-$edge of acetone and agrees well with the experiment. To provide an outlook towards future work, we discuss application of the developed formalism to crystalline materials.

Résumé

Les phonons contribuent à la diffusion inélastique résonante des rayons X (RIXS) du fait du couplage entre les degrés de liberté électronique et ceux du réseau. Contrairement à d'autres techniques sensibles aux interactions électron-phonon, la technique RIXS peut donner accès aux constantes de couplage dépendantes du moment. Des informations sur la dispersion de l'interaction électron-phonon sont très précieuses dans le contexte de la supraconductivité anisotrope conventionnelle et non conventionnelle [1, 2].

Nous avons considéré la contribution des phonons sur la diffusion RIXS d'un point de vue théorique. Contrairement aux études précédentes, [3–5], nous soulignons le rôle du couplage du réseau avec les trous de coeur. Notre modèle, avec les paramètres obtenus *ab-initio*, montre que même dans le cas d'un trou de coeur profond, la technique RIXS sonde le couplage exciton-phonon plutôt qu'un couplage direct électron-phonon.

Cette différence conduit à des écarts quantitatifs et qualitatifs pour le couplage électron-phonon implicite par rapport à l'interprétation standard dans la littérature. Ainsi, notre objectif est de développer une approche rigoureuse pour quantifier le couplage électron-phonon dans le contexte des mesures de diffusion RIXS. La possibilité de reproduire avec précision les résultats expérimentaux à partir des calculs *ab-initio*, sans recourir à des paramètres ajustés, doit être considérée comme le test ultime d'une compréhension correcte de la contribution des phonons sur la diffusion RIXS.

Nous commençons notre travail en considérant uniquement l'interaction trou de coeur-phonon dans le contexte de la spectroscopie par photoémission de rayons X. Nous combinons un calcul *ab-initio* de la fonction de réponse en espace réel avec des techniques de fonctions de Green à plusieurs corps pour reproduire les bandes latérales vibrationnelles dans les molécules SiX_4 ($X = H, F$). L'approche que nous avons développée peut être appliquée aux matériaux cristallins.

Nous examinons ensuite la contribution des phonons aux spectres d'absorption des rayons X. Contrairement aux excitations chargées générées par la photoémission par rayons X, l'absorption des rayons X crée une excitation neutre que nous approchons en tant que trou de coeur et électron excité. Nous résolvons d'abord la partie électronique du problème au niveau de l'équation de Bethe-Salpeter, puis nous habillons la quasi-particule excitonique à 2 particules résultante avec les interactions exciton-phonon en utilisant l'Ansatz des cumulants. La viabilité de cette méthode a été testée en calculant le seuil K XAS de la molécule N_2 et le seuil K d'Oxygène de l'acétone. Les spectres vibrationnels obtenus concordent avec les résultats expérimentaux.

Enfin, nous construisons une formulation hybride de la section transversale RIXS qui préserve la sommation explicite sur un petit nombre d'états finals, mais remplace la sommation sur les états intermédiaires, ce qui pourrait être extrêmement coûteux, par une fonction de Green. Nous avons obtenu un développement de la fonction de Green et dérivé des solutions analytiques exactes (dans la limite de non-recul) et approximatives. Le formalisme a de nouveau été testé sur le seuil K de l'acétone et est bien en accord avec l'expérience. En perspectives des travaux futurs, nous discutons de l'applicabilité de notre formalisme aux matériaux cristallins.

List of Figures

List of Tables

Abbreviations

EPC(I) – Electron-phonon coupling (interaction)

RIXS – Resonant inelastic X-ray scattering

XAS – X-ray absorption spectroscopy

XES – X-ray emission spectroscopy

XPS – X-ray photo-emission spectroscopy

ARPES – Angular resolve photo-emission spectroscopy

IXS — inelastic X-ray scattering

DFT – Density functional theory

SCF – Self-consistent field

DFPT – Density functional perturbation theory

PES – Potential energy surface

KHE – Kramers-Heisenberg equation

BO – Born-Oppenheimer

MD – Molecular Dynamics

HF – Hartree-Fock

RPA – Random phase approximation

TDA – Tamm-Dancoff approximation

BSE – Bethe-Salpeter equation

FM – Fan-Migdal

DW – Debye-Waller

Units

Unless otherwise explicitly specified atomic units were used ($\hbar = e = m_e = 4\pi\epsilon_0 = 1$)

Atomic units (conventional / SI units):
Length: bohr (≈ 0.529 Å / 5.29×10^{-11} m)
Mass: m_e (9.11×10^{-31} Kg)
Energy: Ha (27.212 eV / 4.36×10^{-18} J)
Time: $\hbar$/Ha (2.42×10^{-17} s)

Chapter 1

Introduction

This chapter introduces some general aspects of the electron-phonon interaction, particularly as it related to the theory of superconductivity. We further discuss experimental techniques that are used to obtain information about the coupling between the electronic and lattice degrees of freedom.

Contents

1.1 Electron-phonon interaction

Electron-phonon coupling (EPC) is an inescapable aspect of condensed matter systems that has a pronounced influence on many quantities of interest. Interactions between electrons and phonons induce structural and magnetic transitions and contribute to the temperature dependence of charge and spin transport [6–11]. We first introduce a generic many-body Hamiltonian which describes the interaction between electronic and lattice subsystems, following [12, 13] we have

$$H = H_e + H_I + \sum_{ij} V_{ei}(\boldsymbol{r}_i - \boldsymbol{R}_j) \ . \tag{1.1}$$

Here, the electronic part H_e part normally contains the electron kinetic term and all electron-electron interaction; H_I describes the lattice subsystem. The electron-lattice interaction (V_{ei}) is governed by the potential which depends on both coordinates of the electrons $\boldsymbol{r}_i$ and ions $\boldsymbol{R}_j$. The origin of this potential is the electron-ion attractive interaction, but the explicit form depends on the particular approximation for the generic many-body problem [11]. In the absence of the electron-lattice interaction one can write the total wave-function simply as a product of the electronic and lattice parts $|\psi_{tot}\rangle = |\psi_e\rangle\,|\psi_I\rangle$. This is not any more correct in the presence of the mutual interaction. The solution in the fully interacting case can be found by expanding the electron-lattice potential around the equilibrium positions. Atomic displacements $\boldsymbol{Q}_j$ are taken to be a small parameter, and the resulting potential which acts on an electron becomes

$$V_{ei}(\boldsymbol{r}_i) = \sum_j V_{ei}(\boldsymbol{R}_j^0 - \boldsymbol{r}_i) + \sum_j \boldsymbol{\nabla}_{\boldsymbol{R}} V_{ei}(\boldsymbol{R}_j^0 - \boldsymbol{r}_i)\boldsymbol{Q}_j + \frac{1}{2!}\sum_{j,j'} (\boldsymbol{\nabla}_{\boldsymbol{R}})^2 V_{ei}(\boldsymbol{R}_j^0 - \boldsymbol{r}_i)\boldsymbol{Q}_j\boldsymbol{Q}_{j'} + O(Q^3) \ . \tag{1.2}$$

It follows that we can first solve the electronic problem in the presence of the static external potential which is defined by the term $V_{ei}(\boldsymbol{R}_j^0 - \boldsymbol{r}_i)$. Then the dynamics of the electron-ion potential can be accounted for using Eq. 1.2 in a perturbative way. Combing Eqs. 1.1 and 1.2 in the second quantization formalism we have [11, 12]

$$H = \sum_\alpha \epsilon_\alpha c_\alpha^+ c_\alpha + \sum_\nu \omega_\nu (b_\nu^+ b_\nu + 1/2) + \sum_{\alpha_1,\alpha_2,\nu} M^\nu_{\alpha_1,\alpha_2} c^+_{\alpha_1} c_{\alpha_2} (b_\nu + b_\nu^+)$$

$$+ \sum_{\alpha_1,\alpha_2,\nu,\nu'} (M^{(2)})^{\nu,\nu'}_{\alpha_2,\alpha_1} c^+_{\alpha_1} c_{\alpha_2} (b_\nu + b_\nu^+)(b_{\nu'} + b_{\nu'}^+) \ . \tag{1.3}$$

Here we assumed harmonic lattice vibrations (phonons) and b_ν^+ and b_ν are the phonon creation and annihilation operators, respectively. The energy of an electron ϵ_α is defined in the presence of the equilibrium ion potential and c_α^+, c_α are electron creation and annihilation operators respectively. The subscript $\alpha = \{n, \boldsymbol{k}\}$ represents the band index and momentum vector of the electron, while $\nu = \{\lambda, \boldsymbol{q}\}$ stands for the phonon mode and wave-vector. Electron-phonon interaction terms are defined in this context by the first and the second order coupling constants $M_{\alpha,\alpha}^{\nu}$, $(M^{(2)})_{\alpha,\alpha}^{\nu,\nu'}$, respectively.

1.2 Superconductivity

In addition to dictating the electronic transport properties of metals [6, 14] and renormalizing the electronic bands in semiconductors and insulators [15–18], the electron-phonon interaction produces the attractive force between electrons that binds Cooper pairs in conventional Bardeen–Cooper–Schrieffer (BCS) superconductors [19].

The theory of conventional superconductivity requires the presence of an attractive potential apart from the Coulomb repulsion. This competitive interaction leads to the formation of the quasi-particle states close to the Fermi level. For conventional superconductors, the attractive potential is generated by the electron-phonon interaction. Thus, the critical temperature $\mathrm{T_c}$ of the normal-superconducting state transition depends on the strength of the electron-phonon interaction (λ). The approximate relation between $\mathrm{T_c}$ and λ is given by McMillan [20]

$$T_c = \frac{\theta_D}{1.145} exp[-\frac{1.04(1+\lambda)}{\lambda - \mu^* - 0.62\lambda\mu^*}] \tag{1.4}$$

where μ^* is related to the double average of the Coulomb potential on the Fermi surface. The parameter λ is a double average of the Eliashberg function [7] on Fermi surface

$$\lambda = \sum_{\boldsymbol{k}\boldsymbol{k'}} \frac{1}{N(0)^2} \int_0^\infty d\omega' \alpha^2 F_{\boldsymbol{k}\boldsymbol{k'}}(\omega') \frac{2\omega'}{\omega_n^2 + (\omega')^2} \delta(\epsilon_{\boldsymbol{k}}) \delta(\epsilon_{\boldsymbol{k'}}) \ , \tag{1.5}$$

where the Fermi energy is set to zero and the momentum dependent Eliashberg function is

$$\alpha^2 F_{\boldsymbol{k}\boldsymbol{k'}} = \sum_\lambda |M_{\boldsymbol{k},\boldsymbol{k'}}|^2 \delta(\omega - \omega_\lambda(\boldsymbol{k} - \boldsymbol{k'})) \ . \tag{1.6}$$

The latter reflects the Migdal [6] approximation for the self-energy, i.e., neglects the electron-phonon vertex correction. The parameter λ also gives the electron mass enchantment at the Fermi energy. Improvements of Eq. 1.4 can found elsewhere [11, 13]. In general, one finds the critical temperature by solving the coupled equations for the temperature dependent energy gap Δ and the quasi-particle renormalization function $Z(i\omega)$ in the Eliashberg theory [21] (for the isotropic case)

$$Z(i\omega_n) = 1 + \frac{1}{|2n+1|}\sum_{n'}[\lambda(n-n') + \delta_{nn'}(\gamma_N + \gamma_P)]\delta_{nn'}$$

$$Z(i\omega_n)\Delta(i\omega_n) = \sum_{n'}^{|\omega'_n<\omega_c|}[\lambda(n-n') - \mu^* + \delta_{nn'}(\gamma_N - \gamma_P)]\Delta(i\omega_n)\ . \tag{1.7}$$

The n for which a non-trivial solution of Δ exists gives the critical temperature. The inverse lifetimes γ_P and γ_N correspond to the average over the Fermi surface of the interaction with paramagnetic and non-magnetic impurities receptively.

The isotropic approximation is mainly valid for metallic superconductors. In this case, the momentum dependence of the electron-phonon coupling constant does not play an essential role since all modes and wave-vectors contribute to the formation of the superconducting states. This is, however, not the case for the unconventional superconductors which show strong anisotropic properties [1] and thus need careful treatment of the momentum dependence of the coupling strengths.

The discovery of the high-temperature copper-based superconductors [22] proves that there are still missing parts in the description of the superconducting state. The description of the modern theories of unconventional superconductivity goes beyond the purpose of this section and can be found elsewhere [23, 24]. Although we do not want to make any claim in favor of one or another interpretation, we would like to emphasize the role of the mutual influence of the electron and lattice degrees of freedom in phase transitions in general.

Unconventional superconductivity is accompanied by a complex phase diagram, i.e., different symmetry breakings with respect to the carrier level dopping or other external parameters. This can be seen as a result of the existence of multiple intertwined orders, including spin, charge and lattice degrees of freedom [2, 23]. This interplay between different degrees of freedom is particular to excitations around quantum critical

points in strongly correlated materials. To get a complete picture, one has to obtain full information on the strengths of these interactions including coupling to the lattice degrees of freedom [1, 25, 26].

Although the electron-phonon interaction on its own is not sufficient for unconventional superconductivity, it may still play a role in the formation of such phenomena [27–29]. The dispersion relation of the electron-phonon interaction is tightly connected with the formation of charge density waves and can boost or suppress the creation of superconducting pairs [30, 31], depending on the wave-vector. This motivates mapping the electron-phonon coupling strength throughout the Brillouin zone.

1.3 Quantifying electron-phonon coupling

Several experimental techniques can measure electron-phonon coupling strengths to varying degrees of efficacy.

Inelastic scattering Inelastic neutron scattering is an excellent and well-established technique to experimentally measure the dispersion of low-energy collective excitations such as phonons. Here, the linewidth of phonon features contains information about electron-phonon coupling. The electron-phonon coupling $M^{\nu'}_{kk'}$ contributes to the self-energy of the phonon Green's function through the vertices in the polarization diagrams. Phonon self-energy then contains double average over BZ and all electronic energies of this matrix elements and defines linewidth for every phonon mode2. However, the overall broadening of the phonon peaks is quite small, which makes it difficult to determine charateristic coupling constant even for compounds with strong electron-phonon interaction [32]. Conventional inelastic X-ray scattering can provide similar information as inelastic neutron scattering [33, 34].

Charged and neutral excitations The electron-phonon interaction can also be probed by investigating electronic spectra of materials. For example, in angle-resolved photo-emission spectroscopy (ARPES), which can map the dispersion of the valence electron bands, the electron-phonon interaction manifests as an anomalous 'kinks' on the band structure, or even produces satellite structure [35–37]. The dispersion of

the electron-phonon coupling constant appears as a correction to the quasi-particle picture and renormalizes quasiparticle energies and spectral weights, and bestows them with lifetimes [18, 38, 39]. But ARPES probes an effective coupling constant averaged over the phonon modes and wave-vectors. One can also consider scanning tunneling spectroscopy [40, 41] or electron energy loss spectroscopy [42]. In the same spirit, neutral excitations can be used to detect the electron-phonon interaction, such as in Raman and optical spectroscopies [43, 44].

All of these approaches have certain unsatisfactory limitations concerning accurately quantifying the electron-phonon interaction strength throughout the full Brillouin zone. Resonant inelastic X-ray scattering (RIXS) – which can generate collective excitations by the perturbation present in the intermediate, resonantly core-excited state – has emerged in the last decade as a new technique for accomplishing this objective [2, 3]. RIXS holds certain advantages over these other techniques including element and orbital selectivity, sensitivity to small sample quantities, and momentum resolution. Most importantly, it is commonly assumed that RIXS offers a *direct* probe of electron-phonon coupling [2, 45], contrary to the indirect nature of some of the other measurements.

Chapter 2

Resonant Inelastic X-ray Scattering

The purpose of this chapter is to provide an overview of the RIXS technique and motivate our subsequent studies. We will briefly discuss different methods to calculate the phonon contribution in RIXS, and will show the importance of the core-hole in the formation of the phonon contribution in RIXS.

Contents

2.1 Introduction

Resonant inelastic X-ray scattering (RIXS) is a technique based on the second order interaction of an X-ray photon with matter. This means that RIXS involves two photons, which we label incoming and outgoing. The energy of the incoming photon is normally tuned to be close to the resonant transition of a core-electron to a conduction level; this leads to the resonant photon absorption. The following de-excitation and emission of the outgoing photon creates the final state, which might be different from the ground-state. Quantities of particular interest are the energy loss ($\omega_{loss} = \omega_i(\boldsymbol{k}_i) - \omega_o(\boldsymbol{k}_o)$), momentum transfer ($\boldsymbol{q} = \boldsymbol{k_{in}} + \boldsymbol{k}_{out}$) and change in the polarization of the photons. The energy and momentum transferred to the sample during the scattering process generate various excitations in the material, such as orbital, magnon, phonon, charge transfer, charge density wave, etc. One of the advantages of RIXS is the long life-time of the final states and consequently high resolution of the spectra. The latter is mainly defined by the instrumental broadening and today the overall resolution can be better than 25 meV [46]. This gives access to very low energy excitations and offers a powerful probe for studying unconventional superconductors, strongly correlated systems, and other materials [1, 26]. Detailed reviews on the RIXS technique can be found here [3, 47].

The RIXS cross-section can be approximated by the second order contribution from the electron-photon operator with respect to the vector potential A. The electron-photon interaction in the non-relativistic limit contains terms linear and quadratic in $\boldsymbol{A}$ [12, 49]

$$V = \sum_i \left[-\frac{1}{c}\boldsymbol{p_i} \cdot \boldsymbol{A}(\boldsymbol{r}_i) - \frac{1}{c}\boldsymbol{\mu}_i \cdot \boldsymbol{B}(\boldsymbol{r}_i) + \frac{1}{2c^2}|\boldsymbol{A}(\boldsymbol{r}_i)|^2 \right] ; \ \boldsymbol{B} = \boldsymbol{\nabla} \times \boldsymbol{A} \ . \tag{2.1}$$

The above expression obtained expanding square term ($[\boldsymbol{p}_i - \frac{1}{c}\boldsymbol{A}]^2$) in the Hamiltonian of an electron in the electromagnetic field and accounting for the magnetic field - spin interactions. This form reflects the choice of gauge $\nabla \cdot \boldsymbol{A} = 0$. Coordinate position, momentum and magnetic moment of a given electron are denoted as $\boldsymbol{r_i}$, $\boldsymbol{p_i}$ and $\boldsymbol{\mu_i}$ respectively. Here and after we will refer to the first two terms as V^I and to the term with $|\boldsymbol{A}|^2$ as V^{II}. The vector potential may be written in terms of field creation and

annihilation $a^+_{\boldsymbol{k},\alpha}, a_{\boldsymbol{k},\alpha}$ operators as

$$\boldsymbol{A}(\boldsymbol{r},t) = \sum_{\boldsymbol{k},\alpha} \sqrt{\frac{2\pi c^2 \omega_{\boldsymbol{k}}}{V}} \boldsymbol{\xi}(\boldsymbol{k},\alpha)(a_{\boldsymbol{k}\alpha} e^{-i\omega_{\boldsymbol{k}} t + \boldsymbol{k}\cdot\boldsymbol{r}} + h.c.) \ . \tag{2.2}$$

Here the index $\boldsymbol{k}$ stands for the momentum of the photon and the subscript α runs over all different modes and the polarization unit vector ξ gives the polarization of each mode. The photon field operators obey boson commutation relation $[a_{\boldsymbol{k},\alpha}, a^+_{\boldsymbol{k},\alpha}] = \delta_{\boldsymbol{k'k}}\delta_{\alpha,\alpha'}$. For the seek of simplicity we will introduce the following notation for electron-photon interaction, separating the photon parts ($l = k_l, \alpha_l$)

$$V^I_l(t) = [\Delta^I_l a_l e^{-i\omega_{\boldsymbol{l}} t} + h.c.]$$

$$V^{II}_{l_1,l_2}(t) = [\tilde{\Delta}^{II}_{l_1,l_2} a_{l_1} a_{l_2} e^{-i(\omega_{l_1}+\omega_{l_2})t} + h.c.] + [\Delta^{II}_{l_1,l_2} a^+_{l_1} a_{l_2} e^{-i(\omega_{l_2}-\omega_{l_1})t} + h.c.] \tag{2.3}$$

The rate of electronic transitions due to interaction with the electromagnetic field and consequently the cross-section of the inelastic scattering process can be found from perspectives of time-dependent perturbation theory. Here we should consider time evolution of initial many-body state which is driven by the following operator in the interaction picture representation $U(t) = e^{iH_0 t} e^{-iHt}$, where $H = H_0 + V$ and $H_0 = H^s_0 + H^p_0$ describes the unperturbed electronic system and the free photon parts respectively. The practilce way to proceed is to expand the time-evolution operator in the powers of interaction (see Appendix F). Terms which are quadratic in the vector potential will contribute to the transition rate of the two-photon processes $W_{FI} \sim \frac{d}{dt}\left|\langle o, \Psi_F| \, U(t) \, |\Psi_I, i\rangle^{(2)}\right|^2$. However only two of them are relevant for the scattering [48]

$$\langle \psi_F, o| \, U(t) \, |\Psi_I, i\rangle^{(2)}_{scattering} = \left[\langle \Psi_F| \, \Delta^{II}_{i,o} \, |\Psi_I\rangle + \sum_M \frac{\langle \Psi_F| \, (\Delta^I_o)^+ \, |\Psi_M\rangle \, \langle \Psi_M| \, \Delta^I_i \, |\Psi_I\rangle}{(E_{MI} - \omega_i + i\Gamma_M)}\right]$$

$$\times \frac{(e^{-i(E_{FI}-\omega_{loss}+i\Gamma_F)t} - 1)}{E_{FI} - \omega_{loss} + i\Gamma_F} \ . \tag{2.4}$$

Here we factorized out non-interacting photon's parts in initial and final wavefunctions leaving only explicit energy dependence. The subscripts i, o represents properties of incoming and outgoing photon respectively. The following shorthand notation

are used $\omega_{loss} = \omega_o - \omega_i$, $E_{MI} = E_M - E_I$ and similarly $E_{FI} = E_F - E_I$. Here Ψ_M, Ψ_I and Ψ_F are the many-body wave-functions and E_M, E_I, E_F are the eigenvalues of unperturbed Hamiltonian H_o^s. The decay of the intermediate and final states are represented by the inverse lifetimes Γ_M and Γ_F respectively. Due to the resonant nature of the process, i.e. resonant regarding the transition to the intermediate state $\omega_i \sim E_M - E_I$, the contribution from the first term in Eq. 2.4 in the RIXS process is negligible. The Δ^{II} portion of the first term dominates in non-resonant inelastic X-ray scattering (NRIXS). Since we will work only with the resonant part from now, we will drop the superscript of $\Delta^I = \Delta$ to simplify the notations.

Roughly speaking, RIXS can be viewed as a two step process in which the intermediate states are populated by an XAS-like absorption of the incident photon. The intermediate states subsequently decay to the final states through an XES-like emission of the outgoing photon, leaving some set of lower energy excitations in the final state. In practice, these two processes are poorly separable due to mutual interference effects, though this view offers an approximate formulation of RIXS in terms of the convolution of XAS and XES spectra [50]. The full cross-section is given by the Kramers-Heisenberg equation [51]

$$\sigma(\omega_i, \omega_{loss}) = \frac{\omega_o}{\omega_i} \sum_F \left| \sum_M \frac{\langle \Psi_F | \, \Delta_o^+ \, | \Psi_M \rangle \, \langle \Psi_M | \, \Delta_i \, | \Psi_I \rangle}{E_{MI} - \omega_i + i\Gamma_M} \right|^2 \delta(E_{FI} - \omega_{loss}) \ . \tag{2.5}$$

In practice, due to the local character of a core excitation, Δ_i, Δ_o can be approximated by the dipole expansion. The inverse core-hole lifetime is defined by Γ_M. In principle, the excited state might decay through different channels. The Auger process, where the de-excitation of the excited electron is non-radiative and leads to the creation of another electron, gives a significant contribution to the broadening of the final state in X-ray absorption in total electron yield measurements. It remains unclear whether RIXS is sensitive to the Auger decay rate or it the intermediate state lifetime is instead governed by the fluorescence decay channel, which gives longer core-hole lifetimes.

Equation 2.5 is written with the assumption that the final state has an infinite lifetime. The final state contains various kinds of excitations that have different lifetimes, but these tend to be much longer than the intermediate state lifetime. This fact makes RIXS features quite sharp compared to the XAS energy resolution and consequently

allows access to the fine structure of the electronic transitions.

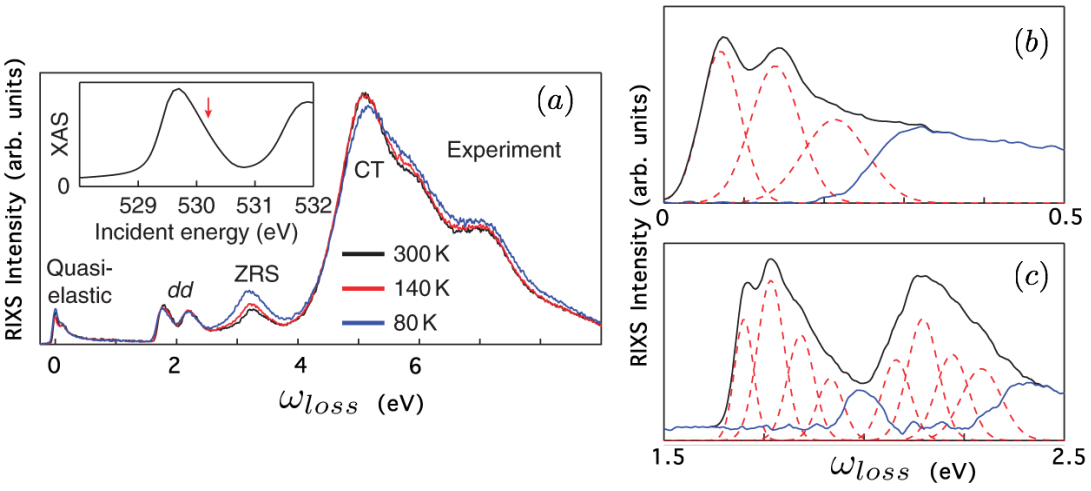

Figure 2.1: Low energy part of RIXS O K-edge spectrum of quasi-one-dimensional cuprate compound (Li_2CuO_2) [4]. The RIXS spectrum (a) showing dd excitations, phonon satellites, Zhang-Rice singlet and charge transfer peak. The right panel shows phonon satellites around the elastic peak (b) and on the dd electronic excitations (c). Figure adapted from the work of Johnston *et al* [4].

There is a common separation between the contributions to RIXS. For the so-called direct RIXS the energy of the emitted photon is generally independent of the incident photon energy. The direct contribution to RIXS can often be explained by the density of states, and is also referred to as the fluorescence contribution [45]. The other, indirect contribution, arises from secondary excitations generated by the perturbation caused by the intermediate state. This contribution can only be explained with a many-body picture. Since the emission energy varies with the incident energy, keeping the energy loss constant, these features are sometimes called Raman-like. Thus, the indirect contribution includes collective excitations (phonons, magnons) which accompany the electronic transitions. These various secondary excitations can often be distinguished by the loss energy at which they appear, however, sometimes it is not obvious to separate low energy (e.g. phonon and magnon) features, since they can have similar energies and show higher harmonics.

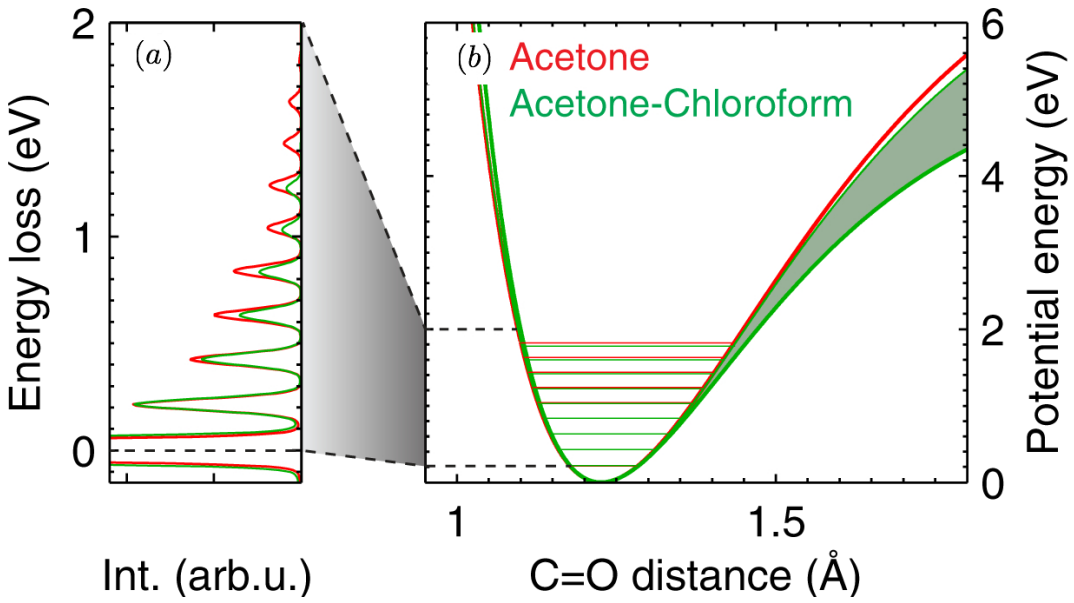

Figure 2.2: Mapping of the ground state potential energy surface. By obtaining the peak positions of the phonon satellites around the elastic line (a), one can reconstruct the parameters of the Morse potential and consequently the potential energy surface of the ground state (b). As an example, one can see the ground state reconstruction done by for acetone compounds from RIXS spectra. Figure adapted from work of Schreck *et al* [52].

2.2 Low-energy excitations

The main focus of our work is the phonon contribution. Typical phonon lifetimes in the final state are of the order of a few ns, corresponding to a broadening of $\sim$ 10 meV, which is smaller than the characteristic phonon energy. Only recently have the instruments reached sufficient resolving power to distinguish phonon excitations in crystalline materials. This progress in resolution makes RIXS a very powerful technique [1, 25, 26] to study collective excitations and their coupling to the electronic system [4]. The phonon contribution to RIXS has an indirect nature. After absorbing the incident photon, the lattice responds to the perturbation present in the intermediate state, time-evolving on an excited-state potential energy surface for the duration of the core-hole lifetime. When the photo-excited electron decays back to the core-state, the lattice will inevitably be caught out of equilibrium with respect to the ground-state potential energy surface, leaving some occupation of phonons in the final state. In different words, this process involves transitions from initial phonon level to multiple phonon

levels of the intermediate state and from all populated intermediate state phonon levels to each phonon level of the final state (Fig. 2.3). The probabilities of those transitions defined by the overlap of phonon wavefunctions in the ground state, core-excited state, and final state, and consequently by the relative position of the corresponding potential energy surfaces.

The RIXS phonon cross-section reflects a combination of couplings of initial, intermediate and final states configurations to the collective modes. This means that apart from the dispersion relation of the phonon, which one can obtain by tuning both the energy loss and the momentum transfer, one can also extract the coupling constants from the relative intensities of the harmonics of these excitations.

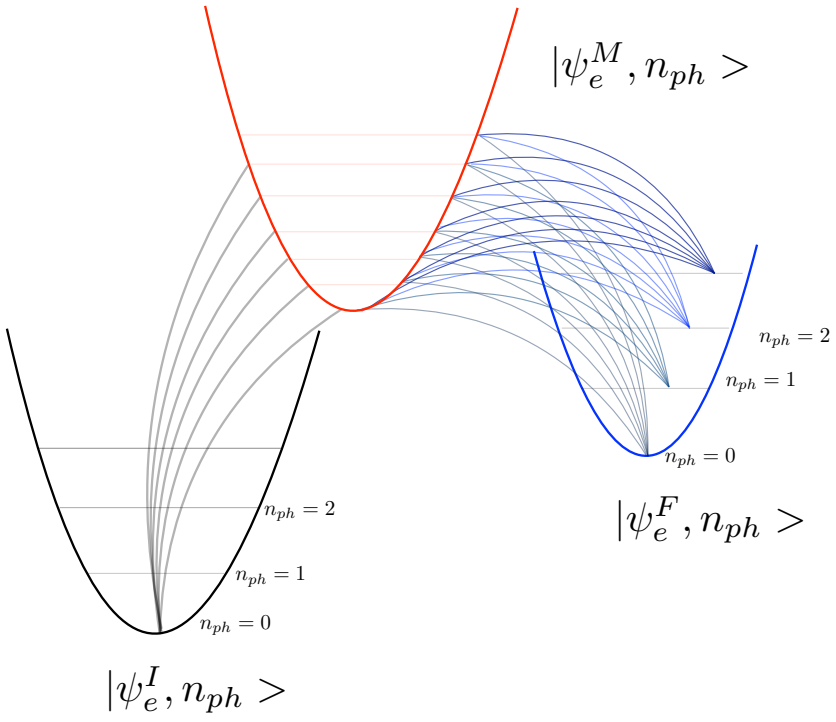

Figure 2.3: Schematic representation of the RIXS process regrading phonon contribution. Superscripts I, M and F correspond to electronic initial, intermediate and final state, respectively. Only one intermediate and final electronic state are shown. Each final state contains contributions from all possible intermediate phonon states.

Knowledge about the electron-phonon coupling at all points in the Broilloun zone

would help for rigorous testing of competing theories of unconventional superconductivity [1, 23]. The ability to resolve collective excitations for different momenta transfer makes RIXS a potentially valuable new tool for studying electron-phonon coupling. Assuming zero phonon population in the initial state, the phonon mainly would be created during the propagation of an excited, intermediate state, which reflects the coupling of excited electron-core-hole pairs to the lattice. However, the electron-phonon coupling which is relevant for transport properties involves the electronic ground state. Thus, it is important to correctly identify the meaning of the coupling constant that is observed by RIXS and how it is related to the transport electron-phonon coupling.

A standard interpretation of the electron-phonon interaction from RIXS is given by Ament *et al* [45]. The model constructed by the authors is inspired by cuprates, which have a single unoccupied d orbital. To treat the electron-phonon interaction they use a Holstein-type Hamiltonian, where a single electronic orbital couples to a single (Einstein) phonon mode. The RIXS cross-section can then be obtained using an analytical solution of the Hamiltonian by the Lang-Firsov canonical transformation: $H' = e^{-S} H e^{S}$, where $S = \sqrt{g} c^{+} c (b - b^{+})$ [12]. The overlap between vibrational wave-functions in the Kramers-Heisenberg equation is given by Franck-Condon factors ($B(n, n')$)

$$\sigma(\omega_i, \omega_{loss}) = \sum_{n_f} \left| \sum_{n_m} \frac{B_{n''n'}(g) B_{n_m 0}(g)}{\omega_i - (g - n_m)\omega_0 + i\gamma_m} \right|^2 \delta(\omega_{loss} - n_f \omega_0) \ . \tag{2.6}$$

Here $n' = \min(n_m, n_f)$, $n'' = \max(n_m, n_f)$, and $g = (M/\omega_0)^2$ is the dimensionless coupling strength. The inverse core-hole life-time γ_m is defined by the decay of vibronic intermediate state. The analytical expression for the Franck-Condon factors is [45]

$$B_{mn}(g) = (-1)^m \sqrt{e^{-g} m! n!} \sum_{l=0}^{n} \frac{(-g)^l \sqrt{g}^{m-n}}{(n-l)! l! (m-n+l)!} \, . \tag{2.7}$$

The simplicity of this model has led to its widespread use for quantitative explanation of experimental results [5, 53]. This model produces multiple phonon peaks around the elastic line, the relative intensities of which are proportional to the absolute of the coupling strength $g = \frac{M_{eff}^2}{\omega_{vib}^2}$ (see Fig 2.2). The main parameters of this model are the electron-phonon coupling, the phonon frequency and the core-hole life-time. The latter

is well defined form other experiments.

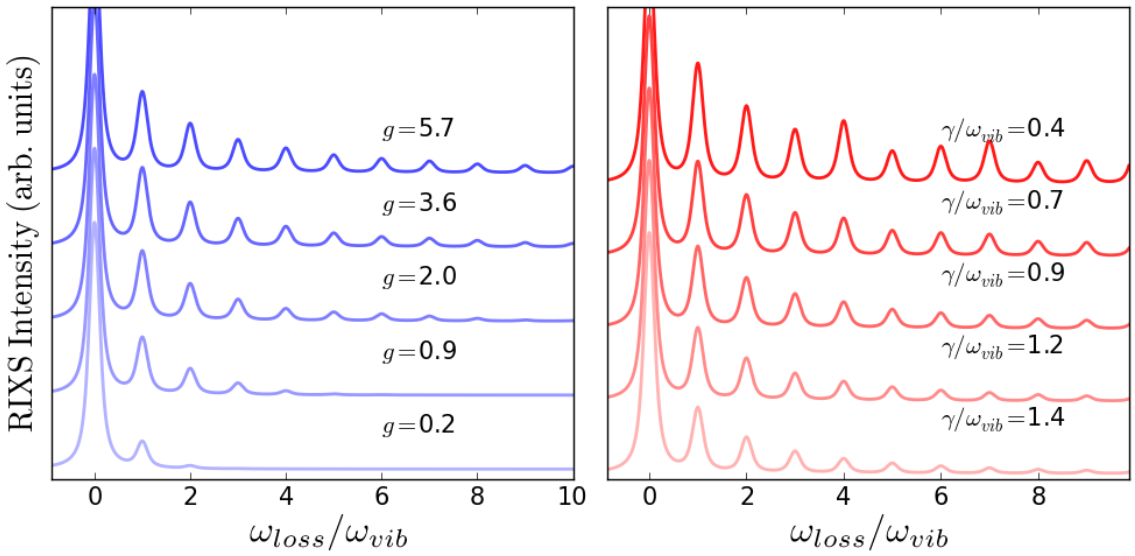

Figure 2.4: Phonon contribution to RIXS calculated using model Hamiltonian 2.8. Different spectra are offset arbitrarily in vertical axis. The two main dimensionless parameters of the model are the coupling strength $g = \frac{M^2}{\omega_{vib}^2}$ and the ratio between the inverse intermediate life-time and the vibrational frequency γ/ω_{vib}. On the left, RIXS spectra are presented with respect to variation of the coupling strength; the intermediate state life-time was fixed $\gamma \sim \omega_{vib}$. The coupling strength controls the final state population of the phonon levels. The monotonic damping of the peak intensities, however, can be broken by increasing the intermediate state lifetime (right). If the lifetime is longer then the characteristic time of oscillation ($\gamma/\omega_{vib} < 1$) the spectra start to deviate from monotonic decay.

Another recent paper by Johnston *et al* [4] focused on RIXS studies of the quasi 1D cuprate Li_2CuO_2. They applied exact diagonalize to a small CuO cluster using an extended Hubbard-type Hamiltonian with a few bands. A linear electron-phonon interaction was included for a dispersionless mode. The presence of the core-hole in the intermediate state was included through an on-site Coulomb attraction, but direct core-hole–phonon coupling was neglected.

The dispersion of the one-phonon contribution to RIXS for an 8-band CuO cluster was calucalted using digramatic techniques by Devereaux *et al* [2]. Although this study makes progress by including phonon dispersion, the direct coupling of the core-hole to phonons was still neglected. Also, application of such results is limited to the weak coupling limit since it includes only one lowest order diagram. Example results were

provided assuming a generic form for the q dependence of the electron-phonon coupling strength [54].

Another application of the phonon contribution to RIXS is to quantify (valence) excited-state potential energy surfaces. At the true elastic line of the RIXS signal, the electronic (and vibrational) system returns to the ground state. For the quasielastic contribution, the system returns to the electronic ground-state, but with some number of phonon excitations. The frequency spacing of these phonon features corresponds to the curvature of the ground-state potential energy surface. RIXS features corresponding to final states with electronic excitations may also be accompanied by a phonon tail. In this case, the frequency spacing of the phonon features may differ from that at the quasielastic region, indicating that the curvature of the corresponding excited-state potential energy surface differs from the ground-state potential energy surface. In this way, it has been demonstrated by the group of Föhlisch that RIXS is a valuable technique for revealing excited-state potential energy surfaces [52].

Taking everything into account there are three different approaches to study the phonon contribution in RIXS: (i) simplified model approaches [5, 45, 53]; (ii) an approaches based on the model calculations of the small clusters and exact diagonalization; (iii) advanced quantum chemistry calculations using an explicit electronic and vibrational Hilbert spaces for small molecules [55–58]. The simplified model approaches are clearly not satisfactory, and the last two cases are difficult to scale for proper calculations with full momentum dependence. This creates the necessity for a new approach which has to treat correctly both the electronic structure of the excited state and the dispersion of the collective excitations and can be scaled to crystalline materials.

However, before we will discuss possibilities for the approaches, we would like to point out the critical difference between the ground state coupling to the lattice and coupling to the lattice in the presence of core-excitation. This aspect was missing in previous studies based on model approaches.

2.3 *Ab-initio* + model study

To show the importance of the electron-hole and hole-phonon interactions we preformed a model study based on parameters calculated from first principles.

The objective is to see how the model proposed by Ament *et al* [45] can reproduce an experiment using an *ab-initio* calculations of the coupling constant. Usually, the series of the phonon satellites from the experiment can be closely fitted with this model by adjusting the coupling constant. The resulting coupling might be misinterpreted as the electron-phonon coupling constant, though this will not be correct if the contribution from the core-hole-phonon coupling is non-negligible. To clarify this point, we calculated coupling constants for three types of electronic excitations. We considered excited electron, core-hole and exciton type of electronic excitations. The phonon contribution to RIXS was obtained using Eq. 2.6 and the results were compared to the experimental data.

For this, we considered the O K-edge RIXS of the acetone molecule. The choice of this compound was based on two factors: (i) availability of a high-resolution experimental data [52] and (ii) that the compound should be relatively simple/well studied, to avoid uncertainties in the ground state calculations.

After photo-absorption, the excited electron is well localized in an anti-bonding orbital. According to the experimental data, the main contribution to the vibrational part of RIXS comes from the CO stretching mode. The RIXS process was considered in the spirit of the Holstein Hamiltonian with one local mode and single electronic orbital

$$H = \epsilon c_i^+ c_i + \omega_{vib}(b^+ b + \frac{1}{2}) + M_{eff} c_i^+ c_i (b + b^+) \ . \tag{2.8}$$

First, we assumed that RIXS is a direct probe of electron-phonon coupling. This means that the excited state consists only of the excited electron and that the core-hole is omitted. The structure was first relaxed in the ground state and then an extra electron was added to the lowest unoccupied (anti-bonding) orbital. The gradient of the potential energy surface was obtained by varying the C-O inter-atomic distance around the ground-state equilibrium and calculating within SCF DFT the total energies for the excited state electronic configuration and all distances. Thus the tangent of the slope

of the excited potential energy surface at the ground state equilibrium distance gives the gradients, and consequently the coupling constant $M = \sqrt{\frac{\hbar}{\omega_{vib}\mu}}F$. The phonon contribution to RIXS obtained using model 2.6 and this calculated electron-phonon coupling constant is shown in Fig. 2.3 in red (see also Tab. 2.1).

Second, the same procedure was repeated for the electronic excitations including only the core-hole. The $1s$ core-hole on the oxygen site was modeled with a pseudo-potential. In this case, the operators c_i^+ and c_i correspond to the creation and annihilation of the core-hole and M_{eff} is coupling of the core-hole to the local vibration. The force was found as well from the excited state potential energy surfaces and the resulting phonon contribution to RIXS is shown in Fig. 2.3 in green.

Third, the exciton configuration of the excited state was created using both a core-hole on the 1s level and an extra electron in the lowest unoccupied orbital [59, 60]. Such an excited state generaly has to be treated within the Bethe-Salpeter equation (BSE) [61–63]. For this particular case DFT SCF relaxation of the electronic density gives similar results to the solution of the BSE (see Chapter 5). At this point to preserve the form of the Hamiltonian 2.8 one has to use an effective treatment of the two-particle problem, which we will discuss at the end of this section to avoid distraction from the main conclusion. Again the excited state potential energy surface along C-O stretching mode was used to calculate the exciton-phonon coupling constant. The phonon RIXS contribution from exciton-phonon coupling is shown in blue (Fig. 2.3).

Table 2.1: Vibronic forces for acetone obtained from the slope of the excited-state PES (CO stretching mode) evaluated at the ground-state equilibrium bond length with respect to different types of excitations.

Excitation type	Force (eV/Å)
electron	-1.0
core-hole	-3.5
exciton	-7.7

The resulting phonon contribution for the three types of electronic excitations are shown in Fig. 2.3 along with the experimental data from the work of [52]. The comparison clearly shows that satisfactory reproduction of the experimental data is

possible only with the exciton-phonon interaction. This leads to the conclusion that RIXS in fact is a probe of exciton-phonon coupling even in the case of a deep core-hole. An interesting aspect is that the phonon coupling of an exciton is stronger then the sum of the core-hole and excited electron coupling. This can be explained considering the structure of the LUMO in terms of atomic orbitals. The presence of the core-hole potential on the oxygen site tends to shift the energy of the atomic orbitals, and consequently modifies the contribution from oxygen orbitals. Thus, the electron-hole interaction also indirectly contributes to the strength of resulting exciton-phonon interaction. Our study of the O K-edge RIXS of acetone clearly shows the importance of direct coupling of the core-hole to vibrations.

Cu L-edge Since many RIXS studies are performed at the Cu L_3 edge, we now estimate the contribution from a Cu $2p$ hole in generating lattice dynamics. We select crystalline Cu_2O for this test and approximate the forces on nearest neighbor oxygen sites due to an excitation on a copper site. As in the acetone example, we model an extra electron, a core-hole, and an exciton.

The resulting forces are given in Table 2.2. The force resulting from the introduction of a Cu $2p$ core-hole is approximately 60 % of the force due to an exciton, and slightly larger than the force from the addition of an electron localized at the copper site. From this, we conclude that the Cu $2p$ hole is not screened enough to neglect it's coupling to phonons.

Table 2.2: Forces on the nearest neighbor oxygens due to an electronic excitation on a Cu site in crystalline Cu_2O.

Excitation type	Force (eV/Å)
effective electron	0.135
core-hole	0.165
exciton	0.257

The experimental structure was initially relaxed in order to minimize the electron-ion forces for the ground-state configuration. Keeping the ground-state atomic positions fixed, SCF calculations were made for core-hole and 'exciton' configurations. For these,

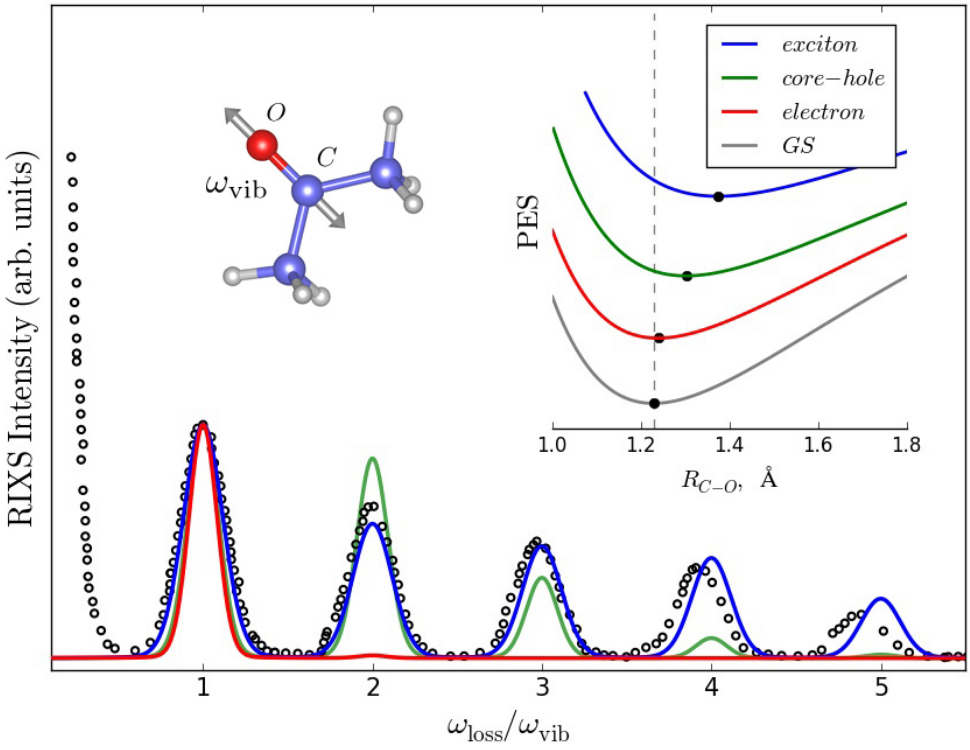

Figure 2.5: RIXS spectrum at the O-K edge of acetone showing a progression of phonon excitations. Calculations resulting from an electron-phonon coupling constant assuming an intermediate state with an excited electron (red), an oxygen core-hole (green), and an exciton (blue) are compared to experimental results (open symbols) [52]. Calculated spectra are shown without the elastic contribution and are normalized to the intensity of the first phonon peak. Inset: calculated potential energy surfaces (PES) for the three possible excited states along with the ground-state (GS) PES (gray). The dashed vertical line indicates the ground-state equilibrium C=O bond length and the black dots are placed at the minima of each PES. All PES curves are offset arbitrarily in energy.

we made a copper pseudopotential with one electron removed from the $2p$ shell and used this pseudopotential on one of the copper sites in the supercell. The core-hole configuration has an overall positive charge of $1|e|$ for the supercell that can be compensated by a uniform negative charge.

Explicitly adding an extra electron to the bottom of the conduction band (instead of using a uniform neutralizing charge density) gives the exciton configuration since this extra electron will be localized around the core-hole site. For each configuration, we

obtain the force on the oxygen atoms nearest to the copper site with the core-hole. We find that the force on the nearest oxygen atoms for the core-hole configuration is 64 % of the force resulting from the exciton configuration. This strongly suggests that even for the deeply bound Cu $2p$ levels a core-hole is not completely screened and contributes directly to the generation of phonons.

To mimic the addition of an extra, localized electron, to otherwise neutral Cu_2O, we substituted Zn for one of the Cu sites. Due to the impurity nature of the Zn atom, the highest occupied electron level is localized around the zinc site. We repeated the calculation after removing this electron (giving a supercell with total positive charge of $1|e|$) and defined the force due to the excited electron as the difference between forces on nearest oxygen atoms for the neutral and charged (Zn and Zn^{+1}) impurity configurations ($F_e = (F_{Zn-O}) - (F_{Zn^{+1}-O})$). The resulting force on the nearest oxygen site is smaller than for either the exciton or core-hole configurations, possibly due to the less localized nature of the extra electron compared to the bound exciton. Although more effective schemes for localizing an extra electron can likely be constructed with a local orbital basis DFT code, the comparison between the core-hole and exciton configurations already indicates that the core-hole–phonon coupling should not be neglected at the Cu L_3-edge.

Model Hamiltonian for exciton-phonon interaction For the case of a single exciton which couples to the vibrational mode, the model Hamiltonian 2.8 has to be rewritten in terms of two-particle operators which are $a_i = \sum_{e,h} A^i_{eh} c^+_e c_h$ and $a^+_i = \sum_{e,h} A^{i*}_{eh} c_e c^+_h$

$$H = \epsilon_i a^+_i a_i + \omega_{vib}(b^+ b + \frac{1}{2}) + M_{eff} a^+_i a_i (b + b^+) \ . \tag{2.9}$$

Here ϵ_i is an exciton energy and coefficients A^i_{eh} contain information about particle-hole interactions in general defined by the eigenvectors of two interacting particles Hamiltonian such as BSE one which is in details discussed in Chapters 3 and 5. However the main parameter of this model is an effective exciton-phonon coupling and in this study was found again using constrained DFT calculation of the potential energy surface along CO stretching mode $M_{eff} = -\sqrt{\frac{\hbar}{2\mu\omega_{CO}}} \partial_{R_{CO}} E^{DFT}_i(R_0)$. The electronic excitation is charge neutral, and it is no longer obeys Fermi statistics and in general, as well deviates from regular bosonic commutation relation [64]. However the limit of low

exciton density, this commutator can be approximate as a quasi-bosonic one $[a_p^+, a_{p'}] \cong \delta_{pp'}$ [65]. Thus in contrast to the initial model Hamiltonian, Eq. 2.9 describes boson-boson interactions. Although it does not change the analytical expression in Eq. 2.6 for the RIXS cross-section, one has to be aware that it leads to a sign change in the expression for the canonical exciton creation and annihilation operators (see Appendix D).

Numerical details For all calculations in this section, we used a pseudopotential based plane-wave DFT code (QUANTUM ESPRESSO) [66] with periodic boundary conditions. The applicability of the DFT plane-wave methods was checked by calculation of well known ground state properties, such as the molecule orbitals and vibrational frequencies. The acetone molecule was modelled in the gas phase using a $(20\mathring{A} \times 20\mathring{A} \times 20\mathring{A})$ supercell with one molecule in the middle. We used ultrasoft, PBE/GGA pseudopotentials taken from the Quantum-ESPRESSO pseudopotential library, and a plane-wave cutoff of 60 Ry for the wave-functions and 600 Ry for the charge density. For the Cu_2O crystal, DFT calculations were performed on a $(3 \times 3 \times 3)$ supercell using LDA norm-conserving pseudo-potentials.

2.4 Conclusion

In this section, we investigated the nature of electron-phonon coupling as probed by RIXS. Despite the advantages of this technique, such as momentum selectivity and long final state lifetime, we caution that the resulting coupling constant obtained from RIXS is an excited state-lattice coupling, and thus contains contributions from both excited electron and core-hole.

Using the model proposed by Ament *et al* [45] and *ab-initio* based calculations of the coupling constants for three types of the electronic excitations present in the intermediate state of RIXS (excited electron, core-hole and exciton), we showed that only exciton-phonon coupling can reproduce the experimental spectra. As an example, we considered the acetone molecule and vibrational contribution to O K-edge RIXS. We also showed the importance of the core-hole contirbution to the resulting exciton-lattice coupling in the crystalline copper based material Cu_2O with a deep $2p$ hole. This study highlights the importance of the direct core-hole phonon coupling, which was omitted in previous studies [2, 5, 45, 53, 67].

Results of this model study show a clear need for a rigorous approach to reproduce the phonon contribution to RIXS from first-principles for crystalline materials.

Chapter 3

Spectral functions

The objective of this chapter is to introduce the Green's functions and spectral functions techniques. We consider and compare different types of Green's function expansions (Dyson's equation and cumulant) for electron-phonon interactions. We also discuss the two-particle problem with electron-electron interactions and the Bethe-Salpeter equation (BSE), which is relevant in the context of neutral excitations.

Contents

3.1 Green's functions

The Green's function is a powerful tool of many-body physics which provides insight about the response of a system to a perturbation. From the strict mathematical definition, it follows that a Green's function (G) gives the response of a linear differential operator (L) to an impulse perturbation

$$LG(x, x', t, t') = \delta(x - x')\delta(t - t') \ . \tag{3.1}$$

This helps turn the differential non-homogeneous equitation $L\phi(x', t') = f(x', t')$ into the integral equation

$$\phi(x, t) = \phi^0(x, t) + \int dx'dt'G(x, x', t, t')f(x', t') \ , \tag{3.2}$$

where ϕ is a solution of the homogeneous equation. Another advantage is if the right side of the inhomogeneous differential equation depends on ϕ ($f(x) = V\phi(x)$) the resulting solution can be found in a self-consistent way. If the system is described by the Hamiltonian H_0 then the Green's function can be written using its eigenstates and eigenvectors

$$G(\boldsymbol{r}, \boldsymbol{r'}, \omega) = \sum_m \frac{\langle \boldsymbol{r}|\phi_m\rangle \langle \phi_m|\boldsymbol{r'}\rangle}{\epsilon_m - \omega \pm i\gamma} \, . \tag{3.3}$$

An infinitesimal γ is introduced to remove singularities at $\omega = \epsilon_m$; the plus and minus shifts the pole to the upper or lower half of the complex plane. In the time domain this corresponds to either causal (forward) or anti-causal (backward) propagation of the particle. The Green's function may be written in the time domain for forward or backward propagation as

$$G^{>}(\boldsymbol{r}, \boldsymbol{r}, t, t') = -i \langle 0| \psi(\boldsymbol{r}, t)\psi^+(\boldsymbol{r'}, t') |0\rangle$$

$$G^{<}(\boldsymbol{r}, \boldsymbol{r'}, t, t') = -i \langle 0| \psi^+(\boldsymbol{r}, t)\psi(\boldsymbol{r'}, t') |0\rangle \ . \tag{3.4}$$

The field creation (annihilation) operator $\psi^+(\psi)$ inserts a test particle (anti-particle) at space-time point $\boldsymbol{r'}, t'$ and removes it at another point r, t. In this sense the Green's function can be viewed as a correlation function or particle propagator. Both forms of Eq. 3.4 satisfy Eq. 3.1 [12], and this brings uncertainties in the definition of the Green's

function. One possible choice is the time-ordered Green's function, which involves both causal and anti-causal solutions. Using the time-ordering operator (see Appendix F) the Green's function reads

$$G(\boldsymbol{r},\boldsymbol{r},t,t') = -i\left\langle 0\right| T\psi(\boldsymbol{r},t)\psi^{+}(\boldsymbol{r'},t')\left|0\right\rangle \ , \tag{3.5}$$

although this choice is not unique [12] (here we will work by default with the time-ordered Green's function). The field operator can be expanded as a linear combination of momentum creation operators (under the assumption that we are working with fermions) as $\psi^{+}(\boldsymbol{r},t) = \frac{1}{\sqrt{N}}\sum_k c_k^{+}(t)e^{i\boldsymbol{k}\cdot\boldsymbol{r}}$. The spin index will be omitted for simplicity. The initial wave-function $\langle 0|$ is considered to be the many-body ground state of the system. Here and after we will stick to the zero-temperature case, neglecting initial population of phonons (n_{ph}^0). It is a reasonable choice for both high energy optical phonon modes in the low-temperature regime (e.g. high temperature superconducting cooper based materials $\omega_{ph} \sim 70-80\ meV;\ kT = 25-8\ meV;\ n_{ph}^0 \sim 10^{-2}-10^{-4}$ and for vibrational population in case of molecules even within at the room temperature ($\omega_{vib} \sim 200\ meV;\ kT = 25\ meV;\ n_{ph}^0 \sim 10^{-4}$). Further consideration of the finite-temperature effects can be performed using Matsubara frequency technique [12]. The Green's function can be related to the density of states using completeness of the basis states $H_0\left|n\right\rangle = \epsilon_n\left|n\right\rangle$ and inserting the identity $1 = \sum_n \left|n\right\rangle\left\langle n\right|$

$$G_m(t,t') = -i\sum_n \left\langle 0\right| Tc_m(t)\left|n\right\rangle\left\langle n\right| c_m^{+}(t')\left|0\right\rangle$$

$$= -i\sum_n |\left\langle n\right| c_m^{+}\left|0\right\rangle|e^{i\epsilon_m t}e^{-i\epsilon_n t'}\theta(t-t') - i\sum_n |\left\langle n\right| c_m\left|0\right\rangle|e^{-i\epsilon_m t}e^{-i\epsilon_n t'}\theta(t'-t)\ . \tag{3.6}$$

Fourier transforming gives

$$G_m(\omega) = \sum_n \frac{|\left\langle n\right| c_m^{+}\left|0\right\rangle|^2}{\epsilon_n - \epsilon_m - \omega + i\gamma} + \sum_n \frac{|\left\langle n\right| c_m\left|0\right\rangle|^2}{\epsilon_n - \epsilon_m - \omega - i\gamma}\ . \tag{3.7}$$

Using the relation $\lim_{\gamma\to 0}\frac{1}{x\pm i\gamma} = P\frac{1}{x} \pm \pi\delta(x)$, the imaginary part of the Green's function Eq. 3.7 gives the density of states (spectral function)

$$A_m(\omega) = -\frac{1}{\pi}\mathrm{Im}\ G_m(\omega)\ . \tag{3.8}$$

This makes the Green's function a convenient tool to study many electronic properties that relate to the density of states. By definition, the spectral function is non-negative and the first moment of the one particle spectral function is 1 ($\int d\omega A_m(\omega) = 1$).

So far we have only considered unperturbed systems. However, it is typically the case that the full Hamiltonian, H, of a system cannot be solved exactly. One then separates the Hamiltonian into a solvable part, H_0, and a (hopefully small) perturbation, V. The Green's function formalism allows access to the solution of the perturbed system. The Green's function will now deviate from the initial definition of Eq. 3.1 since the field operator is normally defined by the eigenstates of H_0 (ψ_α) while the total wave-functions $|\Psi\rangle$ are unknown and corresponds to H

$$iG_\alpha(t,t') = \langle\Psi(t)|\, Tc_\alpha(t)S(t,t')c_\alpha^+(t')\,|\Psi(t')\rangle \ . \tag{3.9}$$

In the interaction picture the time evolution of operators is driven by H_0 but the propagation of the wave-function is defined by the interaction potential and scatterring matrix $S(t',t)$ (see Appendix F). To find a relation between $|\Psi\rangle$ and the unperturbed wave-function $|0\rangle$ one of the possible assumptions is that the interaction potential is turned on very slowly, this means $|\Psi(t)\rangle = S(t,\infty)\,|0\rangle$. The analogous treatment can be applied to the bra state assuming that the potential vanishes in the limit of infinite time. This leads to the same final state apart of the phase factor $\frac{\langle 0|S(\infty,t)}{\langle 0|S(\infty,-\infty)|0\rangle}$ [12]. Eq. 3.16 then becomes

$$iG_\alpha(t,t') = \frac{\langle 0|\, Tc_\alpha(t)S(\infty,-\infty)c_\alpha^+(t')\,|0\rangle}{\langle 0|\, S(\infty,-\infty)\,|0\rangle} \ . \tag{3.10}$$

Using an expansion of the S-matrix one can rewrite Eq. 3.10. The expansion leads to a series of correlation functions which due to the Wick's theorem can be related to a set of integrals constructed using single particle Green's functions and interaction vertices. Those integrals can be expressed as Feynman diagrams. The denominator in Eq. 3.10 cancels all disconnected diagrams in the numerator and will be omitted. Contributions from all connected terms is indicated with a subscript $\langle|\,|\rangle_c$. This leads to the expansion of the Green's function

$$iG_\alpha(t,t') = \sum_n \frac{(-i)^n}{n!}\int ..\int dt_1..dt_n\,\langle 0|\, Tc_\alpha(t)V(t_1)V(t_n)c_\alpha^+(t')\,|0\rangle_c \ . \tag{3.11}$$

The challenge will be how to evaluate Eq. 3.11 in practice.

3.2 Dyson's expansion

Feynman diagrams can be used to visualize the terms in the expansion of Eq. 3.11 after applying Wick's theorem. The latter states that the expectation values of time-ordered operators can be expressed in terms of all different combinations of time-ordered pairs $\langle TABCD\rangle = \langle TAB\rangle \langle TCD\rangle + \langle TAC\rangle \langle TBD\rangle + \langle TBC\rangle \langle TDA\rangle$, though one has to be careful with sign changes coming from odd permutations of fermion operators. Since the main focus of this work is the electron-phonon interaction, the perturbation term that we consider is the electron-phonon interaction

$$V(t) = \sum_{\alpha,\alpha',\nu} M^{\nu}_{\alpha\alpha'} c^{+}_{\alpha'}(t) c_{\alpha}(t) B_{\nu}(t) \ . \tag{3.12}$$

The series expansion of the electron Green's function is

$$G_{\alpha}(t,t') = \sum_{n} W_n(t,t')$$

$$= G^0_{\alpha}(t,t') + i \sum_{\alpha,\nu} \int\int dt_1 dt_2 M^{\nu}_{\alpha\alpha'} M^{\nu}_{\alpha\alpha'} G^0_{\alpha}(t,t_1) G^0_{\alpha'}(t_1,t_2) D_{\nu}(t_1,t_2) G^0_{\alpha'}(t,t_1) + .. \tag{3.13}$$

The odd terms in the interacting potential vanish because of the parity of the phonon operator in Eq. 3.12. The momentum conservation for the second term implies $q_{\nu} = k_{\alpha} - k_{\alpha'}$, where q_{ν} is a phonon wave-vector and $k_{\alpha} - k_{\alpha'}$ is a difference between momenta of the initial and scattered electron. The Fourier transform of this series gives

$$G_{\alpha}(\omega) = G^0_{\alpha}(\omega) + G^0_{\alpha}(\omega)\Sigma_0(\omega)G^0_{\alpha}(\omega) + G^0_{\alpha}(\omega)(\Sigma^0_{\alpha})^2(\omega)G^0_{\alpha}(\omega) + G^0_{\alpha}(\omega)\Sigma^1_{\alpha}(\omega)G^0_{\alpha}(\omega) .. \ , \tag{3.14}$$

where $\Sigma_0(\omega) = \sum_{\alpha,\nu} |M^{\nu}_{\alpha\alpha'}|^2 \int d\omega G^0_{\alpha'}(\omega) D_{\nu}(\omega - \omega')$ is the kernel of the expansion. One can notice that the third term involves replicas of the the second order term (as well as other contribution with crossings of the phonon lines $\Sigma^1_{\alpha}(\omega)$, see Fig. 3.1$d, e$) and so

on. This series may be expressed succinctly as the Dyson equation

$$G_\alpha(\omega) = \frac{G^0_\alpha(\omega)}{1 + G^0_\alpha(\omega)\Sigma_(\omega)} \ . \tag{3.15}$$

If one calculates the self-energy including higher orders irreducible diagrams, the resulting Green's function will converge to the exact one

$$\Sigma_\alpha(\omega) = \sum_j \Sigma^{(j)}_\alpha(\omega) \ , \tag{3.16}$$

here j run over all irreducible diagrams. Dyson's equation is very powerful because instead of calculating each term in the series of Eq. 3.13 individually, one can just calculate a single (or small number) self-energy diagram, which will then be included to infinite order. Dyson's equation can also be found using the equation of motion and variation of the functional derivatives [68]. For the case of screened electron-electron interactions, the self-energy can be expressed with Hedin's set of self-consistent equations [69]. However, due to numerical difficulties, it is common to use a lowest order term in the self-energy together with Dyson's equation, which formally can be denoted as G^0W^0 in contrast to GW.

Self-energy Regarding the electron-phonon problem there are two types of the lowest order terms in the self-energy. The first, so called Fan-Migdal term, [11, 12], originates from the linear electron-phonon interaction in Eq. 1.2 and has a visual analogy to G^0W^0 (see Fig. 3.1)

$$\Sigma^{FM}_\alpha(t,t') = -i\sum_{\nu,\alpha_1} M^\nu_{\alpha\alpha_1} G^0_{\alpha_1}(t,t') D_\nu(t,t') \ . \tag{3.17}$$

This term is represented by the electron-phonon bubble diagram, and describes the scattering of an electron due to interaction with a phonon of momentum and wave-vector $\nu = \{q_\nu, \lambda_\nu\}$ to the state α_1 and back. The second is the Debye-Waller term (see Fig. 3.1). It is proportional to the second order electron-phonon interaction (last term in Eq. 1.2) and reads

$$\Sigma^{DW}_\alpha(t,t') = \sum_{\nu,\alpha} (M^{(2)})^\nu_{\alpha\alpha}(2N_\nu + 1) \ . \tag{3.18}$$

Here N_ν is the number of phonons in the initial state, which in thermal equilibrium is defined by the temperature of the system. In the limit of zero-temperature, however, it gives a constant shift to the energy of the quasi-particle.

Spectral function Using Eqs. 3.15 and 3.8 one can write the spectral function of the one particle Greeen's function. The spectral function ($A(\omega) = \frac{1}{\pi}|\mathrm{Im}G_\alpha(\omega)|$) from Dyson's equation is

$$A^D(\omega) = \frac{1}{\pi}\frac{|\mathrm{Im}\ \Sigma_\alpha(\omega)|}{|\omega - \epsilon_\alpha - \mathrm{Re}\ \Sigma_\alpha(\omega)|^2 + |\mathrm{Im}\ \Sigma_\alpha(\omega)|^2}\,. \tag{3.19}$$

Here the self-energy is $\Sigma_\alpha = \Sigma_\alpha^{FM} + \Sigma_\alpha^{DW}$. The quasi-particle peak is shifted by the electron-phonon interaction. The shift is primarily given by Re $\Sigma_\alpha(\omega)$, however if the contribution from Im $\Sigma_\alpha(\omega)$ at $\omega = \epsilon_\alpha + $Re $\Sigma_\alpha(\omega)$ is non-negligible it also contributes to the final shift of the quasi-particle peak. Eq. 3.19 gives rise to one satellite. The weight which was transferred from the quasi-particle peak to the satellite due to the electron-phonon interaction can be found by expanding the self-energy around the position of the quasiparticle peak (E_α^{qp}). The renormalization of the quasipraticle weight is [69, 70]

$$Z_\alpha^{qp} = \left(1 - \mathrm{Re}\ \frac{\partial\Sigma_\alpha(\omega)}{\partial\omega}\bigg|_{\omega=\mathrm{E}_\alpha^{\mathrm{qp}}}\right)^{-1}\,. \tag{3.20}$$

Despite the fact that Dyson's equation accounts for an infinite number of replicas of the FM and DW self-energy terms, the spectral function defined by Eq. 3.19 is not fully satisfactory and poorly reproduces the experimental spectral function [70, 71].

3.3 Cumulant expansion

The cumulant ansatz to the interacting Green's function originates in the linked-cluster expansion [73] and provides an exact solution with only the lowest order self-energy for the case of an isolated, deep core-hole [74, 75]. This is similar to the observation that the Holstein-type vibronic Hamiltonian can be solved exactly by a canonical transformation when electronic recoil is neglected. The cumulant expansion is no longer exact when recoil becomes important, such as for valence level electrons and holes, nevertheless, its

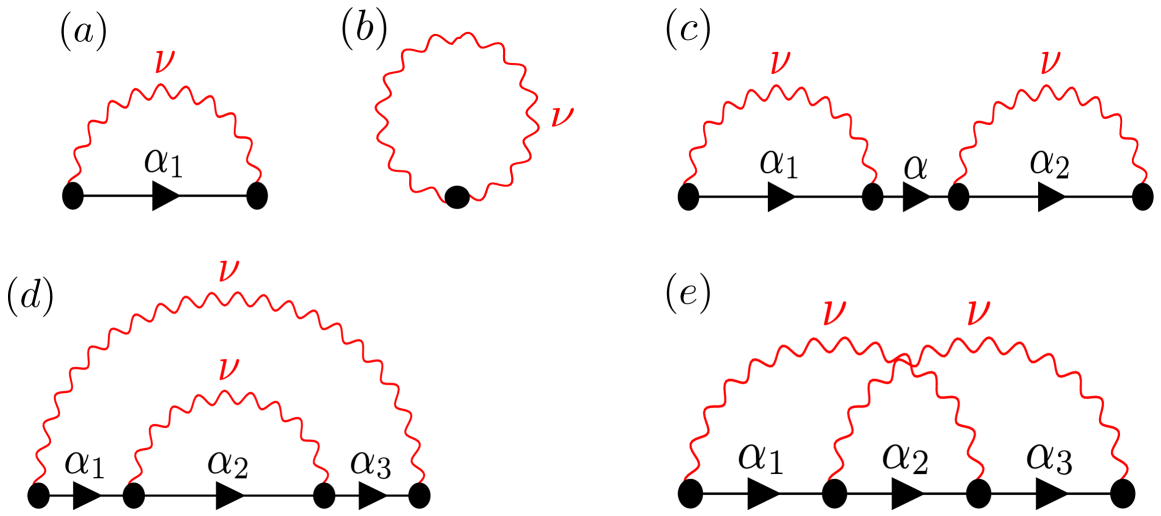

Figure 3.1: Few lowest order diagrams representing electron-phonon interactions. Diagrammatic form of the Fan-Migdal (a) and Debye-Waller (b) terms of electron-phonon self-energy. (c) Replica of the FM term which appears in both Dyson's and cumulant expansions in the fourth order. The fourth order terms which includes self-consistent inclusion (d) and vertex correction (e), which are neglected in the Dyson+FM expansion and approximately treated within the cumulant+FM expansion [70, 72]

recent use in such cases has been promising [70, 76–79].

The moments expansion of the Green's function in orders of the interactions (see Eq. 3.1) can be written as

$$G(t,t') = \sum_n W_n(t,t') \ . \tag{3.21}$$

The general idea is to find the functions $C_m(t,t')$ in terms of $W_n(t)$. Here m and n correspond to the orders in the interaction potential. The existence of such a solution is guaranted by a one to one correspondence between the statistical distributions defined by moments and cumulants [12]. By expanding the exponential function in Eq. 3.22 we have

$$G(t,t') = G^0(t,t') exp(\sum_m C_m(t,t')) \ . \tag{3.22}$$

The general idea is to find the functions $C_m(t,t')$ in terms of $W_n(t)$. By expanding the exponential function in Eq. 3.22 we have

$$exp(\sum_m C_m(t)) = \sum_n \frac{1}{n!}(\sum_m C_m(t)) = 1 + C_1 + C_2(t) + ... + \frac{C_1^2}{2!}(t) + .. \ . \tag{3.23}$$

Equating terms of the same order in Eqs. 3.21 and 3.22, the cumulants for any order can be find from

$$\begin{aligned} W_1(t) &= C_1(t)G^0(t) \\ W_2(t) &= (C_2(t) + \frac{C_1^2(t)}{2!})G^0(t) \\ W_3(t) &= (C_3(t) + \frac{C_1^3(t)}{3!} + C_2(t)C_1(t))G^0(t) \\ &... \end{aligned} \tag{3.24}$$

In practice, often only the lowest order cumulant is evaluated ($C \approx C_1$), but even such truncation of the cumulant series accounts for infinite numbers of diagrams due to the exponential form.

To be more specific we will focus on the electron-phonon interacting terms Eq. 3.12. Due to the parity of the phonon operator the odd terms in the interaction potential vanish in the expansion Eq. 3.1 (i.e. $W_1 = 0$ and $C_1 = 0$) and the lowest non-zero term has the second order in the electron-phonon interaction (the notation for electronic

states α is omitted for simplicity)

$$W_2(t,t') = (-i)^2 \int\int dt_1 dt_2 \sum_\nu |M_\nu|^2 G^0(t,t_1) G^0(t_1,t_2) D_\nu(t_1,t_2) G^0(t_2,t') \qquad (3.25)$$

and the resulting lowest order cumulant is (form Eq. 3.24 $C_2 = W_2/G^0$)

$$C_2(t,t') = -[G^0(t,t')]^{-1} \int\int dt_1 dt_2 \sum_\nu |M_\nu|^2 G^0(t,t_1) G^0(t_1,t_2) D_\nu(t_1,t_2) G^0(t_2,t') \ . \qquad (3.26)$$

Using notation for the lowest order Dyson's self-energy (Eq. 3.17) the second order cumulant reads

$$C_2(t,t') = -[G^0(t,t')]^{-1} \int\int dt_1 dt_2 G^0(t,t_1) \Sigma(t_1,t_2)(t_1,t_2) G^0(t_2,t') \ . \qquad (3.27)$$

Combing Eqs. 3.24 and 3.27 the interacting Green's function using the second order cumulant becomes

$$G(t,t') = G^0(t,t') e^{C_2(t,t')} \, . \qquad (3.28)$$

To highlight the difference between expansions 3.15 and 3.29 one sees that the lowest order self-energy leads to the inclusion of quite different types of diagrams. Rewriting the exponent as a series in C^2 we can keep track of the terms which are treated by the second order cumulant

$$\begin{aligned} G(t,t') &= G^0(t,t') \\ &+ \int\int dt_1 dt_2 G^0(t,t_2) \Sigma(t_1,t_2) G^0(t_2,t') \\ &+ \frac{1}{2!}[G^0(t,t')]^{-1} [\int\int dt_1 dt_2 G^0(t,t_2) \Sigma(t_2,t_3) G^0(t_2,t')]^2 \\ &+ \ldots \end{aligned} \qquad (3.29)$$

The first two terms are the same as in Dyson's series, but already the third term is new. The resulting interacting Green's function includes all replica of the FM term, and partially includes self-consistency and vertex correction terms (see Fig. 3.1 d, e). Further, one can rewrite the time integrals in Eq. 3.27 using the energy representation

of the Green's function

$$C(t,t') = -[G^0(t,t')]^{-1} \int d\omega [G^0(\omega)]^2 \Sigma(\omega) e^{-i\omega(t-t')} \,. \tag{3.30}$$

Using the explicit definition of non-interacting Green's function and the spectral representation of the self-energy, the second order cumulant becomes [70, 78]

$$C_\alpha(t,t') = \frac{1}{\pi} \int d\omega \frac{|\mathrm{Im}\ \Sigma_\alpha(\omega+\epsilon_\alpha)|(\mathrm{e}^{-\mathrm{i}\omega(\mathrm{t}-\mathrm{t}')} + \mathrm{i}\omega(\mathrm{t}-\mathrm{t}') - 1)}{\omega^2} \,. \tag{3.31}$$

The factor $(e^{-i\omega t} + i\omega t - 1)$ defines the structure of the spectral function in the cumulant representation. The exponential term gives rise to multiple satellites, while the term linear in t leads to the quasiparticle shift and the -1 generates the quasiparticle weight. In the case of the time-ordered Green's function, the limits of integration in Eq. 3.32 are taken over all occupied states for holes and all unoccupied state for particles. In an alternative formulation using the retarded formulation of Green's function both solutions are mixed, which leads to particle-hole recoil effects [78]. For the case of core-level spectroscopy, this effect likely contributes less to the resulting spectral function, and we will use the time ordered formulation. The DW appears due to the lowest order quadratic electron-phonon coupling, and by analogy to the FM term can be treated within the cumulant expansion. However, the DW term contributes only to the shift of the quasiparticle. The interacting particle Green's function can be written as

$$G(t,t') = -ie^{-i(\epsilon_\alpha + \Sigma_\alpha^{DW})(t-t')} e^{C_\alpha(t,t')} \tag{3.32}$$

where the cumulant C_α is defined by the FM term. Unlike in Dyson's equation, the weight of the quasiparticle line is defined by the exponential factor

$$Z = exp\left(\mathrm{Re}\ \frac{\partial \Sigma_\alpha^{\mathrm{FM}}(\omega)}{\partial \omega}\bigg|_{\omega=\epsilon_\alpha}\right) . \tag{3.33}$$

The spectral function can be found as

$$A^C(\omega) = -\frac{1}{\pi}\mathrm{Im} \int \mathrm{dte}^{-\mathrm{i}\omega\mathrm{t}}\mathrm{G(t)} \,. \tag{3.34}$$

The expansion of the Greens function in terms of cumulants appears to be quite

a powerful tool for some types of interactions. From a statistical point of view, the exponential generating function relates to random processes. Thus, presumably such an ansatz for the solution will work well in cases where the interacting events are weakly correlated.

First-principles work with the cumulant expansion has mainly been employed to describe plasmon satellites in conjunction with Hedin's GW self-energy (G is the single particle Green's function and W the screened Coulomb interaction). This has proven to be quite successful at reproducing the valence-level photoemission spectrum of silicon [76, 80–84] and has even reasonably reproduced the low energy plasmon satellites in $SrVO_3$ [85, 86] and charge transfer effects in the XPS [87] and XAS [88] spectra of NiO, suggesting the applicability of the GW-cumulant approach may extend to moderately correlated materials. Only very recently has the cumulant expansion been applied to the vibronic coupling problem [35, 70, 71, 89]. Here, one exchanges the plasmonic GW self-energy for the Fan-Migdal vibronic self-energy GD (D is the phonon propagator). These studies focused on valence level photoemission.

Dyson *vs* Cumulant The spectral functions for the Green's functions constructed from Dyson's equation and the cumulant expansion, for the same level of approximation (non self-consistent Fan-Migdal) are shown in Fig. 3.2. The simple model of one non-dispersive electronic band, one non-dispersive phonon mode with linear electron-phonon coupling was considered. Such strong disagreement comes from the fact that an exponential series tends to treat not only the replicas of self-energy diagrams, as is the case when using Dyson's expansion, but also approximately [72] includes diagrams with vertex corrections and self-consistent parts. Thus, the cumulant expansion produces superior spectral functions even without computationally expensive self-consistent calculations.

This observation is in agreemnet with recent works on the electron-phonon coupling for valence spectroscopy [70] and studies of the core-hole-plasmon interactions [77, 84, 85]. From the results of the model study, one can see that the electron-phonon interaction tends to break the quasi-particle picture. Moreover, it tends to redistribute spectral weight between quasi-particle peak and multiple satellites and attributes an energy shift [12, 71, 78]. We find that combining the cumulant expansion with FM self-energy leads to a more accurate spectral function [35, 70] in analogy to results based on

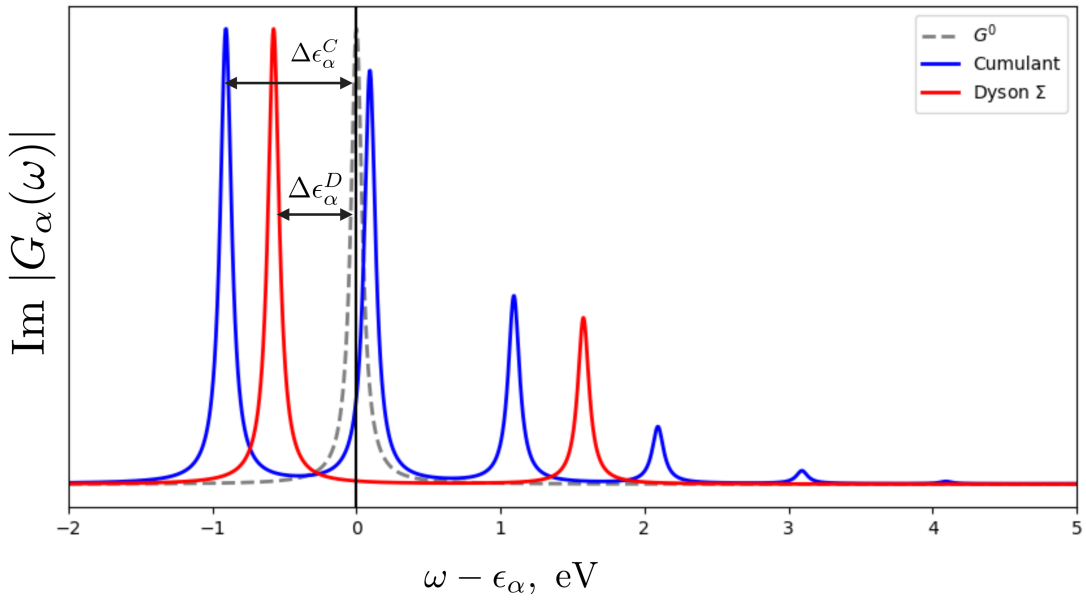

Figure 3.2: Comparison between model core-hole spectral functions obtained using cumulant (blue) and Dyson (red) expansions and FM type self-energy. The cumulant ansatz gives an exact solution in this limit (see text) and can be seen as a reference [75]. The coupling strength was chosen in the intermediate regime $g \sim 1$. The grey line corresponds to the quasi-particle spectral function without electron-phonon interaction. A small broadening is added to model the lifetime effects. Apart from the incorrect shifts of the quasi-particle energy, the spectral function of the Dyson expansion also fails to reproduce the satellite structure, and produces only one misplaced phonon peak instead of several equally spaced phonon satellites.

the mixture of the *GW* self-energy and cumulant expansion for plasmons [77, 79, 80, 82].

3.4 Bethe-Salpeter equation

Apart from the electron-phonon interactions, we treat the electron-hole interaction on the level of the Bethe-Salpeter approach. In this section, we will follow [68] considering variation of the correlation function with respect to the external potential in the spirit of linear response. This approach is analogues to the standard diagrammatic techniques, which we used in the previous sections.

One particle properties obtained within the regular KS DFT approach often have to be corrected by including many-body effects. For example, to predict optical /

electronic properties of insulators, one has to deal with one electron removal / addition events. For example, the ability to accurately predict electronic band gaps is of general interest.

DFT does not guarantee the excited state configuration to be realistic, and not surprisingly tends to underestimate the band gap [84]. Improvements involve many-body corrections beyond the mean-field DFT level. These corrections can be accounted for with Dyson's equation, considering the KS DFT states as an unperturbed solution. Instead of working with bare electron-electron interactions one can write the expansion of the Green's function in terms of the screened Coulomb interaction W, which makes the series converge faster. Following [69], the set of self-consist equations for calculating the self-energy and appropriate vertex are $(1 = t_1, \mathrm{r}_1)$

$$\begin{aligned}
\Sigma(1,2) &= iG(1,\bar{3})W(1,\bar{4})\Gamma(\bar{3},\bar{4},2) && (3.35)\\
W(1,2) &= v(1,2) + v(1,\bar{3})P(\bar{3},\bar{4})W(\bar{4},2) && (3.36)\\
P(1,2) &= -iG(1,\bar{3})\Gamma(\bar{3},\bar{4},2)G(2^+,\bar{4}) && (3.37)\\
\Gamma(1,2,3) &= \delta(1,2)\delta(2,3) + \frac{\delta\Sigma(1,2)}{\delta G(\bar{4},\bar{5})}G(\bar{4},\bar{6})G(\bar{7},\bar{5})\Gamma(\bar{6},\bar{7},3)\ . && (3.38)
\end{aligned}$$

Here $G(1,2)$ is defined by Dyson's equation, which is also a part of the self-consistent scheme. Due to computational expenses, the vertex function Γ is often set to 1 in all equations and the resulting set of equation defines the GW approximation. In the lowest approximation, we can obtain the self-energy as just G^0W^0, where W^0 is the screened Coulomb potential with the polarization $P = iGG$ calculated in the random phase approximation (RPA).

While we have defined the self-energy correction for the one particle problem, we now look at the two particle problem. The two particle correlation function is formally defined by a functional derivative of the one-particle Green's function with respect to a non-local perturbation

$$L(1,2,3,4) = \left.\frac{\delta G(1,3)}{\delta U_{ext}(2,4)}\right|_{U_{ext}=0}\ , \qquad (3.39)$$

and the functional derivative in Eq. 3.41 is

$$\frac{\delta G(1,2)}{\delta V_{ext}(3,4)} = G(1,\bar{5})\frac{\delta G^{-1}(\bar{5},\bar{6})}{\delta U_{ext}(3,4)}G(\bar{6},2) \ . \tag{3.40}$$

Expressing $G^{-1}(5,6)$ from Dyson's equation for the two-particle correlation function we have

$$L(1,2,3,4) = G(1,3)G(2,4) + G(1,\bar{5})\frac{\delta\Sigma(\bar{5},\bar{6})}{\delta G(\bar{7},\bar{8})}\frac{\delta G(\bar{7},\bar{8})}{\delta U_{ext}(3,4)}G(\bar{6},2) \ . \tag{3.41}$$

Finally the Bethe-Salpeter Equation reads

$$L(1,2,1',2') = L^0(1,2,1',2') + L^0(1,2,3,3')\Xi(\bar{3},\bar{3'},\bar{4},\bar{4'})L(\bar{4},\bar{4'},2,2') \ , \tag{3.42}$$

where L_0 is an uncorrelated part and the four point vertex function is derived from the chain rule [68] as $\Xi = \frac{\delta\Sigma}{\delta G}$. Here, we explicitly use the Hartree and screened Coulomb term in the GW approximation for the self-energy and this gives for the vertex function [61]

$$i\Xi(1,2,3,4) = \delta(1,3)\delta(2,4)v_c(1,2) - \delta(1,2)\delta(3,4)W(1,3) + G(1,3)\frac{\delta W(1,3)}{\delta G(4,2)} \ . \tag{3.43}$$

The approximation which implies that the response to the external potential is static

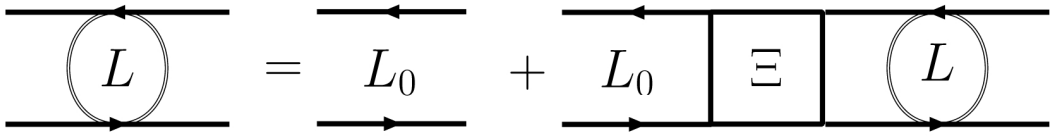

Figure 3.3: Bethe-Salpeter equation in diagrammatic form. The four point vertex function is defined as a functional derivative of the one-particle self-energy $\frac{\delta\Sigma(1,2)}{\delta(G(1,2))}$.

(there is no dependence on the energy of excitations), comes from neglecting the functional derivative of the screened potential $\frac{\delta W(1,2)}{G(3,4)} \approx 0$. This approximation completely misses the dynamical response such as the plasmonic contribution, but in general it still captures a lot of physics and shows good agreement for XAS [62, 90].

The lowest approximation for the self-energy G^0W^0 neglects higher order contributions, e.g., diagrams with crossed lines and with electron-electron vertex corrections. It leads to the so-called ladder approximation where the electron-hole interaction events occur one after another without entanglements. The validity of such approximation was discussed in the original paper of Salpeter and Bethe [91] for the small coupling limit.

By definition, the Green's function operator is a resolvent of the linear differential equation

$$\hat{L}(\omega) = \frac{1}{H_{BSE} - z} \ , \tag{3.44}$$

where z is an imaginary frequency and H_{BSE} is an effective two-particle Hamiltonian. The important comment on such a representation of the BSE is that the effective Hamiltonian is not fully hermitian [92], due to the possible mixing of causal and anti-causal excitons (coupled particles). The approximation we use neglects such effects and is known as the Tamm-Dancoff approximation (TDA) [93, 94] (where only forward propagation of an exciton was considered) and it works reasonably well for bulk materials [95]. We start by writing H_{BSE} in the independent particle-hole basis

$$H_{BSE} = h_e - h_h + \Xi \ , \tag{3.45}$$

where the single particle parts might be dressed $h_e = H_{KS} - h_{xc} + \Sigma_{GW}$. The core-hole also normally includes local spin-orbit terms χ and life-time effects $H_h = E_\alpha + \chi + \Sigma_\alpha$. The electron-hole interaction includes two terms $\Xi = -V_D + V_x$. The first is the screened direct attractive Coulomb term

$$V_D = \int\int d\boldsymbol{r}' d\boldsymbol{r} c_\alpha(\boldsymbol{r}') c_k^+(\boldsymbol{r}) W(\boldsymbol{r}, \boldsymbol{r}', \omega = 0) c_k(\boldsymbol{r}) c_\alpha^+(\boldsymbol{r}') \ , \tag{3.46}$$

the second is the repulsive exchange term

$$V_X = \int\int d\boldsymbol{r} d\boldsymbol{r}' c_\alpha(\boldsymbol{r}') c_k^+(\boldsymbol{r}) \frac{1}{|\boldsymbol{r} - \boldsymbol{r}'|} c_k(\boldsymbol{r}') c_\alpha^+(\boldsymbol{r}) \ . \tag{3.47}$$

In the equations above the spin index was omitted, but one has to keep in mind that the exchange term acts on the spin states of the particle too. The static response calculations mean that there is no energy dependence in the screened interaction $W(\omega = 0)$. The transition energies differ from the difference between quasi-particle levels due

to these Coulomb interactions. This captures electron-hole interactions which occur during the XAS process. Apart from this, to obtain the absorption coefficient one has to calculate a transition matrix elements $d_{\alpha,k}$ [90].

Chapter 4

XPS: Charged excitations

Due to doubts in the RIXS community about the role that the core-hole plays in generating the phonon contribution to RIXS spectra [2, 4, 5, 96], we first focused on the problem of the core-hole phonon coupling. This section is dedicated to the calculation of X-ray photo-emission spectra including phonon sidebands. This effect is mainly intrinsic and thus reflects coupling of the deep core-hole to lattice degrees of freedom. We apply a Green's function formalism and develop a numerical approach for parameter-free calculations of the phonon contribution to the spectra. To demonstrate our approach, we preform calculations on SiX_4 ($X = F, H$) molecules.

Contents

4.1 Photo-current

X-ray photoemission spectrocopy (XPS) is a well-established technique to measure electronic binding energies [97, 98]. An incoming X-ray photon knocks out a core-electron, and the quantity which is measured is the photo-current. By scanning the emitted energy one can access different states within the system, e.g., the spin-orbit split $2p_{1/2}$ and $2p_{3/2}$ levels.

The photo-current is proportional to the rate of the bound-state–continuum transitions per atom. The first order of the electron-photon interaction gives this rate according to Fermi's golden rule as [48]

$$J(\omega) \approx \sum_F |\langle\psi_F|\,\Delta\,|\psi_I\rangle|^2 \delta(\omega - E_{FI}) \ . \tag{4.1}$$

Here the capital letters F, I correspond to many-body initial and final states, and the photon energy ω and photon operator Δ describes the linear electron-photon interactions . We will consider the latter in the generic form of the second quantization formalism

$$\Delta = \sum_{k,\alpha} d_{k,\alpha} c_k^+ c_\alpha + h.c. \ . \tag{4.2}$$

Here the matrix elements $d_{k,\alpha}$ are the projection of the core state α wave-function after the interaction with the photon onto the continuum state wave-function of the photo-electron with momentum k. The actual form of the photon operator is presented in Eq. 2.1 and in the lowest order is proportional to $\boldsymbol{A} \cdot \boldsymbol{p}_i$. The electron-photon matrix elements are roughly independent of k ($d_{\alpha,k} \approx d_\alpha$) assuming that $k \gg k_F$.

In the independent particle picture the many-body wavefunction can be written as a single Slatter determinant, and the difference between the initial and final energy is just the binding energy of the core-electron. The transition rate is nominally proportional to the density of occupied states.

$$J_k^0(\omega) \approx \sum_\alpha^{occ} |d_\alpha|^2 \delta(\omega - \epsilon_\alpha - \epsilon_k) \ . \tag{4.3}$$

This simple picture is insufficient to reproduce the real experimental spectra, which

might contain multiple satellites around the binding energy of the photo-electron [39, 78, 99]. These additional satellite features can be explained in the context of many-body theory and are related to the interaction of the core-hole with the electronic (plasmonic effects) [75] and atomic (phonons) [100, 101] structures. This leads to changes in the effective energy of the core-hole. These satellites can provide information about the strength of coupling between the electronic and lattice degrees of freedom, which is of particular interest for us.

In principle, the XPS signal includes intrinsic (related to the core-hole) and extrinsic (photo-electron) contributions as well as interactions that lead to interference effects [88]. Taking into account that the high energy photo-electron interacts less with the system than the bound hole, we can neglect extrinsic contributions in this problem [75]. The final state many-body wave-function can be then written as a product of $|k\rangle$ photo-electron wave-function and many-body wave-function of the system with a core-hole $|\psi_f\rangle$ ($|\Psi_F\rangle = |\psi_f\rangle\,|k\rangle$) and the same for initial state $|\Psi_I\rangle = |\psi_i\rangle\,|0\rangle$. Expanding the square in Eq. 4.3 we obtain

$$J_k(\omega) \approx \sum_f |\,\langle k|\, c_k^+\,|0\rangle\,|^2 \sum_\alpha |d_\alpha|^2\,\langle\psi_i|\, c_\alpha^+\,|\psi_f\rangle\,\langle\psi_f|\, c_\alpha\,|\psi_i\rangle\,\delta(\omega - \epsilon_{fi} - \epsilon_k)\ . \tag{4.4}$$

Here the $\epsilon_{fi} = \epsilon_f - \epsilon_i$ is the energy difference between the systems with and without a core-hole. This leads to the formulation of the photo-current in terms of spectral functions ($|\,\langle k|\, c_k^+\,|0\rangle\,|^2 = 1$)

$$J_k(\omega) \approx -\sum_\alpha |d_\alpha|^2 A_\alpha(\omega - \epsilon_k)\ , \tag{4.5}$$

where the spectral function accounts for the density of the core-hole in the presence of many-body interactions. The spectral function is obtained from the core-hole Green's function as

$$A_\alpha(\omega) = -\frac{1}{\pi}\mathrm{Im}\ G_\alpha(\omega)\ . \tag{4.6}$$

The independent particle picture can be viewed as a lowest-order approximation. In this case the spectral function is a delta function, centered around the core-hole binding energy $\mathrm{Im}\ G_\alpha^0(\omega) \sim \delta(\omega - \epsilon_\alpha)$. Moreover, the many-body interactions can be

accounted for using Green's functions techniques. One can start with a quasi-particle picture $G_\alpha^{qp}(\omega)$ and include electron-phonon interactions as a correction to the 'static' (fixed nuclei) quasi-particle spectral function [87, 102]

$$J(\omega) = \sum_\alpha \int d\omega' J_\alpha^0(\omega - \omega') A_\alpha(\omega') \ . \tag{4.7}$$

The pure electronic XPS spectra (J^0) are obtained in the presence of the core-hole-electron interactions, which lead to the quasi-particle corrections (screening of the core-hole and life-time effects). The core-hole spectral function ($A(\omega)$) then dresses the core-hole propagator with the electron-phonon interactions.

The interaction of the core-hole with surrounding atoms (ions) can be accounted for with the Green's function techniques. Taking into account the different time and, consequently, energy scales of the electron-electron ($\sim fs$) and electron-phonon ($\sim ns$) interactions, one can treat them separately. Thus, we assume the core-hole is instantaneously screened by the valence electron density.

Recent studies of the plasmonic contribution to valence and core-level photoemission spectra show the advantage of the cumulant ansatz for the electronic Green's function [77, 78, 84]. The extension of this approach to the electron-phonon interaction problem also seems to be promising for the valence photoemission spectra of both metals [71] and insulators [70]. In the same spirit, we combine the cumulant expansion of the Green's function with an *ab-initio* based method to treat the phonon contribution to XPS.

4.2 Core-hole Green's function

The problem of the hole interacting with phonons is governed by the Fröhlich type Hamiltonian [11] (see also Chapter 1)

$$H = h_{ch}^0 + h_{vib}^0 + \sum_{\lambda,\boldsymbol{q},\alpha} M_\alpha^{\lambda,\boldsymbol{q}} c_\alpha^+ c_\alpha (b_{\lambda,\boldsymbol{q}} + b_{\lambda,-\boldsymbol{q}}^+) \ . \tag{4.8}$$

Here $h^0_{ch} = \sum_\alpha \epsilon_\alpha c^+_\alpha c_\alpha$ and ϵ_α is the energy of the core-hole level, which was found in the absence of the electron-phonon interaction. The core-hole state could be found, e.g. by a Hartree-Fock or density functional calculation. The free phonon part is assumed to be harmonic with arbitrary q dispersion, and c^+_α, c_α are the hole creation and annihilation operators, respectively. $M^{\lambda,\boldsymbol{q}}_\alpha$ is the core-hole phonon coupling and λ represents phonon mode.

The typical electron-phonon self-energy in the second order (lowest non-zero term) contains the Fan-Migdal and the Debye-Waller [11] terms. The last one involves non-linear electron-phonon coupling and is responsible only for the shift of the quasi-particle energy. The structure of the spectral function however is controlled by the energy-dependent Fan-Migdal terms [12]. It has a visual analogy to the electronic G_0W_0 approximation (neglecting vertex corrections $\Gamma = 1$)

$$\Sigma^{FM}_\alpha = \sum_{\alpha,\lambda,\boldsymbol{q}} |M^{\lambda,\boldsymbol{q}}_\alpha|^2 \int d\omega' G^0_\alpha(\omega) D^0_{\lambda,\boldsymbol{q}}(\omega - \omega') \ . \tag{4.9}$$

The objective is to calculate the core-hole Green's function dressed by the electron-phonon interactions. Recalling the cumulant ansatz which was introduced in the previous chapter we have

$$G_\alpha(t) = G^0_\alpha(t) e^{C_\alpha(t)} \ , \tag{4.10}$$

where the core-hole Green's function in the absence of the electron-phonon interaction is $G^0_\alpha(t) = -i\theta(t)e^{i\epsilon_\alpha t}$, and the quasi-particle energy without electron-phonon interaction is assumed to be known. Therefore we will focus on the influence of the electron-phonon interaction. We employed a modified second-order cumulant from Eq. 3.27 using the bosonic excitations spectrum ($\beta_\alpha(\omega)$)

$$C_\alpha(t) = \int d\omega \frac{\beta_\alpha(\omega)(e^{-i\omega t} + i\omega t - 1)}{\omega^2} \ . \tag{4.11}$$

The intensity with which the perturbation generates bosons of energy ω is given by $\beta_\alpha(\omega)$. It takes into account the response of the system to the perturbation caused by a core-excitation, and it is related to the imaginary part of the self-energy as

$$\beta(\omega) = |\text{Im } \Sigma(\omega + \epsilon_\alpha)| \ . \tag{4.12}$$

The energy shift as well as renormalization factor of the quasi-particle peak can be expressed in terms of the excitation spectrum as [70, 78]

$$\Delta E_\alpha = \int d\omega \frac{\beta_\alpha(\omega)}{\omega} \quad \text{and} \quad Z_\alpha = \exp\left[\int d\omega \frac{\beta_\alpha(\omega)}{\omega^2}\right] . \tag{4.13}$$

Thus, to find the interacting core-hole Green's function one has to calculate the bosonic excitation spectrum or the self-energy itself, which consists of the response function, in our case a phonon Green's function and the core-hole phonon couplings. The excitation spectrum can be constructed in the time domain from the phonon response function and the core-hole – phonon coupling constants

$$\beta_\alpha(t) = \sum_{\boldsymbol{q}\lambda} |M_\alpha^{\boldsymbol{q}\lambda}|^2 D(t-t') . \tag{4.14}$$

4.3 Core-hole phonon interaction

To go beyond the Born-Oppenheimer approximation the interaction of the electronic and ionic subsystems should be treated explicitly. We will start our discussion considering a single core-hole with quasi-particle energy calculated in the presence of other electrons, however neglecting any vibrational contribution. We assume the vibrational part of the Hamiltonian to be harmonic with a frequency calculated, e.g. from density functional perturbation theory (DFPT). The interaction is driven by the total effective potential at the core-hole site. Within a real-space representation the potential is

$$V_{eff} = \int \psi_\alpha^+(r)\psi_\alpha(r)V_{eff}(r)dr = \int \rho_\alpha(r)V_{eff}(r)dr , \tag{4.15}$$

where $\rho_\alpha(r)$ is the density operator for the localized core-hole, which can reasonably be modelled as a delta function on the core-hole site (r_α). The effective potential differs from a bare electron-nuclear term since it also includes screening effects from the rest of the electronic system. Without explicitly writing an exact analytical expression for V_{eff} we can expand it in a Taylor series using displacements form the nuclear equilibrium positions $\boldsymbol{Q}_{\boldsymbol{R}_i}$ as parameters of the expansion, following Eq. 1.2

Assuming that the creation of the core-hole can be tread as a small perturbation to the system, we will consider only the linear term in this expansion. The first term

is responsible for the renormalization of the atomic equilibrium positions. Following standard texts [12] (see Eq. 1.3), the interacting potential (V_{eff}) in the first order approximation is

$$V_{eff} = \sum_{\lambda,q} M_{\alpha}^{\lambda,\boldsymbol{q}} c_{\alpha}^{+} c_{\alpha} B_{\lambda\boldsymbol{q}} \ . \tag{4.16}$$

It involves one phonon operator, the linear electron-phonon coupling $M_{\alpha}^{\lambda,\boldsymbol{q}}$ and the number operator for the core-hole. The phonon momentum, $\boldsymbol{q}$ runs over the full Brillouin zone taking into account translation invariance of the crystalline material. The phonon operator is $B_{\lambda,\boldsymbol{q}} = b_{\lambda,-\boldsymbol{q}}^{+} + b_{\lambda,\boldsymbol{q}}$. Since the core-hole is localized in space we will first find the coupling constants in real-space and then Fourier transform them. The linear electron-phonon coupling constant is defined as

$$M_{\alpha}^{\lambda,\boldsymbol{q}} = \sum_{\boldsymbol{G}} \sqrt{\frac{\hbar}{2\mu N \omega_{\lambda,\boldsymbol{q}}}} \boldsymbol{\xi}_{\lambda,\boldsymbol{q}} \cdot \sum_{i} \langle \psi_{\alpha} | \, \boldsymbol{\nabla}_{\boldsymbol{R_i}} V(r_{\alpha} - R_i^0) \, | \psi_{\alpha} \rangle \, e^{-i(\boldsymbol{q}+\boldsymbol{G})\boldsymbol{R}_i} \ . \tag{4.17}$$

Here μ is the reduced mass of the unit cell, and N comes from the normalization of the Fourier transform.

Noticing that the gradient of the interaction potential is a force which is acting on the core-hole from the atom with position $\boldsymbol{R}_i$ we can relate the coupling constants to the forces in real-space. Another numerical simplification comes from the symmetry between forces acting on the core-hole and forces acting on the surrounding atoms due to the core-hole creation. Thus, using DFT based calculations of the atomic response to suddenly switching on the core-hole one can find the interatomic forces

$$\boldsymbol{F}_{\boldsymbol{R}_i} = \langle \psi_{\alpha} | \, \boldsymbol{\nabla}_{\boldsymbol{R_i}} V(r_{\alpha} - R_i^0) \, | \psi_{\alpha} \rangle \ , \tag{4.18}$$

and those forces can be used to obtain the coupling constant as

$$M_{\alpha}^{\lambda,\boldsymbol{q}} = \sum_{G} \sqrt{\frac{\hbar}{2\mu N \omega_{\lambda,q}}} \sum_{i} \boldsymbol{F}_{\boldsymbol{R}_i} \cdot \boldsymbol{\xi}_{\lambda,\boldsymbol{q}} e^{-i(\boldsymbol{q}+\boldsymbol{G})\boldsymbol{R}_i} \ . \tag{4.19}$$

To calculate this forces we performed supercell DFT calculations, placing a core-hole on a central atom and calculating the forces resulting on all other atoms.

Eq. 4.19 contains a sum over all projections of the forces onto the polarization

of the phonon with momentum $\boldsymbol{q}$ and mode λ. The coupling constant can be found without calculating explicitly the forces by applying the frozen phonon approach. Thus now we will look at the total force which appears in the system due to the distortion along mode $\boldsymbol{\xi}_{\lambda,\boldsymbol{q}}$. The total force can be found, using the Hellman-Feynman theorem, as a first derivative of potential energy surface along a normal mode displacement

$$F_{\alpha}^{\lambda,\boldsymbol{q}} = -\langle\psi| \frac{dH_{\alpha}}{dQ_{\lambda,\boldsymbol{q}}} |\psi\rangle = -\frac{dE_{tot}}{dQ_{\lambda,\boldsymbol{q}}} \ . \tag{4.20}$$

4.4 Real-time approach and nuclear response function

Since the final state of the XPS experiment describes the system with a core-hole, it is not a surprise that the response of both electronic and nuclear subsystems contribute a lot to the formation of this state. Due to the sudden creation of the core-hole (the time of transition is much smaller than the characteristic time of the atomic movements) the nuclei do not have time to adjust their positions to the new charge density distribution. The nuclear response to such a perturbation leads to collective excitation of phonons, and the electron-phonon coupling defines how many of them will be activated. From the Kubo formula, it follows that the linear response function is proportional to the retarded correlation function of the observable

$$\chi(t, t', \mathrm{r}, \mathrm{r}') = \langle 0| \left[\mathrm{Q(t, r)Q(t', r)}\right] |0\rangle \ . \tag{4.21}$$

In our case, the observable is the atomic positions (Eq. 4.22), and the correlation function gives the retarded phonon Green's function. The phonon operator can be found form real-space displacement operators Q transformed into momentum space. This allows us to use real-space calculations to obtain the system response as well as the excited state phonon Green's functions. The phonon field operator is

$$B_{\boldsymbol{q},\lambda}(t) = \sum_{i} \sqrt{\frac{\mu\omega_{\boldsymbol{q}\lambda}}{2\hbar N}} \delta\boldsymbol{R}_i(t) e^{i\boldsymbol{q}\cdot\boldsymbol{R}_i} \cdot \boldsymbol{\xi}_{\boldsymbol{q},\lambda} \ . \tag{4.22}$$

The summation index runs over all atoms in the supercell and δR_i defines the time-dependent displacements of the nuclei from their equilibrium positions. The displace-

ment - displacement correlation function gives the dynamical response and time-dependent phonon Green's function. From now on, we will assume the correlation function in context of classical displacements. Moreover we will neglect thermal disorder, though it can be added using MD calculations. Finally the phonon Green's function becomes

$$D_{\boldsymbol{q},\lambda}(t) = -i \sum_{ij} Q_i^{\lambda,\boldsymbol{q}}(t) Q_j^{\lambda,\mathbf{q}}(0) e^{iq(R_i - R_j)} \ . \tag{4.23}$$

The normalized displacement along a given mode is $Q_j^{\lambda,\boldsymbol{q}} = \sqrt{\frac{\mu\omega_{\mathbf{q}\lambda}}{2\hbar N}} \delta \boldsymbol{R}_i \cdot \boldsymbol{\xi}_{\mathbf{q},\lambda}$. These displacements can be found from the DFT based molecular dynamics calculation. The quantum nature of the electronic interactions and screening can be captured within BO MD calculations. The time dependence of the nuclear positions has to be projected onto the normal phonon coordinates. In the end one has a real-time, real-space displacement-displacement correlation function.

Molecular dynamics simulations are also suitable for non-linear responses since they will capture any an-harmonic response. The an-harmonic effects can be seen as a phonon-phonon interaction and can be added to the harmonic, non-interacting phonon Green's function, using the self-energy concept and Dyson expansion. Thus in the case of an-harmonicity of the correlation function, the obtained phonon Green's function is implicitly dressed by the phonon-phonon interactions.

4.5 Numerical results

The theory developed in the previous sections is meant to be applied to crystalline material, although this section is dedicated to tests on small molecules. Molecules often show strong electron-vibrational coupling with vibrational frequencies that are usually higher than in solids. Therefore the fine vibrational structure in the XPS spectra can be well pronounced, despite the short lifetime of the core excitation. This availability of experimental spectra with well resolved vibrational side-band makes molecules good references for theoretical testing.

Here we consider excitation of the Si 2p core-level in a family of tetrahedral molecules SiX_4 (X = H, F). Calculations were performed to mimic the gas-phase by placing a single molecule in the center of a 15 Å vacuum cell. All density functional

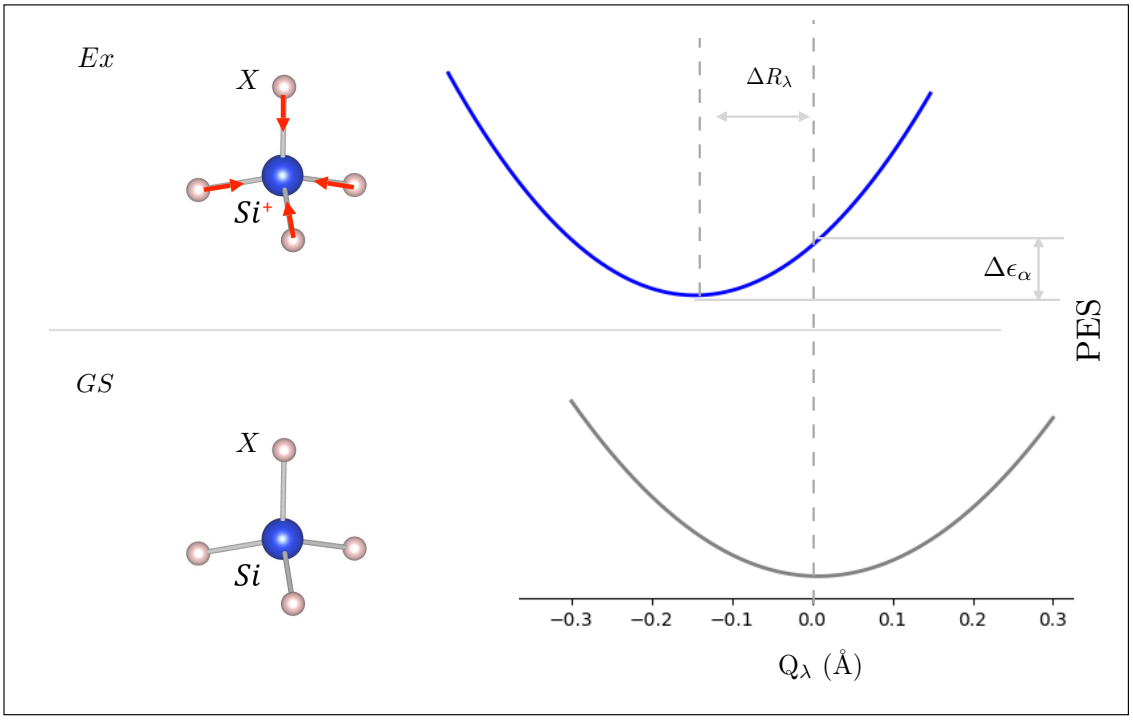

Figure 4.1: Diagram for the core excitation process. Bottom: the ground state (GS) potential energy surface (PES) of the SiX_4 ($X = F, H$) molecule. Top: the excited (Ex) state configuration of the same molecule, after emission of the photo-electron form the core-level. Due to uncompensated charge on the silicon site ligands moves along normal mode coordinate around new equilibrium. The shift of the minimum of excited state PES with respect to GS proportional to the electron-phonon coupling constant $\Delta R_\lambda = g^\lambda_\alpha \sqrt{\frac{\hbar}{2\mu\omega_\lambda}}$. The energy shift of the zero-phonon line is $\Delta\epsilon_\alpha$ and in harmonic approximation is equal to $g^\lambda_\alpha \omega_\lambda$.

theory, density functional perturbation theory, and ab initio molecular dynamics calculations were performed with a pseudopotential-based, plane-wave DFT code (QUANTUM ESPRESSO) [66] with periodic boundary conditions. Unless stated otherwise, we used ultrasoft, PBE/GGA pseudopotentials taken from the Quantum-ESPRESSO pseudopotential library, and a plane-wave cutoff of 50 Ry for the wave-functions and 400 Ry for the charge density. For MD we used time step of 50 $\hbar/E_{\mathrm{Ryd}}$.

First, the electronic and atomic structures were relaxed in the absence of a core-

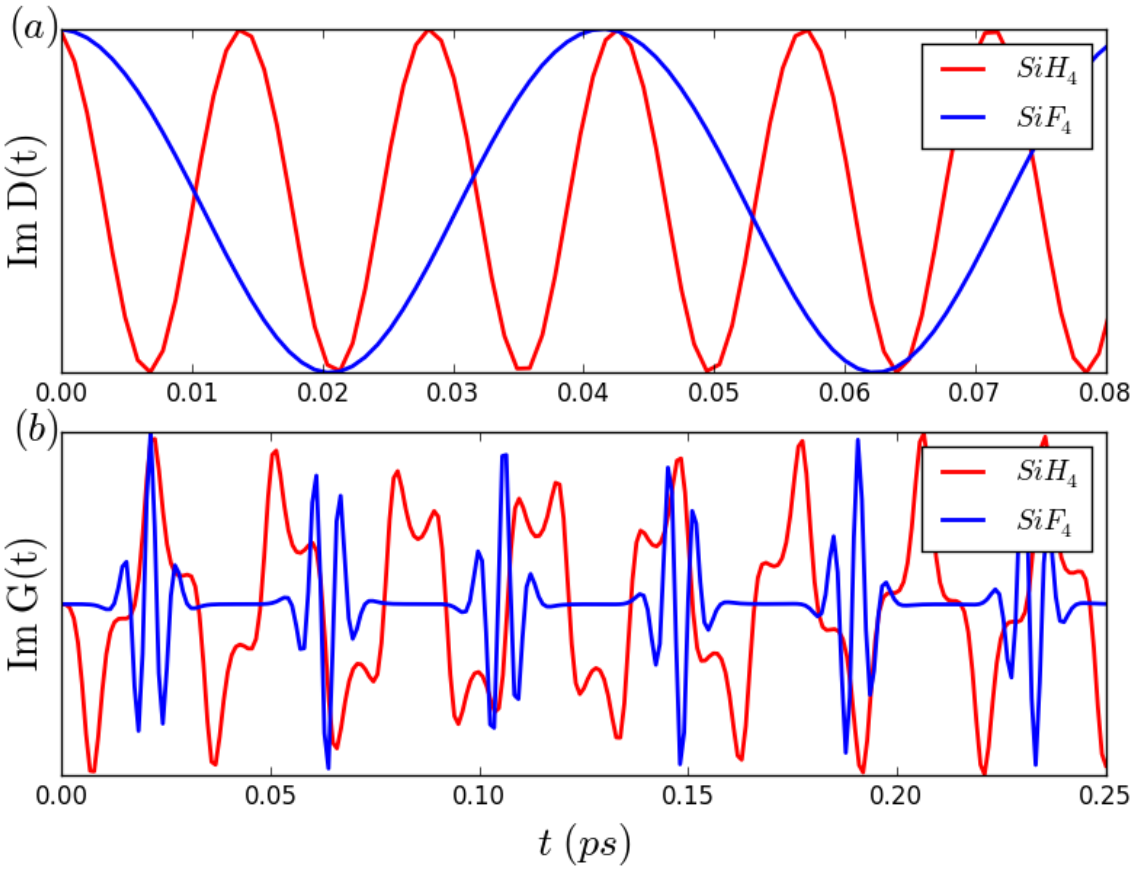

Figure 4.2: The time-dependent core-hole Green's function calculated using *ab-initio* based MD and cumulant ansatz. (a) The imaginary part of the phonon Green's function calculated obtained as displacement autocorrelation function from the atomic response to the sudden creation of the Si 2p core-hole. (b) The fully interacting core-hole Green's function calculated using Eq. 4.14 for secondary excitation spectrum and the second order cumulant expansion in the limit of harmonic response.

hole. Then the sudden creation of the core-hole was introduced by changing the Si pseudopotential to one with a 2p core-hole calculated using the pseudopotential generator code OPIUM (GIPAW).

Using Born-Oppenheimer molecular dynamics (BO MD) we let the ligands respond to this charge perturbation on the silicon site. BO MD involves self-consistent relaxation of the electronic structure at each time step. After the introduction of the core-hole, the system develops new Born-Oppenheimer surfaces due to the rapid screening response of the electron density. The nuclei, which were initially at equilibrium with respect to the ground-state BO surfaces, are suddenly away from the minima of the new BO surfaces

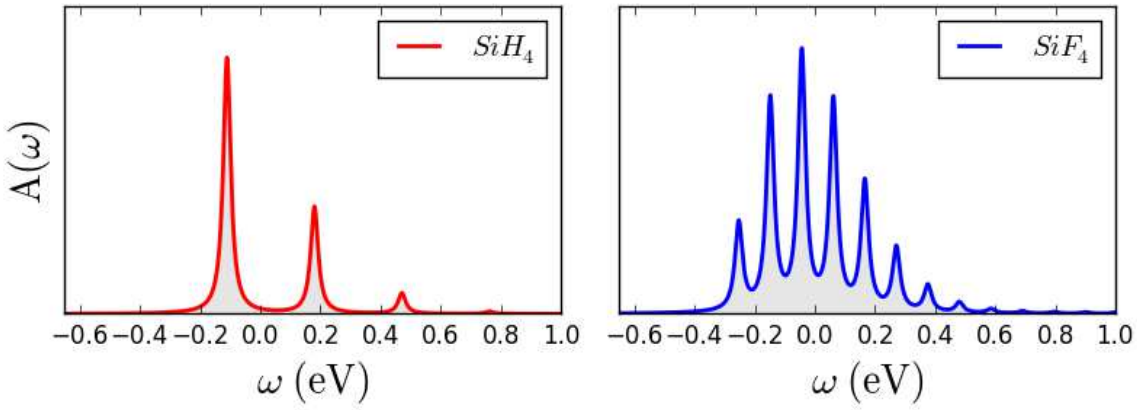

Figure 4.3: Core-hole spectral functions for SiX_4 (X = F, H). The energy of the single particle is set to zero, and the energy of the zero-phonon peak gives an absolute value for the quasiparticle energy shift $\Delta\epsilon_\alpha$. The broadening has a Lorentzian shape and originates from the finite core-lifetime.

(Fig. 4.1).

We extract the forces corresponding to Eq. 4.20 at the $t = 0$ time step and build the phonon Green's function from the temporal autocorrelation function according to Eq. 4.23.

The only vibrational mode which was activated in the MD simulations is a fully symmetric (a_1) ligand stretching mode. As expected, it is clear from the period of oscillations that the frequency strongly depends on the mass of ligands. The obtained correlation function and the vibrational Green's function in real space can then be projected onto the normal coordinates.

In this specific case, the response can be well approximated as harmonic, which also means that we are in the linear response regime. In the energy domain the vibrational Green's function is given by a delta function at the vibrational frequency. Both the vibrational frequencies and coupling constants obtained from the molecular dynamics are listed in Tab. 4.5. As an alternative approach to obtain the excited state vibrational frequency we fit the bottom of the excited state potential energy surface with a quadratic polynomial. We used the coefficients to calculate the frequency of vibrations in the classical limit. Those values obtained from the BO MD simulation are in agreement with the frequency and coupling constant calculated form the potential energy surface.

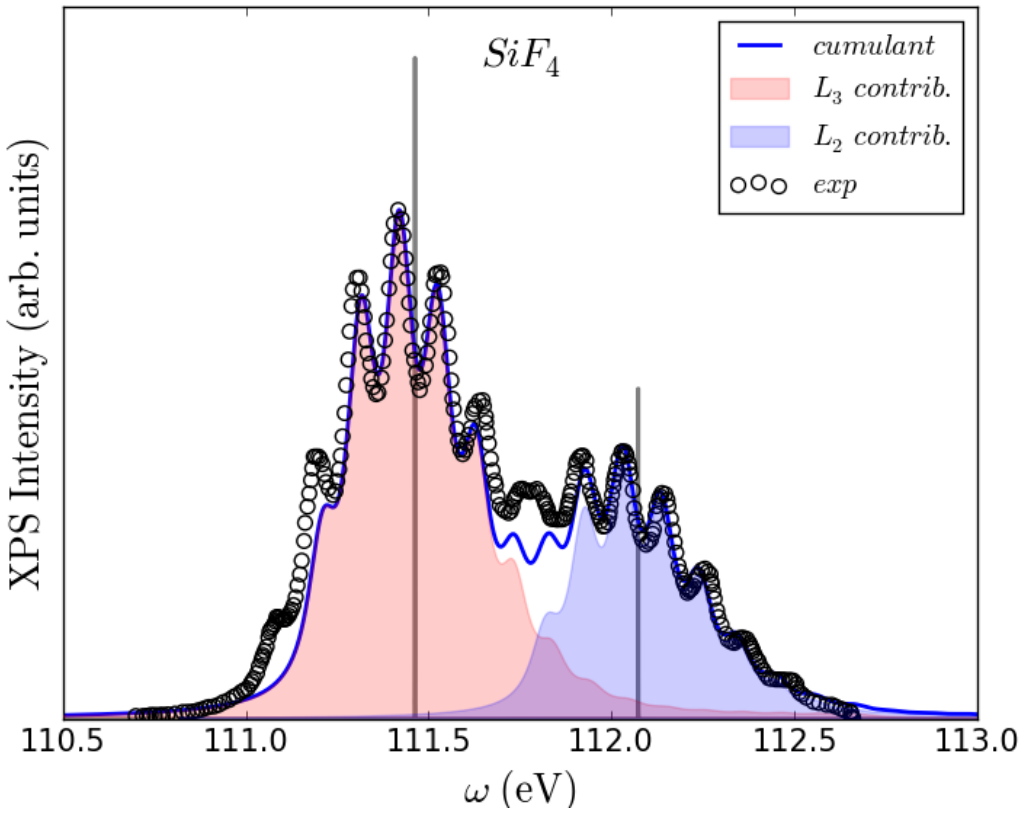

Figure 4.4: Calculated XPS spectra of SiF_4 compared to experimental results [99] (open symbols). Shaded curves represent the individual $2p_{3/2}$ (red) and $2p_{1/2}$ (blue) contributions. Vertical gray lines indicate the positions of electronic peaks in the absence of electron-phonon interactions.

Table 4.1: Parameters of core-hole vibrational coupling calculated from BO MD for SiX_4 (X = F, H) for vibrational mode with a_1 symmetry λ. The coupling strength ($g = \frac{M^2}{\omega^2}$) is a unitless parameter of the interaction.The experimental frequency obtained from the energy separation of the vibrational side-bands.

Compound	M_α^λ, **meV**	g_α^λ	ω_λ, **meV**	ω_λ^{exp}, **meV**
SiH_4	200	0.25	290	290
SiF_4	270	2.4	105	110

In order to calculate the core-hole Green's function one can Fourier transform the secondary excitation spectrum $\beta_\alpha(t)$ obtained in time the domain (see Eq. 4.14) and

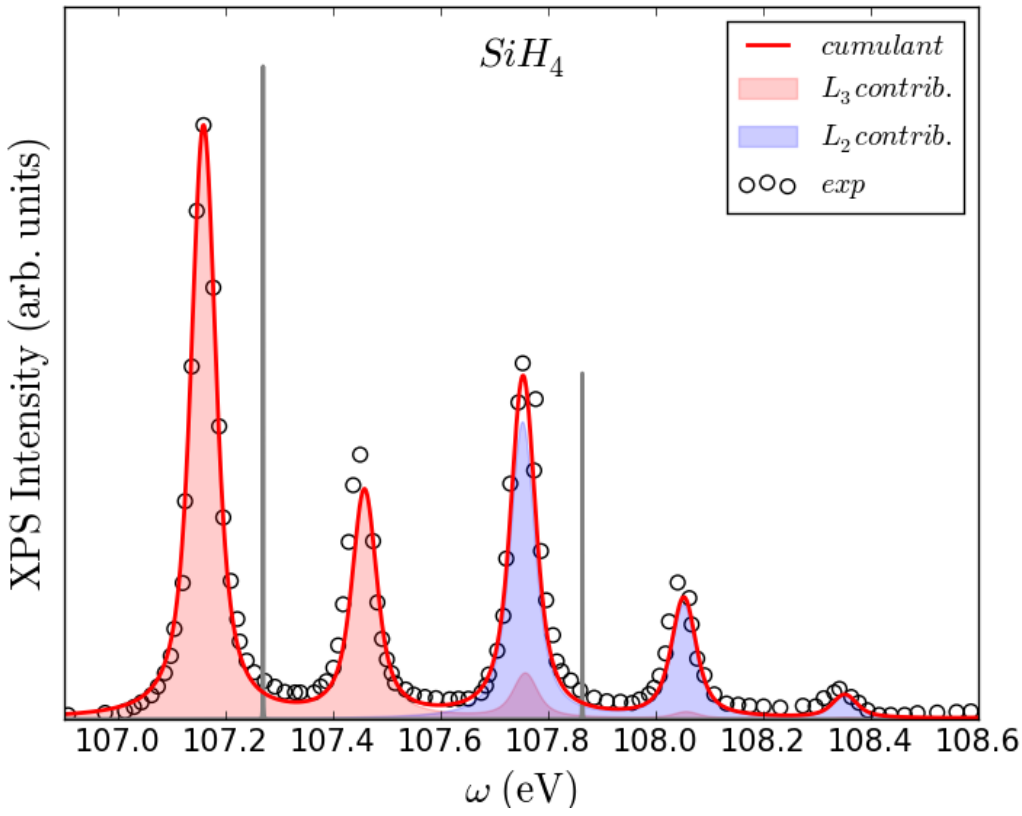

Figure 4.5: Calculated XPS spectra of SiH_4 compared to experimental results [99] (open symbols). Shaded curves represent the individual $2p_{3/2}$ (red) and $2p_{1/2}$ (blue) contributions. Vertical gray lines indicate the positions of electronic peaks in the absence of electron-phonon interactions.

calculate the cumulant using Eq. 4.11. Noticing that in the harmonic limit $\beta(\omega)$ is a weighted delta function centered at the vibrational frequency, the integral in Eq. 4.11 can be taken analytically, and the expression for the cumulant simplifies to

$$C_\alpha(t) = \sum_\lambda (M_\alpha^\lambda)^2 \frac{e^{-i\omega_\lambda t + i\omega_\lambda t - 1}}{\omega_\lambda^2} \tag{4.24}$$

The resulting core-hole Green's function in the time domain for the Si 2p hole is presented in Fig. 4.2b. The resulting spectral functions for SiF_4 and SiH_4 are shown after shifting the quasi-particle energy to zero in Fig. 4.3. The overall shape of the spectral function dramatically depends on the ratio between the coupling constant and the phonon frequency, i.e., on the coupling strength. The smaller coupling strength

corresponds to a more asymmetric spectral function (the case of SiH_4).

Inspecting Eq. 4.24 one can notice that the core-hole Green's function is proportional to the double exponential function $G_\alpha(t) \sim e^{-g_\lambda} e^{g_\lambda e^{-i\omega_\lambda t}}$. By expanding the first exponent in powers of the coupling strength $G_\alpha(t) \sim e^{-g_\lambda} \sum_n \frac{g^n}{n!} e^{-i\omega_\lambda n t}$ which gives a set of delta functions separated by the vibrational energy and weighted by the factor $e^{-g_\lambda} \frac{g^n}{n!}$. Those weights correspond to the Poisson probabilities of a random process. Thus the shape of the spectral function in the limit of small g is given by the Poisson generating function. However, in the limit of strong coupling the overall shape of the spectral function becomes more Gaussian-like because the intensity of the first peak goes down due to e^{-g} [12]. This explains the shape of the vibrational spectra.

Turning finally to the XPS spectra, the silicon $2p$ orbitals are split by spin-orbit coupling into $2p_{3/2}$ and $2p_{1/2}$ levels, which are separated by about 0.6 eV [103]. To compare our calculations with experimental results [99], we obtain the full silicon $2p$ XPS signal by convolving each spectral function with a bare core-hole spectrum. This consists of two delta functions (for the $2p_{3/2}$ and $2p_{1/2}$ levels) that have a 2:1 intensity ratio. This comparison is presented in Fig. 4.4 and 4.5. An additional linewidth, beyond the Lorentzian core-hole broadening, was added by further convolving with a Gaussian to account for the experimental resolution [99]. The bare core-hole spectral function used in the convolution with the vibronic spectral function was constructed by hand from experimental knowledge of the Si $2p$ spin-orbit splitting and binding energies. Values for the spin-orbit splitting and the respective binding energies (which depend moderately on the local chemical environment) could be obtained numerically, *e.g.* from all-electron DFT or Hartree-Fock calculations.

4.6 Conclusions

In this section, we showed that the fine vibrational structure in the experimental XPS spectra comes from the strong coupling between the deep core-hole and the vibrational degrees of freedom. Thus neglecting such effects in the RIXS process might lead to significant qualitative and quantitative mistakes.

To reproduce the XPS vibrational side-bands, we applied the cumulant ansatz for the interacting core-hole Green's function. Taking into account the localized character of the core-hole, we performed calculations of the coupling constants using the interatomic forces from the core-excited state at time zero. The excited state phonon Green's function was calculated using the displacement-displacement correlation function obtained from BO molecular dynamics. We tested the approach on small molecules. The calculated XPS spectra are in a good agreement with the experimental ones.

The benefits of this approach are that it can be applied directly to crystalline materials and is also capable of capturing anharmonic effects as they will occur naturally during the MD simulation. To account for strong electronic correlations one can go beyond the present DFT study and calculate the electronic structure with various kinds of techniques (DFT+U, DMFT, Gutzwiller, slave bosons).

Chapter 5

XAS: Neutral excitations

Characterizing the coupling of neutral excitations to phonon degrees of freedom is essential for the general understanding of the phonon contribution to RIXS. In contrast to XPS, where the sample becomes charged after interaction with a photon, RIXS involves only neutral excitations. In this sense, despite the conceptual differences between XAS and RIXS, both probe the same type of electronic excitations and consequently reflect the same interactions. In the present chapter, we focus on phonon contributions to XAS, regarding this problem as a reference for the correct understanding of the processes that form the intermediate state in RIXS.

Contents

5.1 Introduction

X-ray absorption spectroscopy (XAS) is a resonant technique that probes unoccupied states. The absorption cross-section is defined by the first order electron-photon interaction (due to the resonant nature of the process other contributions are negligible) within time-dependent perturbation theory [48]. In contrast to photo-emission techniques, after interaction between the X-ray photon and the core-electron, the latter remains in the sample filling an unoccupied orbital. Tuning the energy of the incoming photon to be close to the resonant transitions between atomic levels and conduction states one can achieve orbital and element selectivity. XAS paired with XES (which probes occupied states) provides information on the electronic structure of the absorber, such as the energy splitting between levels, hybridization of atomic orbitals as well as information about the local environment. One can find detailed reviews on these techniques elsewhere [104, 105]. In the limit of weak overlap between the core and the excited electron wave-functions, one can probe the density of the unoccupied states [105]. However, often the electronic structure appears in a mixed way due to strong multiplet effects [104]. All single electron transitions in reality are accompangied by dynamical effects, such as contributions from plasmons [106] or phonons [44, 107, 108]. The electron-phonon interaction contributes to the absorption process as a self-energy correction to the electronic spectral function. Thus, the resulting spectra contain unique signatures of the electron-phonon interaction.

The electron-phonon interaction tends to break the quasi-particle picture of electronic excitations, i.e., it attributes a shift to the quasiparticle peak and gives rise to phonon side-bands. However, the resulting spectral function in many cases is not a one particle property [88]. Using optical absorption one can measure an energy gap in semiconducting/insulating materials, and the electron-phonon interaction renormalizes this gap even in the zero-temperature limit [109] due to the energy shift of the hole and photo-electron levels. Both non-equilibrium electron-electron and electron-phonon interactions accompany the existence of the hole and an excited electron. Thus, in the general case the electron–phonon and hole–phonon interactions appear to be entangled.

One limitation of the X-ray absorption technique in measuring the electron-phonon coupling is that the lifetime of the excited state is usually very short. The lifetime broadening is often more prominent than the splitting between phonon side-bands and

the fine structure vanishes. In this case, the electron-phonon coupling is reflected in the additional broadening of the quasiparticle peak [108] as well as in small changes in the Lorentzian form of the peak. Also in contrast to RIXS, XAS provides information in a phonon mode and wavevector averaged way.

Fermi's golden rule The absorption cross-section (σ_{abs}) and absorption coefficient ($\mu = \sigma_{abs}/N_a$), where N_a is a concentration of absorbing atoms, is defined by Fermi's golden rule [48]. A transition from the core-level (or levels) occurs due to the interaction with X-rays

$$\mu(\omega) = 4\pi^2\alpha\omega \sum_F |\langle\Psi_F|\Delta|\Psi_I\rangle|^2 \delta(\omega - E_{FI}) \ , \tag{5.1}$$

where $|\Psi_I\rangle$ and $|\Psi_F\rangle$ are the many-body ground and excited states, respectively. The term $4\pi^2\alpha\omega$ where $\alpha \sim 1/137$ is the fine structure constant and ω is the photon energy, will be omitted for simplicity.

Depending on the overlap between the excited electron and the core-level hole wave-function the XAS process might be considered in two different pictures. From the real-space impurity picture it can be seen as a probe of local atomic orbitals with strong exchange interactions (mainly L-edges of transition metals). From the band structure perspective it is seen as a probe of a continuous density of the states if the exchange term is negligible (K-edges). In the latter case, the sum over final states in Eq. 5.1 should be replaced by the integration over the final many-body density of states

$$\mu(\omega) \cong \int dE_F N(E_f) |\langle\Psi_F|\Delta|\Psi_I\rangle|^2 \delta(\omega - E_{FI}) \ . \tag{5.2}$$

The density is weighted by the transition matrix elements which are defined by the electron-photon operator discussed in Chapter 2 . The cross-section depends mainly on the first order terms in time-dependent perturbation theory due to the resonance nature of the transition and the linear (in $\mathbf{A}$) electron-photon operator Δ. A simplification can be achieved by taking into account that the photon wavelength is much larger than the atomic dimension. The electron-phonon interaction can be treated approximately assuming the parameter $\mathbf{k}\cdot\mathbf{r_i}$ to be small.

The energy of the excited core-electron is of the same order as the binding energy $\hbar\omega \sim \frac{Ze^2}{R_{atom}}$. Assuming also that $r_i \sim R_{atom}$ then kr is of the order of $Z\alpha \sim Z/137 < 1$

($\alpha = 1/137$). And thus the exponential factor in many cases can be expanded up to the first few terms $e^{-i\mathbf{k}\cdot\mathbf{r}} \approx 1 + \mathbf{k}\cdot\mathbf{r} + O((\mathbf{k}\cdot\mathbf{r})^2)$.

The first term in this expansion is called the electric dipole (E1) approximation and is proportional to the momentum operator $V^{(0)} \sim \mathbf{p_i}$. The lowest contribution from the magnetic term contributes at higher order in kr then E1 and is called the magnetic dipole (M1). Since in this work we will not be treating any spin involved interactions, the magnetic term will not appear explicitly, but it can be added without any specific requirements.

The transition matrix elements for both E1 and M1 will be zero unless the selection rules are satisfied. The selection rules come from the form of the interacting potential and atomic orbitals. The difference between the total angular momentum of the ground and excited states has to be $\Delta J = 0, \pm 1$. At the same time the difference for the secondary total angular momentum quantum number has to be $\Delta M_J = \pm 1$. The higher order transitions in $\mathbf{k}\cdot\mathbf{r}$ satisfy different selection rules.

In the following text we will use a generic form of Δ^I unless otherwise specified. The coupling of the photon to the electronic structure leads to the annihilation of a core-electron and creation of an excited electron in an unoccupied conduction band orbital. One can express the electron-photon operator using the second quantization formalism

$$\Delta = \sum_{\beta,\alpha} d_{\alpha,\beta} c_\beta^+ c_\alpha + h.c \ , \tag{5.3}$$

where the matrix elements $d_{\alpha,\beta}$ contain all information about the electronic translations. Moreover, the indices α and β represent the core-hole and excited electron, respectively, and consequently run over unoccupied states for the excited electron and occupied for the core-hole, though we usually pick a specific core-level. The electron creation and annihilation operators are c_i^+, c_i respectively.

XAS in terms of many-body Green's functions It is convenient to use the Green's function formalism to obtain the absorption cross-section. By expanding the square of the matrix elements in Eq. 5.1

$$\mu(\omega) = \sum_F \langle\psi_I|\, \Delta^+ \,|\psi_F\rangle \, \langle\psi_F|\, \Delta \,|\psi_I\rangle \, \delta(\omega - E_{FI}) \ , \tag{5.4}$$

and replacing the summation over final states with a propagator
(Im $\Lambda(\omega) = -\frac{1}{\pi}\sum_F |\psi_F\rangle \langle\psi_F| \delta(\omega - E_F)$) we get

$$\mu(\omega) = -\frac{1}{\pi}\mathrm{Im}\,\langle\psi_I|\,\Delta^+\Lambda(\omega + E_I)\Delta\,|\psi_I\rangle \ . \tag{5.5}$$

A distinct advantage of this formulation is an absence of an explicit summation over the final states, which might be enormously expensive for the vibronic problem in crystalline materials. Taking into account that the interaction term is a two-particle operator, the many-body Green's function Λ can be reasonably approximated as a two-particle one [61, 62]. The interaction with other particles will come as a correction to the two particle picture. This approximation, however, is less accurate for open shell compounds.

Eq. 5.5 shows that after the creation of the neutral excitation in the system all information on the internal interactions is hidden in the Green's function, i.e., the main focus will be on the calculation of the two-particle Green's function and related spectral function. For convenience, we will refer to the fully interacting two-particle Green's function as Λ and to the two-particle Green's function in the absence of the electron-phonon interaction as L.

Both electron-hole and electron-phonon vertex parts of the two particle Green's function make calculations non-trivial. One could attempt to treat both types of interaction within a Bethe-Salpeter formalism [109]. Alternatively, as it was done for plasmons, one can consider a cumulant approach to the electron-phonon interaction in the particle-hole basis [88] (See appendix E). However, an important simplification of the problem can be achieved if we change the idea of what we treat as a quasi-particle. Instead of the separately dressed electron and hole, here we suggest to treat the resulting electron-hole exciton as the quasi-particle itself. This approach leads to the separation of the pure electronic and electron-phonon contributions, which can be justified based on the distinctly different time-scales of the interactions. The resulting exciton quasi-particle calculated in the presence of electronic interactions then interacts effectively with phonons, however in a different way than the non-interacting electron and hole. This idea is consistent with the conclusions of the recent work by Antonious and Louie [109] on the optical exciton-phonon coupling, although they use the Dyson approach to treat the exciton-phonon interaction and we will employ the cumulant expansion.

5.2 Cumulant expansion for the exciton-phonon interaction

The advantage of working in the excitonic basis is the possibility to first solve the electronic problem and then, applying approximate methods, to account for the phonon contribution, instead of directly solving the substantial vibronic problem. This scheme can be applied to both solids and molecules. Generally, even the pure electron interaction part cannot be solved exactly [61, 68]. Nevertheless, this separation still significantly reduces the effort one needs to apply to solve the electron-phonon problem. In this section we will rewrite Fermi's golden rule in terms of an exciton Green's function and treat it with a combination of the BSE and the cumulant expansion. First, let us reintroduce the exciton Green's function in the absence of the exciton-phonon interaction

$$L_{\xi,\xi}(\omega) = \sum_{\alpha,\beta} \frac{(A^{\xi}_{\alpha\beta})^* A^{\xi}_{\alpha\beta}}{\epsilon_{\alpha\beta} - \omega \pm i\gamma} \ . \tag{5.6}$$

Using Eq. 3.44 the exciton Green's function and coefficients $A^{\xi}_{\alpha\beta}$ can obtained by solving the BSE Hamiltonian (see Chapter 3). The index $\xi = \{n_\xi, \boldsymbol{k}_\xi\}$ is a shorthand notation for the exciton band and momentum. Using completeness of the excitonic basis, one can rewrite Eq. 5.5 for the absorption coefficient as

$$\mu(\omega) = -\sum_{\xi_2,\xi_1} \frac{1}{\pi} \mathrm{Im} \left\langle \psi_I \right| \Delta^+ \left| \psi_{\xi_1} \right\rangle \left\langle \psi_{\xi_1} \right| \Lambda(\omega + E_I) \left| \psi_{\xi_2} \right\rangle \left\langle \psi_{\xi_2} \right| \Delta \left| \psi_I \right\rangle \ . \tag{5.7}$$

The Green's function operator $\Lambda(\omega) = \sum_m \frac{|\psi_m\rangle\langle\psi_m|}{E_m - \omega - i\gamma}$ is composed of the eigenvectors and eigenvalues of the fully vibronic Hamiltonian. The wave-functions $|\psi_\xi\rangle = |\psi^e_\xi\rangle \, |\chi_{ph}\rangle$ include both electronic ($H_{BSE} \, |\psi^e_\xi\rangle = \epsilon_\xi \, |\psi^e_\xi\rangle$) and phonon ($H^0_{ph} \, |\chi_{ph}\rangle = \omega_{ph} \, |\chi_{ph}\rangle$) degrees. This reduces the initial many-body problem to that of a purely electronic exciton with a self-energy due to interaction with the lattice. Since the initial state wave-function $|\psi_I\rangle$ contains neither electronic nor phonon excitations it will be referred to as $|0\rangle$. The electron-photon operator Δ acts directly only on the electronic states and the initial phonon state remains unchanged. As in the previous section

$$d_\xi = \langle \chi_{ph} | \left\langle \psi^e_\xi \right| \Delta \left| 0 \right\rangle \left| \chi_{ph} \right\rangle = \sum_{\alpha,\beta} d_{\alpha,\beta} \left\langle \psi^e_\xi \right| c_\alpha c^+_\beta \left| 0 \right\rangle = \sum_{\alpha,\beta} d_{\alpha,\beta} A^{\xi}_{\alpha\beta} \, . \tag{5.8}$$

Such matrix elements are projections of the electronic part of the state ξ onto the initial non-interacting electronic wave-functions $|\psi_\alpha\rangle |\psi_\beta\rangle$, where α and β represent states for the hole and particle, respectively. The matrix elements are weighted by the electron transition probability from state α to β. Eq. 5.7 then becomes

$$\mu(\omega) = -\sum_{\xi_2,\xi_1} \frac{1}{\pi}(d_{\xi_2})^* d_{\xi_1} \mathrm{Im}\, \langle 0| a_{\xi_2} \Lambda(\omega) a^+_{\xi_1} |0\rangle \ . \tag{5.9}$$

We now focus on the fully interacting Green's function Λ. It is essential for the following chapter to stress the fact that even if Λ is, in general, non-diagonal in the exciton subspace, it is for sure diagonal in the phonon subspace

$$\Lambda_{\xi,\xi'}(\omega) = \langle \chi^0_{ph}| \langle 0| a_\xi \Lambda(\omega) a^+_{\xi'} |0\rangle |\chi^0_{ph}\rangle \ . \tag{5.10}$$

In the absence of the electron-phonon interaction (or other types of dynamical interactions that are not part of the BSE) Λ is always diagonal in the excitonic basis ($\xi = \xi'$). It reduces to just the electronic Green's function Eq. 5.6. The full spectrum is also proportional to the exciton density of states

$$\mu(\omega) = -\sum_{\xi} \frac{1}{\pi} |d_\xi|^2 \mathrm{Im}\, L_\xi(\omega) \ . \tag{5.11}$$

In contrast, if there is an electron-phonon interaction, these pure electronic states can be mixed. However, non-diagonal elements of the exciton Green's function are only non-zero when $k_{\xi_1} = k_{\xi_2}$ and $n_{\xi_1} \neq n_{\xi_2}$.

Assuming that the excitonic bands, energy-wise, are well separated ($\epsilon_{\xi_1} - \epsilon_{\xi_2} \gg \hbar\omega_{ph}$), the off-diagonal terms in the exciton Green's function can be neglected. The exciton-phonon scattering events are still present in the limit of one band. The fully interacting Green's function can be obtained from the S-matrix expansion by analogy to Eq. 3.13 but starting from the pure electronic BS problem ($a_\xi = \sum_{\alpha,\beta} A^\xi_{\alpha\beta} c_\alpha c^+_\beta$) in the time domain as ($\epsilon_\xi > 0$)

$$i\Lambda_{\xi\xi}(t,t') = \sum_n \frac{(-i)^{2n}}{(2n)!} \int .. \int d\tau_1 d\tau_{2n} \langle 0| T a_\xi(t) V_1(t_1) V_{2n}(t_{2n}) a^+_\xi(t') |0\rangle_c \ . \tag{5.12}$$

Due to the cancellation theorem [12], the expansion contains only connected diagrams

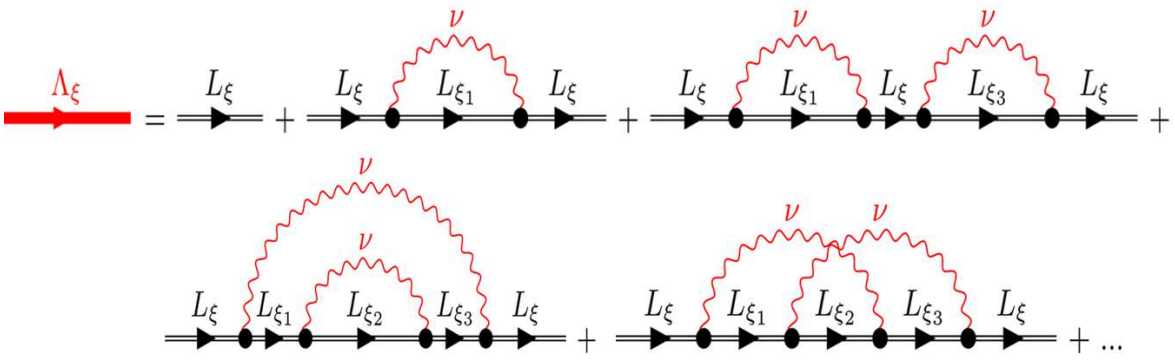

Figure 5.1: Expansion of an exciton propagator dressed by interactions with phonons (wavy red lines). The black exciton-lines include electron-electron interactions. The heavy red line represents the fully interacting exciton propagator within the cumulant expansion.

and all operators are defined according to the Heisenberg representation. Exponential re-summation of the above series (see Chapter 3) leads to a cumulant expansion similar to the one particle case. Denoting the Green's function in the absence of electron-phonon interactions as $L_\xi = -i \langle 0| T a_\xi(t) a_\xi^+(0) |0\rangle$, within the framework of the cumulant ansatz Eq. 5.12 reads

$$\Lambda_{\xi\xi}(t,t') = L_\xi(t,t') e^{C_\xi(t,t')} \ . \tag{5.13}$$

In the lowest order the cumulant can be approximated as a second order term in the exciton-phonon coupling $C_\xi \sim C_\xi^{(2)}(t)$. Equating terms of the same order in the coupling constant this expression for the second-order cumulant can be found in terms of regular moments (Eq. 3.24) and gives

$$\begin{aligned} C_\xi(t,t') &= -[L_\xi(t-t')]^{-1} \sum_{\nu,\xi_1} |M^\nu_{\xi\xi_1}|^2 \\ &\times \int\int d\tau_1 d\tau_2 L_\xi(t-\tau) L_{\xi_1}(\tau_1-\tau_2) D_\nu(\tau_1-\tau_2) L_\xi(\tau_2-t') \ . \end{aligned} \tag{5.14}$$

Using the expression for the Fan-Migdal self-energy $\Sigma = iLD\Gamma$ with $\Gamma = 1$ the above

equation can be written as

$$\begin{aligned} C_\xi(t,t') &= [L_\xi(t-t')]^{-1} \\ &\times \int\int d\tau_1 d\tau_2 L_\xi(t-\tau_1)\Sigma_\xi(\tau_1,\tau_2)L_\xi(\tau_2-t') \ . \end{aligned} \tag{5.15}$$

The second order approximation of the cumulant series seems to be sufficient, although one can improve convergence by including either a higher order cumulant [101] or a different type of self-energy [110]. The above equation can also be formulated as a Fourier transform of frequency dependent functions ($t'=0$)

$$C_\xi(t) = \frac{1}{\pi}\int d\omega \frac{|\mathrm{Im}\Sigma_\xi(\omega+\epsilon_\xi)|(e^{-i\omega t}-i\omega t+1)}{\omega^2} \ . \tag{5.16}$$

The critical difference between the formulation of the problem in the exciton basis is that now the cumulant does not contain a phonon exchange term explicitly. It is now absorbed by the electronic self-energy of the quasi-particle. However, the self-energy has to be carefully evaluated. In contrast to Eq. 3.17, now the self-energy involves the calculation of the exciton-phonon coupling constants and the dispersion of excitonic levels

$$\Sigma_\xi(t,t') = i\sum_{\nu,\xi_1} |M^\nu_{\xi\xi_1}|^2 L_{\xi_1}(t_1,t_2)D_\nu(t_1,t_2) \ . \tag{5.17}$$

The vertices $M^\nu_{\xi\xi_1}$ have to be evaluated in the presence of the electron-electron interactions. Thus, Σ_ξ involves the first-order correction to the electron-electron interaction in the presence of atomic displacements.

Debye-Waller self-energy In general there is one more term present in the second order exciton-phonon self-energy (see Eq. 3.32). The Debye-Waller (DW) term is proportional to higher order exciton-phonon coupling and involves two-phonon operators Eq. 1.2. In the new basis of the excitonic states, one can express the DW part of the self-energy as

$$\Sigma_{DW}(t) = \sum_{\xi,\nu} M^{(2)}_{\xi,\xi'} \langle 0| B_\nu(t)B_\nu(t) |0\rangle = \sum_{\xi,\nu} M^{(2)}_{\xi,\xi'}[2N+1] \ . \tag{5.18}$$

Only coupling constants are affected by the change of the basis. Here, N is the number of phonons in the ground state. This contribution to the spectral function is limited to a constant shift proportional to the second order coupling constant.

Spectral function To find the XAS spectrum one has to combine Eqs. 5.7 and 5.12. The resulting expression for absorption is proportional to the density of states of the fully interacting Green's function

$$\mu(\omega) = -\frac{1}{\pi}\sum_{\xi}(d_\xi)^* d_\xi \text{Im } \Lambda_\xi(\omega) \ . \tag{5.19}$$

The spectral function is nearly diagonal in the electronic space $A_\xi(\omega) = -\frac{1}{\pi}\text{Im } \Lambda_\xi(\omega)$. The above equation accounts for many body corrections in a simple way [88, 102]

$$\mu(\omega) = \sum_{\xi}\int d\omega \mu^0_\xi(\omega - \omega')A_\xi(\omega) \ , \tag{5.20}$$

as a convolution of a pure electronic solution $\mu^0_\xi(\omega)$ with the exciton-phonon spectral function (A_ξ)

$$\mu^0_\xi(\omega) = -\frac{1}{\pi}(d_\xi)^* d_\xi \text{Im } L_\xi(\omega) \ . \tag{5.21}$$

The electronic contribution is an excitonic quasi-particle solution, which is known e.g. from solution of the BSE. The presence of the electron-phonon interaction redistributes the weight of the quasi-particle peak between phonon side-bands while conserving the total weight. This is a convenient way to include many-body corrections if the quasi-particle part is already known. However, such an approach fails when the exciton-phonon interaction mixes different excitonic bands, because off-diagonal terms of the bare excitonic propagator can no longer be neglected.

Exciton-phonon coupling constant The electron-lattice matrix elements

$$M^\nu_{\xi,\xi'} = \sqrt{\frac{\hbar}{2N\mu\omega_\nu}}\boldsymbol{\xi}_\nu \cdot \boldsymbol{F}^\nu_{\xi\xi'} \tag{5.22}$$

are evaluated as an exciton-phonon scattering process rather than separate electron-phonon and core-hole–phonon scattering events. $Q^0_\nu = \sqrt{\frac{\hbar}{2N\mu\omega_\nu}}$ is an amplitude of the

phonon eigenvector with index $\nu = \{\lambda, \boldsymbol{q}\}$. Thus, the exciton-phonon interaction is defined by the variation of an electronic interacting part of BSE Hamiltonian 5.22 with respect to atomic displacements along the phonon polarization vector $\boldsymbol{\xi}_\nu$. We construct the exciton-phonon coupling constants by generalizing the frozen-phonon procedure presented by Tinte and Shirley [63] and Gilmore and Shirley [108] to study the vibrational contribution to the XAS linewidth of $SrTiO_3$. This defines the force constants

$$\boldsymbol{F}^{\nu}_{\xi\xi'} = -\partial_{\boldsymbol{Q}_\nu} \left[E^{GS}_{tot}(\boldsymbol{Q}_\nu) + \langle \psi'_\xi | \, H_{BSE}(\boldsymbol{Q}_\nu) \, | \psi_\xi \rangle \right] \Big|_{\delta \boldsymbol{Q}_\nu = 0} \tag{5.23}$$

as derivatives of the excited-state total energy with respect to given atomic displacements. This expression splits the atomic position dependent excited-state total energy into the sum of the ground-state potential energy surface (PES) $E^{GS}_{tot}(\boldsymbol{Q})$ and the energy separation between the ground- and excited-state PES ($H_{BSE}(\boldsymbol{Q})$). In the above expression, ξ and ξ' are excitonic eigenstates of the equilibrium lattice and Eq. 5.23 accounts also for the scattering between exciton states by phonons.

5.3 Numerical results

The results of this section are limited to small molecules, but the advantage of such an approach is the possibility to apply it to crystalline materials. One should consider the following results as a proof of concept rather than the end stage of the research.

To demonstrate the above methodology we calculate the vibrational contributions to the K-edge of N_2, the O K-edge of CO and the O K-edge of acetone. We select these molecules because for each of them the problem can be well approximated as a single exciton state interacting with a single vibrational stretching mode and also because high-resolution experimental data exist and show multiple phonon side-bands.

To obtain the cumulant using Eq. 5.16 one has to calculate the exciton Green's function and the self-energy using Eq. 5.17 (here we only include the linear electron-phonon coupling). Thus, the quantities one has to evaluate to calculate the exciton-phonon vibrational spectral function are the exciton Green's function, exciton-phonon coupling constants, and the phonon Green's functions.

The acetone O K-edge XAS consists of an isolated feature at 531.5 eV and a

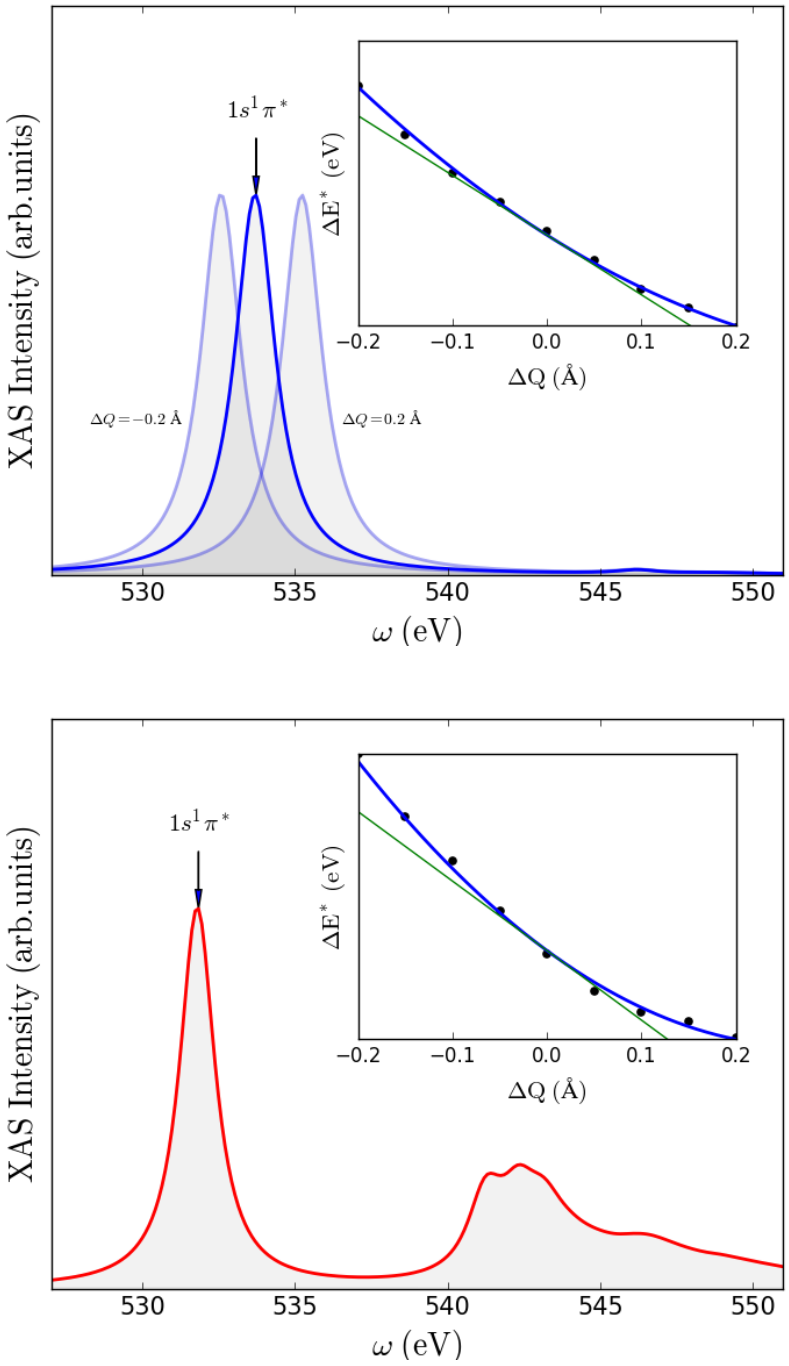

Figure 5.2: Calculation of the O-K XAS of CO (top) and acetone (bottom). The arrows indicate the $1s^1\pi^*$ resonance. The insets show the $1s^1\pi^*$ excited-state PES for the C-O bond stretching constructed as the sum of the ground-state PES and the BSE excitation energy. The tangent lines at the ground-state C-O equilibrium bond lengths give the excited-state forces. The blue curves are quadratic fits of the excited state potential energy.

broad continuum at higher energy. The main feature corresponds to the excitation of an oxygen $1s$ electron into a π^* anti-bonding orbital between the oxygen and nearest carbon atom. We obtain the purely electronic absorption spectrum by solving the Bethe-Salpeter equation with all atoms fixed at their equilibrium positions using the OCEAN code [90, 111] with Quantum-ESPRESSO as the underlying DFT engine [66].

To model the gas phase we used a vacuum box of the size 20 $\mathring{A} \times 20$ $\mathring{A} \times 20$ $\mathring{A}$. The size of the box was converged with respect to the excited state forces. For the ground state calculation we used the LDA functional and norm-conserving pseudopotentials with a converged energy cutoff of 100 Ry. Convergence of the BSE calculations was reached for acetone by including 96 unoccupied bands for the core-hole screening calculation and 72 bands for the exciton basis. The result of the calculation is shown in Fig. 5.2. We focus on the $1s^1\pi^*$ feature at 531.5 eV.

To evaluate the exciton-vibron force constant we perform the numerical derivative in Eq. 5.23 explicitly by repeating the BSE calculation several times while moving the oxygen atom in order to make incremental adjustments to the C-O bond length. Then we construct the excited state potential energy surface as

$$E^*_\xi(Q_\nu) = E_{GS}(Q_\nu) + \Delta E_{eh}(Q_\nu) \ . \tag{5.24}$$

The BSE excitation energy $\Delta E_{eh}(Q_\nu)$ is obtained in this case by variation of the core-level energy and the energy of the $2p$ binding energy with respect to the conduction band minimum. The detailed results of the calculation are shown in Fig. 5.3. Finally the excited-state potential energy surface constructed as the sum of the ground-state PES and the BSE excitation energy is given in the inset of Fig. 5.2. The forces were obtained using numerical derivatives of the potential energy surface

$$F^\nu_{\xi\xi} = \lim_{\Delta Q_\nu \to 0} \frac{E^*_\xi(\Delta Q_\nu/2) - E^*_\xi(-\Delta Q_\nu/2)}{\Delta Q_\nu} \tag{5.25}$$

where the index ξ refers to the specific exciton present in the excited state calculation. For the CO and N_2 molecules the same set of calculations were performed for the $1s^1\pi^*$ excitation and the bond stretching mode.

As an alternative approach to obtain the exciton-phonon coupling constants we generated the excited-state potential energy surface with simpler self-consistent DFT

calculations using a core-hole pseudopotential and placing an extra electron in the LUMO orbital [60, 112]. In this case, the calculation for each molecule was done using the Quantum-ESPRESSO DFT package and PBE ultra-soft pseudo-potentials. Additional 1s core-hole pseudopotentials were used to simulate the XAS final state. The validity of the DFT plane-wave methods for the description of the these molecules was further verified by the reproduction of the ground state vibrational frequencies.

The derivative of the BSE-derived excited-state potential energy surface at the ground-state equilibrium bond length gives an exciton-vibrational force constant for the acetone molecule of $F = -7.6$ eV/Å for the bond stretching mode. This is equivalent to a value of $M = 0.35$ eV or $g = 5.4$. This is consistent with the value of $F = -7.7$ eV/Å obtained from the constrained core-hole DFT calculations. The same procedures were done for the CO (N_2) molecule resulting in a BSE force constant of $F = -13.7$ eV/Å ($F = -6.7$ eV/Å), corresponding to $M = 0.51$ eV ($M = 0.24$ eV) and $g = 9.7$ ($g = 0.92$), again showing good agreement with the constrained core-hole DFT result of $F = -11.7$ eV/Å ($F = -7.0$ eV/Å).

The phonon Green's function was modeled in the harmonic limit using the frequency obtained from a quadratic fit to the excited-state potential energy surface. For acetone, this gives $\omega = 0.15$ meV, while for CO we find $\omega = 0.164$ meV and for N_2 $\omega = 0.25$ meV. Although in the present case the frequencies can be observed experimentally as the energy separation between phonon side-bands. Anharmonic vibrational responses could be obtained through atomic displacement autocorrelation functions, as done for XPS, generated by excited-state molecule dynamic simulations or higher polynomial fitting of the excited state PES. However, beyond the challenge of such calculations, in many periodic systems the harmonic response will be sufficient.

With the exciton-phonon coupling constant and the phonon Green's function, we evaluate the exciton self-energy Σ_ξ in Eq. 5.17. The exciton cumulant is then formed by Eq. 5.40 and the imaginary part of the resulting full exciton Green's function gives the effective XAS spectral function. Since the cases we are considering (the oxygen $1s^1\pi^*$ resonance of acetone and CO, and the N K-edge of N_2) involve excitations into isolated levels, the exciton spectral function is effectively equivalent to the XAS signal. The pure electronic spectrum can be approximated as a single Lorentzian with core-hole lifetime broadening. Additional instrumental broadening was added using the

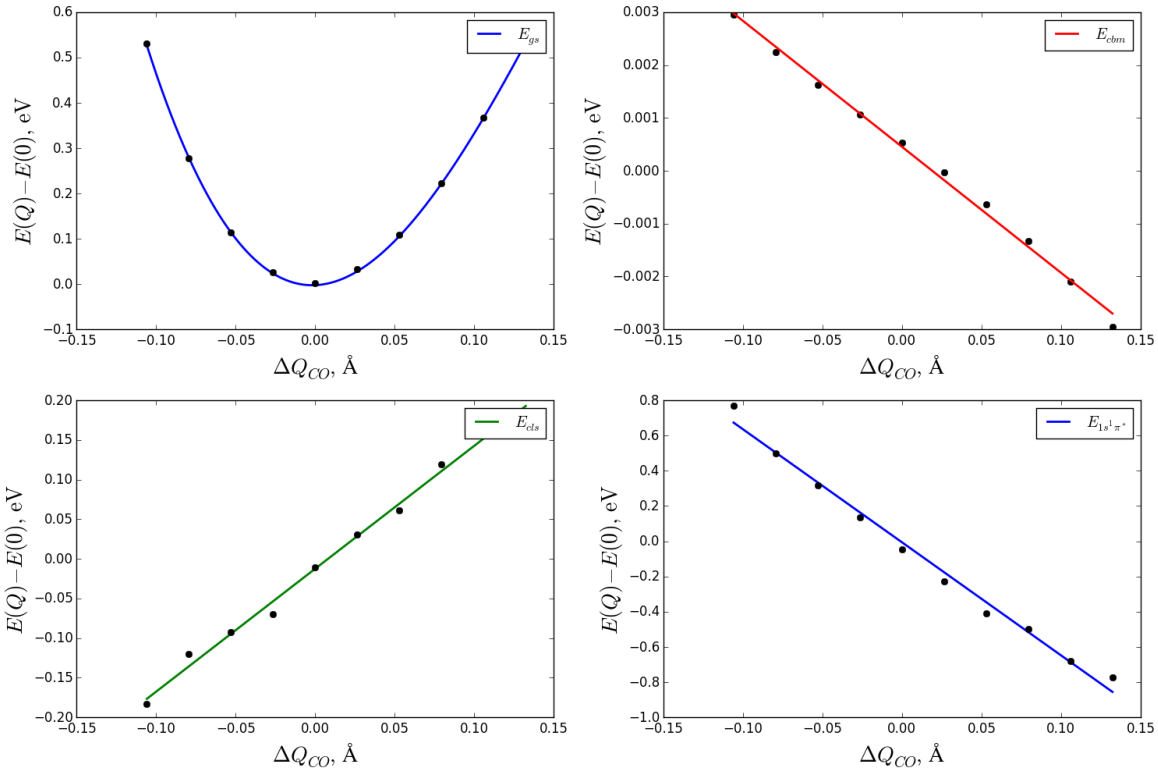

Figure 5.3: Details of calculating the exciton vibrational coupling for the acetone molecule within the frozen phonon framework. All sub-figures show a variation of the quantities used in the calculations with respect to displacement along the C-O stretching mode. From top to bottom and from left to right: variation of the ground state energy, core-level shift, energy of the conducting band minimum, shift of the electronic excitation $1s^1\pi^*$.

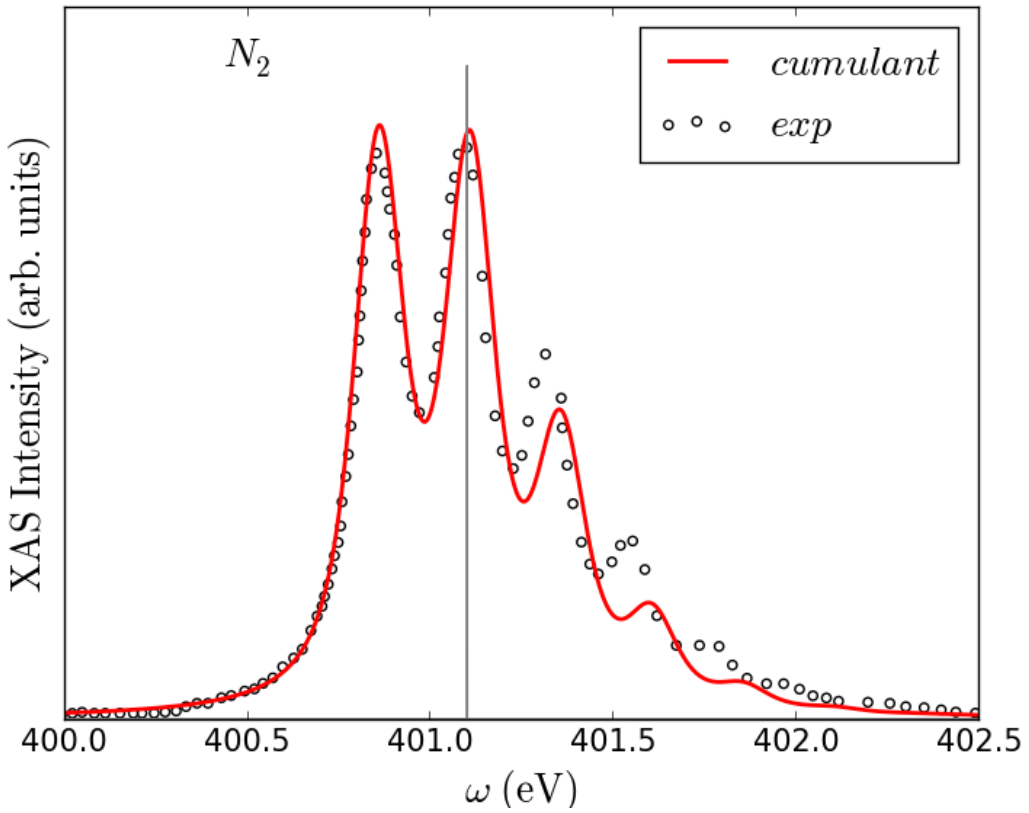

Figure 5.4: Comparison between experimental XAS spectra [113] (black circles) and calculation (red curve) using the cumulant ansatz for the exciton-phonon interaction at the K-edge of the N_2 molecule. The grey line corresponds to the position of the exciton in the absence of the exciton-phonon interaction. Small differences between the calculation and experiment regarding the positions and intensities of the phonon sidebands can be attributed to an-harmonic effects.

HWHM corresponding to the original experimental work [58, 113]. The final spectra are compared to the experimental data in Figs. 5.4 and 5.5, though sufficiently high resolution experimental data is not currently available for the XAS of acetone.

As with the XPS results, the energy shift of the quasiparticle peak and the degree of symmetry of the overall spectral shape depend on the exciton-phonon coupling strength. N_2 has a relatively weak coupling ($g \sim 0.92$), and its spectrum shows noticeable asymmetry while the coupling strength of CO is much larger ($g \sim 9.7$) and the spectrum is more symmetric. The overall agreement between the calculation and experiment for CO is quite good while deviations in the intensities of higher order satellites

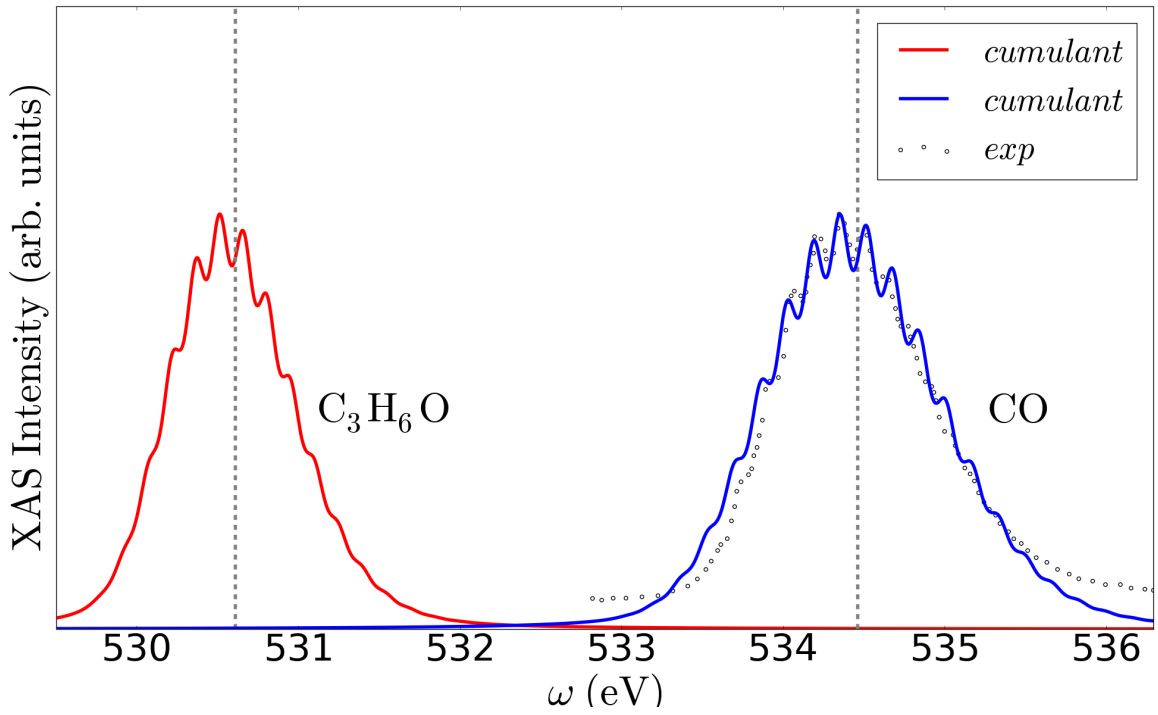

Figure 5.5: Comparison between experimental XAS spectra [114] (black circles) and calculations (red and blue curves) using the cumulant ansatz for the exciton-phonon interaction at the K-edge of oxygen of CO and acetone (C_3H_6O). The dashed lines correspond to the positions of the excitons in the absence of the exciton-phonon interaction.

are noticeable for N_2. This could indicate anharmonicity of the excited-state vibrations that were neglected in the calculation .

5.4 Discussions

We have reformulated the problem of two interacting particles (electron and hole) in the presence of Coulomb and electron-phonon interactions in terms of an excitonic quasi-particle that interacts with bosonic collective modes. This brings certain simplifications to the many-body calculations. However, it also hides the real quantities which are of interest to us, such as the electron-phonon coupling in the absence of a core-hole. We will now discuss how the electron-phonon coupling constant appears in the context of the exciton-phonon interaction, using a model Hamiltonian framework.

Secondly, regarding the numerical evaluation of the Fan-Migdal self-energy in the excitonic basis, it is desirable to find a 'cheaper' way than the frozen phonon approach to calculate the exciton-phonon matrix elements. The limitation of the frozen phonon approach is a necessity to use supercell BSE calculations for each momentum transfer $\boldsymbol{q}$. This, however, can be overcome in framework of the DFPT.

Finally, we address how to include exciton-phonon interband scattering terms. Such scattering may occur close to excitonic band intersections.

Model Hamiltonian Here we start with a simple model that is relevant for the L-edge XAS of transition metals

$$H = \sum_{\alpha} \epsilon_\alpha c_\alpha^+ c_\alpha - \epsilon_\beta c_\beta^+ c_\beta - \sum_{\alpha_1,\alpha_2} J_\beta^{\alpha_1\alpha_2} c_{\alpha_1}^+ c_{\alpha_2} c_\beta^+ c_\beta + \sum_{\alpha} U_{\alpha\beta} c_\alpha^+ c_\alpha c_\beta^+ c_\beta$$

$$- \sum_{\nu} M_{\beta\beta}^{\nu} c_\beta^+ c_\beta B_\nu + \sum_{\nu,\alpha_1,\alpha_2} M_{\alpha_1\alpha_2}^{\nu} c_{\alpha_1}^+ c_{\alpha_2} B_\nu + \sum_{\nu} \omega_\nu (b_\nu^+ b_\nu + \frac{1}{2}) \,. \tag{5.26}$$

We assume a minimal electronic Hilbert space consisting of two electronic levels $\alpha = \{1, 2\}$ and one hole level β. The particle operators c_α and c_β correspond to the electron and hole, respectively. We assume that the single particle energies $\epsilon_\alpha/\epsilon_\beta$ are defined in the presence of the valence electron-electron interactions, and explicitly treat only the electron-hole direct Coulomb $U_{\alpha\beta}$ and exchange $J_\beta^{\alpha_1\alpha_2}$ interactions. The electron and hole phonon interactions are treated by the linear term, neglecting second order couplings. The index ν stands for $\mathbf{q}, \lambda$ phonon wave vector and mode. The phonon operator is $B_\nu = b_{-\mathbf{q},\lambda}^+ + b_{\mathbf{q},\lambda}$. The choice of signs in the Eq. 5.26 implies that all constants are positive. The negative sign of the core-hole–phonon coupling highlights the sign difference of the particles and consequently different attraction/repulsion action on the ions. However it depends on the orbital structure of the absorbing atom and the screening.

We first consider the electronic part H_e of the Hamiltonian H

$$H_e = \sum_{\alpha} \epsilon_\alpha c_\alpha^+ c_\alpha - \epsilon_\beta c_\beta^+ c_\beta - \sum_{\alpha_1,\alpha_2} J_\beta^{\alpha_1\alpha_2} c_{\alpha_1}^+ c_{\alpha_2} c_\beta^+ c_\beta + \sum_{\alpha} U_{\alpha\beta} c_\alpha^+ c_\alpha c_\beta^+ c_\beta \,. \tag{5.27}$$

The corresponding Hilbert subspace has a dimension of 2 and the basis wave-functions

are $|\psi^1_{eh}\rangle = |\psi_{\alpha_1}\rangle\,|\psi_\beta\rangle$ and $|\psi^2_{eh}\rangle = |\psi_{\alpha_2}\rangle\,|\psi_\beta\rangle$. The excitonic basis is the defined by the eigenvectors of H_e which can be generalized to the BSE problem (Eq. 3.45). If the unitary operator S can canonically transform the electronic Hamiltonian $H'_e = S^{-1}H_eS$, then it also defines the expansion of excitonic states in terms of the independent particle-hole basis. The coefficients of the expansion are the elements of the inverse matrix ($|\psi_\xi\rangle = S^{-1}\,|\psi_{eh}\rangle$). For such a small system the matrix of the canonical transformation can be found analytically under the assumption that the Hamiltonian matrix is real and symmetric ($J_{21} = J_{12} = J$).

The coefficients can then be written in terms of model parameters

$$|\psi^e_{\xi_1}\rangle = -\frac{J}{D}\,|\psi^1_{eh}\rangle + \frac{\Delta + D}{2D}\,|\psi^2_{eh}\rangle \tag{5.28}$$

$$|\psi^e_{\xi_2}\rangle = \frac{J}{D}\,|\psi^1_{eh}\rangle + \frac{D - \Delta}{2D}\,|\psi^2_{eh}\rangle \ . \tag{5.29}$$

Here $D = \sqrt{\Delta^2 + 4J^2}$ and the difference between diagonal elements of the Hamiltonian H_e is $\Delta = \epsilon_{\alpha_1} - \epsilon_{\alpha_2} + U_{11} - U_{22} + J_{11} - J_{22}$.

The solution of the electronic Hamiltonian then can be defined on the bigger Hilbert space including phonon states as $|\psi_\xi\rangle = |\psi^e_\xi\rangle\,|\chi_{ph}\rangle$. The states $|\psi_\xi\rangle$ are the eigenstates of the Hamiltonian H with zero electron-phonon coupling. In the new basis $\{\psi_\xi\}$ the Hamiltonian from Eq. 5.26 becomes

$$\tilde{H} = \sum_\xi \epsilon_\xi a^+_\xi a_\xi + \sum_\nu \omega_\nu (b^+_\nu b_\nu + \frac{1}{2}) + \sum_{\nu,\xi_2,\xi_1} M^\nu_{\xi_1\xi_2} a^+_{\xi_1} a_{\xi_2} B_\nu \ . \tag{5.30}$$

The above transformation leads to a partial diagonalization of the Hamiltonian H. The electron-electron interaction is now absorbed by the energies ϵ_ξ and coupling constants in the new basis $M^\nu_{\xi,\xi'}$.

The Hamiltonian 5.30 describes the interaction of an exciton with phonons. The exact expressions for the exciton-phonon coupling for our model system are (under assumption that the variation of the model parameters J and U with respect to the phonon eigenvectors is zero)

$$M^{\nu}_{\xi_1\xi_2} = \sqrt{\frac{\hbar}{2N\mu\omega}} \langle\psi_{\xi_2}| \nabla_\nu V_{eff} |\psi_{\xi_1}\rangle = \sqrt{\frac{\hbar}{2N\mu\omega}} \sum_{i,j} A^{\xi_1}_i (A^{\xi_2}_j)^* \langle\psi^j_{eh}| \nabla_\nu V_{eff} |\psi^i_{eh}\rangle$$

$$= \sum_{i,j} A^{\xi_1}_i (A^{\xi_2}_j)^* [M^{\nu}_{\alpha_i\alpha_j} + M^{\nu}_{\alpha\alpha}] \ . \tag{5.31}$$

Using the relations between transform matrix elements and the parameters of the model 5.29 we obtain

$$\begin{aligned} M^{\nu}_{\xi_1\xi_1} &= \frac{J^2}{D^2}[M^{\nu}_{\alpha_1\alpha_1} + M^{\nu}_{\beta_1\beta_1}] + \frac{(\Delta+D)^2}{4D^2}[M^{\nu}_{\alpha_2\alpha_2} + M^{\nu}_{\beta_2\beta_2}] \\ &- \frac{J(\Delta+D)}{2D^2}[M^{\nu}_{\alpha_2\alpha_1} + M^{\nu}_{\beta_1\beta_2} + M^{\nu}_{\alpha_1\alpha_2} + M^{\nu}_{\beta_2\beta_1}] \end{aligned} \tag{5.32}$$

$$\begin{aligned} M^{\nu}_{\xi_1\xi_2} &= -\frac{J^2}{D^2}[M^{\nu}_{\alpha_1\alpha_1} + M^{\nu}_{\beta\beta}] - \frac{(D-\Delta)J}{2D^2}[M^{\nu}_{\alpha_1\alpha_2} + M^{\nu}_{\beta\beta}] \\ &+ \frac{(\Delta+D)J}{2D^2}[M^{\nu}_{\alpha_2\alpha_1} + M^{\nu}_{\beta\beta}] - \frac{(D^2-\Delta^2)}{4D^2}[M^{\nu}_{\alpha_2\alpha_2} + M^{\nu}_{\beta\beta}] \ . \end{aligned} \tag{5.33}$$

The remaining exciton-phonon matrix elements are simply symmetric to Eqs. 5.32 and 5.33 with respect to permutation of electronic levels.

Terms which can be considered as the exciton-phonon coupling (with no change in exciton states ($M^{\nu}_{\xi_1\xi_1}$)) involve both coupling (M_{α_1,α_1}) and scattering (M_{α_1,α_2}) from the single electron-hole basis representations. Also, even if the scattering term ($M^{\nu}_{\alpha_1\alpha_2}$) is small compared to the coupling term ($M^{\nu}_{\alpha_1\alpha_1}$) in the electron-hole basis this relation might not be satisfied in the exciton basis. This is due to a strong mixing effect of the exchange interaction on the electronic states. In contrast, the difference between the diagonal parts of the electronic interaction Δ in the absence of the exchange interaction does not significantly affect the composition of the resulting exciton-phonon couplings.

This model might be a prototype for the electron-phonon interaction in the L-edge spectra of transition metals in an octahedral crystal structure like $SrTiO_3$ with two conduction bands composed of 3d states (E_g and T_{2g}). Due to the strong multiplet effects the resulting exciton-phonon coupling is composed of many electron-phonon

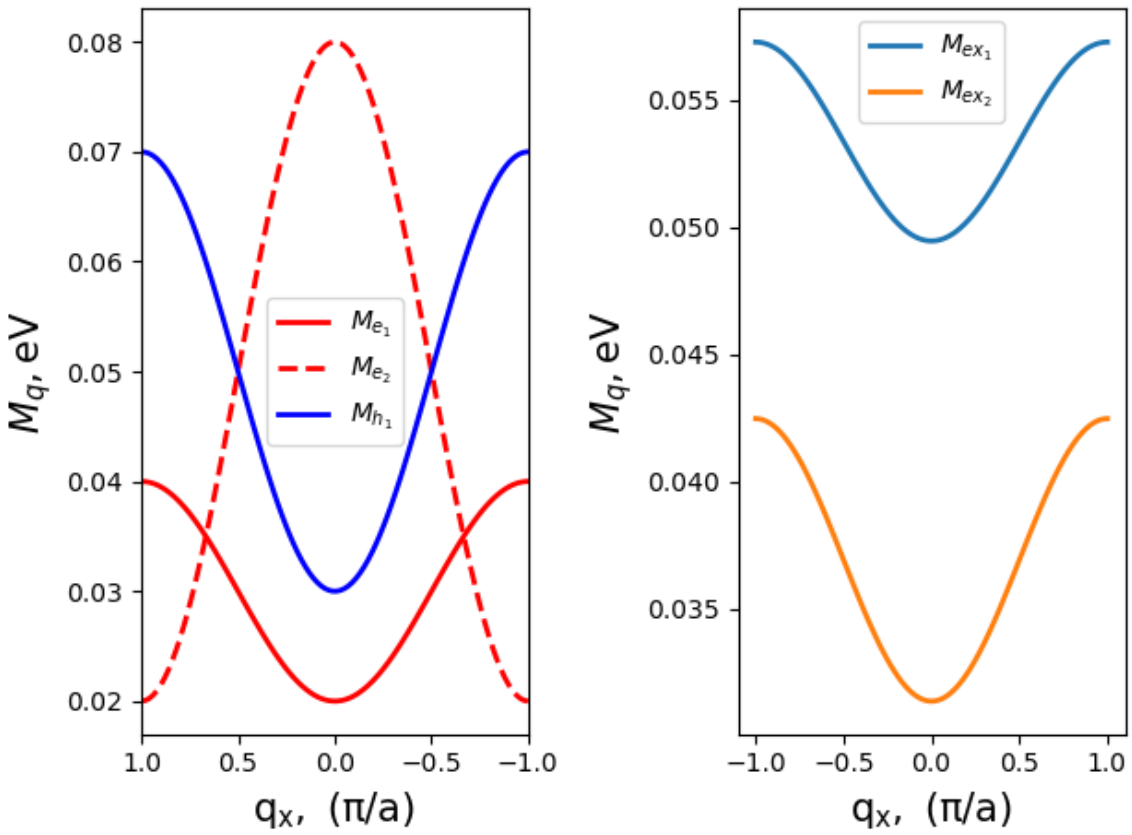

Figure 5.6: Model study of the exciton-phonon coupling. As a starting point the model with two conduction bands and one core-hole level was taken Eq. 5.26. Initial dispersion of the coupling constants is shown on the left side of the figure. Model parameters are $J = 0.3$ eV and $\Delta = 0.1$ eV. The resulting exciton-phonon coupling is shown on the right side of the figure. The interband scattering of the electron-phonon matrix elements is neglected.

coupling terms.

Similar mixing of the electron-phonon coupling may occur due to the strong Coulomb effects of the electronic valence levels. As an example one can consider a one band Hubbard model for a cuprate where the mixing comes from the hopping parts.

Connection to DFPT The calculation of exciton-phonon matrix elemets using density functional perturbation theory is computationally preferable since it employs mainly unit-cell calculations [11]. A reasonable approach for the calculation of excited-state forces within the BSE and DFPT frame-work was formulated in the work of

Ismail-Beigi and Louie [59]. In the following, we suggest a generalization of the excited state force calculation for the cases which includes scattering of an exciton. The excited state calculation of the exciton-phonon coupling should include both variations of the single particle energies and the variation of the interaction terms. In the BSE framework the latter are given by variation of the effective two particle term Eq. 3.45

$$\partial_q H_{BSE} = \partial_q \epsilon_\alpha - \partial_q \epsilon_\beta + \partial_q K_{\alpha,\alpha',\beta,\beta'} \ . \tag{5.34}$$

The first two terms are proportional to the variation of the quasi-particle Hamiltonian, which describes particle and hole excited states (it might include a GW corrections or in the limited cases it might be a regular KS Hamiltonian). From the Hellmann-Feynman theorem we have $\partial_q \epsilon_i = \langle \psi_i | \, \partial_q H_{qp} \, | \psi_i \rangle$. It is common to use static approximation for the BSE calculations [61, 62] $\frac{\delta W(1,2)}{\delta G(3,4)} = 0$. It means that the vertex function includes only a momentary interaction and neglects dynamical effects. The variation of the BSE kernel of Eq. 3.43 includes both variation of the single particle wave-functions and the vertex function. The W is a functional of the electron Green's funciton. From the chain rule the variation of W is $\partial_q W(1,4) = \frac{\delta W(1,\bar{2})}{G(\bar{3},4)} \partial_q G(\bar{3},4)$ and thus it is assumed to be zero [59]. One can argue about the importance of the dynamical effects, but in many cases [90] static calculations provide sufficient results for a pure electronic calculation. The remaining terms contain a variation of the wave-function and unperturbed kernel. The first-order correction to the wave-functions is

$$\partial_q \, | \psi_\alpha \rangle = \sum_{\alpha_1} | \psi_{\alpha_1} \rangle \, \langle \psi_{\alpha_1} | \, \partial_q \, | \psi_\alpha \rangle \cong \sum_{\alpha_1 \neq \alpha} | \psi_{\alpha_1} \rangle \, \frac{\langle \psi_{\alpha_1} | \, \partial_q V_{KS} \, | \psi_\alpha \rangle}{\epsilon_{\alpha_1} - \epsilon_\alpha} \ . \tag{5.35}$$

Finally projecting results of Eq. 5.34 onto the excitonic basis one can write the exciton-phonon coupling as

$$\begin{aligned} M^\nu_{\xi,\xi'} &= \sum_{\alpha,\alpha',\beta,\beta'} (A^\xi_{\alpha,\beta})^* A^{\xi'}_{\alpha',\beta'} [(M^\nu_{\alpha,\alpha} - M^\nu_{\beta,\beta}) \delta_{\beta,\beta'} \delta_{\alpha,\alpha'} \\ &+ \sum_{\alpha_1} \frac{(M^\nu_{\alpha_1,\alpha})^*}{\epsilon_{\alpha_1 \alpha}} K_{\alpha_1,\beta,\alpha',\beta'} + \sum_{\alpha_1} \frac{(M^\nu_{\alpha_1,\alpha'})}{\epsilon_{\alpha_1 \alpha'}} K_{\alpha,\beta,\alpha_1,\beta'} \\ &+ \sum_{\beta_1} \frac{(M^\nu_{\beta_1,\beta})^*}{\epsilon_{\beta_1 \beta}} K_{\alpha,\beta_1,\alpha',\beta'} + \sum_{\beta_1} \frac{(M^\nu_{\beta_1,\beta'})}{\epsilon_{\beta_1 \beta'}} K_{\alpha,\beta,\alpha',\beta_1}] \ . \end{aligned} \tag{5.36}$$

Here $\epsilon_{\alpha\beta} = \epsilon_\alpha - \epsilon_\beta$ and $M^\nu_{\alpha,\alpha'}$, $M^\nu_{\beta,\beta'}$ are electron-phonon and core-hole phonon matrix elements which can be directly found using DFPT formalism [11, 17, 66] (see also Appendix B). Thus one can use the DFPT calculations to obtain the exciton coupling constant including first order corrections to the BSE kernel.

Interband scattering If the non-diagonal exciton-phonon interaction is strong compared to the energy gap between excitonic bands (in areas of intersection) the general form of the expansion of the Green's function is

$$i\Lambda_{\xi\xi'}(t,t') = \sum_n \frac{(-i)^{2n}}{(2n)!} \int .. \int d\tau_1 d\tau_{2n} \left\langle 0 \right| T a_{\xi'}(t) V_1(t_1) V_{2n}(t_{2n}) a^+_\xi(t') \left| 0 \right\rangle_c \ . \tag{5.37}$$

Momentum conservation implies $k_\xi = k_{\xi'}$ and $n_\xi = n_{\xi'}$. The second order self-energy contains electron-phonon matrix elements of two different scattering events. The exciton scatters first from the initial state ξ to the intermediate ξ_1 and then to ξ'

$$\Sigma_{\xi\xi'}(t,t') = i \sum_{n_{\xi_1}, k_{\xi_1}, \nu} M^\nu_{\xi',\xi_1} M^\nu_{\xi',\xi_1} L_{\xi_1}(t-t') D_\nu(t-t') \delta_{k_\xi, k'_\xi} \ . \tag{5.38}$$

The general ansatz for the solution in terms of cumulants is [78]

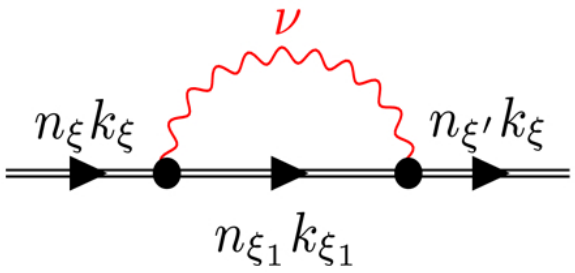

Figure 5.7: Lowest order bubble diagram, which shows the interband scattering event. The momentum and band index of an exciton appear as k_ξ and n_ξ respectively.

$$\Lambda_{\xi\xi'}(t,t') = L_\xi(t,t') e^{C_{\xi\xi'}(t)} \ . \tag{5.39}$$

Following the same steps as in the previous section for the diagonal contribution, the expression for the second order cumulant with non-diagonal matrix elements is formally

(using Eq. 5.38) given by

$$\begin{aligned} C_{\xi\xi'}(t,t') &= -[L_\xi(t-t')]^{-1} \\ &\times \int\int d\tau_1 d\tau_2 L_\xi(t-\tau_1)\Sigma_{\xi\xi'}(\tau_1,\tau_2)L_{\xi'}(\tau_2-t') \ . \end{aligned} \tag{5.40}$$

The above approximation for the cumulant has to be of the same accuracy as for the interband scattering since it includes the same type of diagrams. However, the number of electron-phonon matrix elements increases the total number of possible states for scattering and consequently the computational expense. The presence of the non-diagonal Green's function elements also breaks the approximation to get Eq. 5.21. The full spectrum is no longer proportional to the density of states since it contains a sum over all elements of the imaginary part of the Green's function rather than the trace

$$\mu(\omega) = -\frac{1}{\pi}\sum_{\xi_1,\xi_2}(d_{\xi_1})^* d_{\xi_2}\mathrm{Im}\ \Lambda_{\xi_1\xi_2}(\omega) \ . \tag{5.41}$$

Such a generalization allows accounting for contributions from dark exciton states (not accessible by direct transition from the core-level).

5.5 Conclusion

The main result of this section is the formalism for providing a convenient and efficient solution of the electron-phonon coupling problem for neutral excitations. Using the Green's function formalism, we developed an efficient method to account for the phonon contribution to XAS. In the spirit of the BO approximation, we suggested that the solution of the two particle problem could be effectively found by separating the electron-phonon and the electron-electron interactions. We first solved the problem of the interacting electron and hole in the absence of the electron-phonon interaction. Using the solution of the BSE problem, we constructed an effective quasiparticle exciton propagator. We then dressed the exciton-propagator with phonons using the cumulant ansatz. The exciton-phonon matrix elements were calculated for an excited state configuration using the frozen-phonon approach. The formalism was tested on molecules which show strong vibrational contributions in XAS. The results of these calculations are in good agreement with high-resolution experimental spectra for the oxygen and nitrogen K-edge in CO and N_2.

This result serves as a basis for the correct interpretation of RIXS spectra. In XAS, the Green's function appears to be diagonal in the vibrational space. This makes absorption spectra proportional to the spectral function of the exciton. Even though this condition is not held in the RIXS process, the virtual intermediate state of RIXS is the final state of the XAS process. Thus, with some modifications we can apply this formalism in the context of RIXS.

Chapter 6

Green's function approach to RIXS

To obtain parameters of the electron-phonon interaction from the RIXS experiment one has to understand the formation of the phonon contribution to RIXS. Here we employ the first principle type of calculations as an ultimate test of the approximation we made. The phonon contribution requires treatment which is going beyond the present well-established methods to calculate X-ray spectra for solids. Thus the objective of this section will be the development of a rigorous way to calculate the dynamical (phonon) contribution to RIXS spectra with the possibility of application to the crystalline materials.

Contents

6.1 Introduction

The general introduction to RIXS techniques and in particular to the phonon contribution were given in Chapter 2. The numerical limitations and difficulty of the problem lead to the extensive model studies. The motivation for our work was the absence of the rigorous approach to treat electron-phonon interaction in the RIXS process, which is applicable to solids. Moreover, we argue that previous studies mistreated significant contribution from the electron-hole and hole-phonon interactions. The argument for this was a screening of the core-hole, however, the numerical conformation was missing. Those interactions are generally crucial for the excited state problems and lead to the quantitative and qualitative differences in the resulting value of the electron-phonon coupling. In this section we will focus on the phonon contribution to the quasi-elastic line, i.e., the electronic final state has to be the ground state. However, the low-energy boson excitations will have a non-thermal population at the end of the RIXS process.

6.2 Convolution of XAS and XES

One of common approximations for Kramers-Heisenberg equation presents RIXS as a convolution of the XAS-like spectra and the XES spectra with resonant denominator [50]. The advantage of such approach is a direct connection to the first order processes, but at the same time it is the lowest order approximation

$$\sigma^0(\omega_i, \omega_{loss}) = \int d\omega_1 \frac{\mu_e^0(\omega_1)\tilde{\mu}_a^0(\omega_i - \omega_1 - \omega_{loss})}{|\omega_1 - \omega_{loss} + i\Gamma|^2} \ , \tag{6.1}$$

where μ_e^0 is single particle emission and slightly modified $\tilde{\mu}_a^0$ absorption spectra. $\tilde{\mu}_a^0$ involves incoming energy dependent transition operators instead of regular dipole operators due to the difference between intermediate and final state core-hole potentials. And Γ is an inverse intermediate state lifetime. The zero superscript means that those quantities are calculated in the single particle picture in absence of the electron-phonon interactions.

Taking into account the spectral function representation of the XAS (Eq. 5.20) and XES we can correct the pure electronic transition using a convolution with the

vibronic spectral functions. So the resulting RIXS cross-section can be presented as a convolution of the pure electronic cross-section 6.1 and the effective vibrational spectral function

$$\sigma(\omega_i, \omega_{loss}) = \int\int d\omega' d\omega \sigma^0(\omega_i - \omega', \omega_{loss} - \omega' + \omega")A_{eff}(\omega', \omega'') \ . \tag{6.2}$$

Such form of the convolved cross-section is similar to the one presented in work of Kas *et al* [50] regarding plasmonic contribution to RIXS although the effective spectral function is different

$$A_{eff}(\omega', \omega'') = A_a(\omega')A_e(\omega', \omega'') \ . \tag{6.3}$$

Here the absorption spectral function is the same as in the previous chapter (see 5.20). The transition probabilities for emission case are different for different initial number of phonons n_0. Therefore spectral function has to be modified accordingly $A_e(\omega', \omega'') = \sum_{n_0,\nu} \frac{1}{\pi} \text{Im } G_e^{n_0}(\omega")\delta(\omega' - n_0\omega_\nu)$. The delta function $\delta(\omega' - n_0\omega_\nu)$ allows explicitly connect absorption process and initial population of phonon levels for emission process. Thus A_{eff}^{ae} it takes into account that the initial phonon states for XES process were populated by the XAS process. The details on the XAS/ XES transitions with non-equilibrium phonon population can be found in Appendix C.

Such consideration, however, contains weaknesses and resulting effective spectral function reproduces vibrational RIXS badly. To point out what is missing we will rewrite the KH equation using the notation for interference and incoherent terms. Expanding the square of the matrix elements ($(\sum_i A_i)^2 = \sum_i (A_i)^2 + 2\sum_{i<j} A_i A_j$) we obtain

$$\sigma_{coh}(\omega_i, \omega_{loss}) = \sigma_{incoh}(\omega_i, \omega_{loss}) + \sigma_{interf}(\omega_i, \omega_{loss}) \ . \tag{6.4}$$

Here full cross-section is denoted as coherent one, the incoherent part contains only the sum of the squares

$$\sigma_{incoh}(\omega_i, \omega_{loss}) = \sum_F \sum_M \left| \frac{\langle \Psi_F | \Delta_o^+ | \Psi_M \rangle \langle \Psi_M | \Delta_i | \Psi_I \rangle}{\omega_i - (E_M - E_I) + i\Gamma_M} \right|^2 \delta(\omega_{loss} - (E_F - E_I)) \tag{6.5}$$

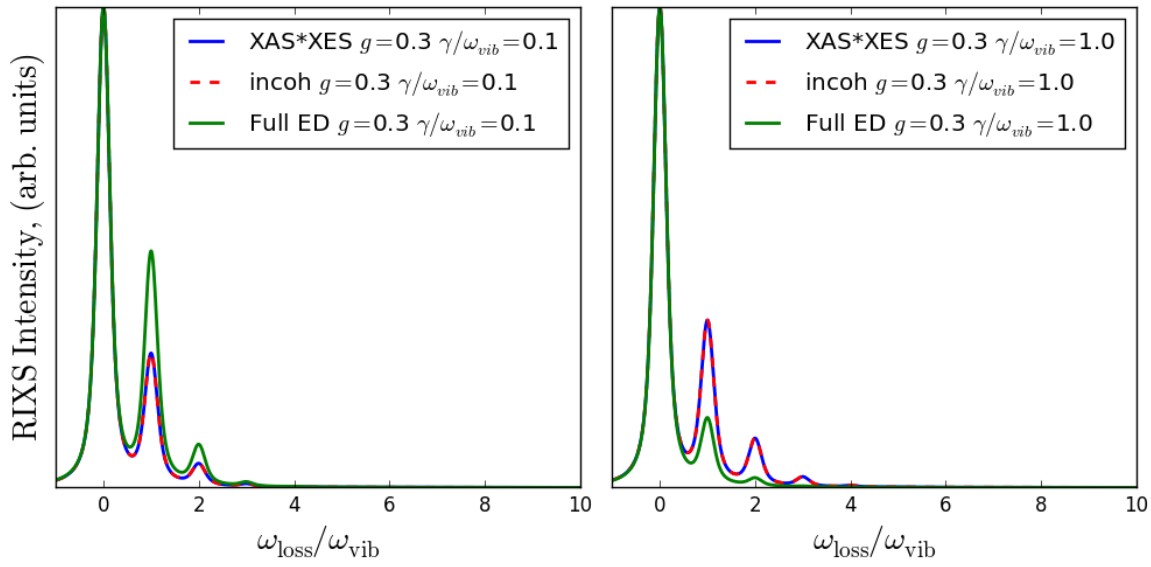

Figure 6.1: Model calculation of the phonon contribution in RIXS using a convolution with spectral function (blue line) and the results of the full Kramer-Heisenberg equation plus exact diagonalization calculations for the coherent and incoherent part σ_{coh} and σ_{incoh}. On the left panel the results are shown for the long core-hole lifetime limit and the opposite case on the right.

The interference part σ_{intef} contains all terms with a cross intermediate states. The results of the model calculation (see Fig.6.2) suggests that the separation of the RIXS effective spectral function into XES and XAS-like components neglects the quantum interference effects which are present in the KH equitation. Inspecting carefully KH and spectral function w given in Eq. 6.3, one can conclude that $|\langle\Psi_f|\,\Delta_o^+\,|\psi_m\rangle|^2$ and $|\langle\Psi_m|\,\Delta_i\,|\Psi_i\rangle|^2$ (i.e. the incoherent parts) are present in the spectral function consideration. However matrix elements $\langle\Psi_f|\,\Delta_o^+\,|\Psi_{M_1}\rangle\,\langle\Psi_{M_1}|\,\Delta_i\,|\Psi_i\rangle$ are omitted, where Ψ_{M_1}, Ψ_{M_1} represent different intermediate phonon states. Due to the importance of the interference part we developed more rigorous approach to find a proper effective spectral function. For this purpose we combined the cumulant expansion and consideration of the off-diagonal exciton Green's function.

6.3 Kramers-Heisenberg equation in the excitonic basis

Green's functions to RIXS In contrast to the absorption cross-section, KH equation is not simply proportional to the two particle spectral function since the final state might has a non-thermal equilibrium population of the phonon excitations. However, we still can rewrite the KH equation in terms of Green's function. Expanding square in Eq. 2.5 we obtained

$$\sigma(\omega_i, \omega_{loss}) = \sum_F \sum_{M_2,M_1} \frac{\langle \Psi_I | \Delta_o | \Psi_{M_1} \rangle \langle \Psi_{M_1} | \Delta_i^+ | \Psi_F \rangle}{\omega_i - (E_M - E_I) + i\Gamma_M} \frac{\langle \Psi_F | \Delta_o^+ | \Psi_{M_2} \rangle \langle \Psi_{M_2} | \Delta_i | \Psi_I \rangle}{\omega_i - (E_M - E_I) - i\Gamma_M}$$

$$\times \delta(\omega_{loss} - (E_F - E_I)) \ . \tag{6.6}$$

The sum over final states together with delta function is proportional to the imaginary part of the many-body Green's function operator Im $G_F(\omega) = -\frac{1}{\pi} \sum_F |\psi_F\rangle \langle \psi_F| \, \delta(\omega - \omega_F)$. Although keeping assumption that the final state wave-function contains no excitations apart from the phonons one can approximate many body final state Green's function as a phonon one ($G_f \sim D$). In the similar way the intermediate state propagation reads in terms of Green's function $\Lambda(\omega) = \sum_M \frac{|\Psi_M\rangle\langle\Psi_M|}{\omega - E_M + i\Gamma_M}$. And finally the cross-section 6.6 in terms of final and intermediate states Green's functions reeds as

$$\sigma(\omega_i, \omega_{loss}) = -\frac{1}{\pi} \mathrm{Im} \ \langle \Psi_I | \Delta_o \Lambda(\omega_i + E_i) \Delta_i^+ D(\omega_{loss}) \Delta_o^+ \Lambda^+(\omega_i + E_I) \Delta_i | \Psi_I \rangle \ , \tag{6.7}$$

In this representation the cross-section is given as an expectation value of three Green's function operators without neither the intermediate nor the final state wave-functions. However, in contrast to XAS, the evolution of such product does not lead to simple representation. Thus we will attack this problem from the different perspective. Going one step back we will introduce explicitly sum over the final state and present the problem in terms of the off-diagonal intermediate state Green's function.

Using completeness of the final state basis which consists of the various phonon states, the final state Green's function operator can be turned into non-thermal prop-

agator

$$\sigma(\omega_i, \omega_{loss}) = -\frac{1}{\pi}\mathrm{Im} \sum_{F_1,F_2} \langle \Psi_I | \Delta_o \Lambda(\omega_i + E_i)\Delta_i^+ | \psi_{F_2} \rangle \langle \psi_{F_2} | D(\omega_{loss}) | \psi_{F_1} \rangle$$

$$\times \langle \psi_{F_1} | \Delta_o^+ \Lambda^+(\omega_i + E_I)\Delta_i | \Psi_I \rangle \ \ i \tag{6.8}$$

The electronic part of the RIXS intermediate state is the same as a final state in the XAS process. In close analogy to the XAS we will approximate the electronic many-body intermediate state Green's function as a two-particle Green's function. We also neglect possible phonon-phonon interaction, and thus the phonon Green's function has to be diagonal (δ_{F_1,F_2}).

Thus evaluation of the RIXS cross-section is directly connected to the evaluation of the off-diagonal elements of the intermediate state Green's function. We will now rewrite it in the excitonic basis (taking into account advantage of the excitonic basis for the XAS problem) and inspect the origin of the off-diagonal parts.

The initial state in the zero-temperature limit contains no-phonons and no-electronic excitations. Here and after we will use $|\psi_I\rangle = |0\rangle |n_i = 0\rangle$, where the $n_i = 0$ is the occupation number of the phonon initial state. The final state $|\psi_F\rangle = |0\rangle |n_f\rangle$ contains no-electronic excitations (and consequently no interaction with phonons), however it describes non-thermal population of the phonon states n_f.

In the excitonic basis KH equation 6.8 can be written using $|\psi_\zeta\rangle = |\psi^e_\xi\rangle |n_{ph}\rangle$. The electronic part of the wave-function $|\psi^e_\xi\rangle = \sum_{e,h} A^\xi_{e,h} |e,h\rangle$ is a solution of the pure electronic BSE problem. Inserting complete set of the new basis states $\sum_\zeta |\psi_\zeta\rangle \langle\psi_\zeta| = 1$ (index $\zeta = \{\xi, n_{ph}\}$ runs over both electronic and vibrational states) in Eq. 6.7 we have

$$\sigma(\omega_i, \omega_{loss}) = -\frac{1}{\pi}\mathrm{Im} \sum_{F,\zeta_1,\zeta_2,\zeta_3,\zeta_4} \langle \psi_I | \Delta_o | \psi_{\zeta_1} \rangle \langle \psi_{\zeta_1} | \Lambda(\omega_i + E_i) | \psi_{\zeta_2} \rangle \langle \psi_{\zeta_2} | \Delta_i^+ | \psi_F \rangle$$

$$\times \langle \psi_F | \Delta_o^+ | \psi_{\zeta_3} \rangle \langle \psi_{\zeta_3} | \Lambda^+(\omega_i + E_I) | \psi_{\zeta_4} \rangle \langle \psi_{\zeta_4} | \Delta_i | \psi_I \rangle D^{n_f}(\omega_{loss}) \quad . \tag{6.9}$$

Let's focus first on the matrix elements with the electron-photon operators. Since they operate only on electronic space the phonon part of the wave-function remains

unchanged

$$d^o_\zeta = \langle\psi_I|\,\Delta_o\,|\psi_\zeta\rangle = \langle n_i=0|\,\langle 0|\,\Delta_o\,|\psi_\xi\rangle\,|n=0\rangle = \langle 0|\,\Delta_o\,|\psi_\xi\rangle$$

$$d^i_\zeta = \langle n_i=0|\,\langle 0|\,\Delta_i\,|\psi^e_\xi\rangle\,|n=0\rangle = \langle 0|\,\Delta_i\,|\psi^e_\xi\rangle \tag{6.10}$$

and similar for final states

$$d^o_\zeta = \langle\psi_F|\,\Delta_o\,|\psi_\zeta\rangle = \langle n_f|\,\langle 0|\,\Delta_o\,|\psi_\xi\rangle\,|n_f\rangle = \langle 0|\,\Delta_o\,|\psi_\xi\rangle$$

$$d^i_\zeta = \langle n_i=0|\,\langle 0|\,\Delta_i\,|\psi^e_\xi\rangle\,|n=0\rangle = \langle 0|\,\Delta_i\,|\psi^e_\xi\rangle\ . \tag{6.11}$$

From the form of the electron-photon interaction one can see that the matrix elements d^o_ξ, d^o_ξ contain information about polarization and wave-vector of the incoming and outgoing photon, although for now we will treat them as known. In an explicit notations of the exciton and the phonon part of the wave-functions the KH equation becomes

$$\sigma(\omega_i,\omega_{loss}) = -\frac{1}{\pi}\sum_{f,n_f}\sum_{\xi_1,\xi_2} d^o_{\xi_2}(d^i_{\xi_1})^+\,\langle n_i|\,\langle\psi_{\xi_2}|\,\Lambda(\omega_i)\,|\psi_{\xi_1}\rangle\,|n_f\rangle$$

$$\times d^i_{\xi_2}(d^o_{\xi_1})^+\,\langle n_f|\,\langle\psi_{\xi_1}|\,\Lambda^+(\omega_i)\,|\psi_{\xi_2}\rangle\,|n_i\rangle\,\mathrm{Im}\ D^{n_f}(\omega_{loss})\ . \tag{6.12}$$

Here $D^n(\omega) = \langle n|\,D(\omega)\,|n\rangle$ is a non-thermal phonon Green's function and it controls the number of phonons in the final state. Two exciton Green's functions are responsible for the amplitude of the peaks with energy loss equals to the energy of the phonon state n_f (their product gives the RIXS amplitude). Both of them are non-diagonal in electronic and vibrational subspaces

$$\Lambda^{(n_i,nf)}_{\xi_1,\xi_2}(\omega) = \langle n_i|\,\langle\psi_{\xi_1}|\,\Lambda(\omega)\,|\psi_{\xi_2}\rangle\,|n_f\rangle\ . \tag{6.13}$$

Assuming zero-initial phonon population ($n_i = 0$) from now on only one superscript will be used to denote off-diagonal elements in vibrational space. In case of $n_f = 0$ (elastic line contribution) the exciton Green's function becomes diagonal in vibrational space and reduces to the one which was evaluated for the XAS case Eq.5.13.

Equation 6.13 does not contain explicit summation over the intermediate states, which can be seen as a significant simplification of the problem. Nevertheless it contains

explicit summation over final state phonons ($f = \lambda, \mathbf{q}, n_{\lambda,\boldsymbol{q}}$), which in fact can be reduced to the manageable range.

In absence of the exciton-phonon interaction $\Lambda^0_{\xi\xi} = L_\xi$ is diagonal in the excitonic basis and the cross-section reduces to merely weighted delta function form

$$\sigma(\omega_i, \omega_{loss}) = -\frac{1}{\pi} \sum_\xi |d^o_\xi|^2 |d^i_\xi|^2 |L_\xi(\omega_i)|^2 \delta(\omega_{loss}) \ . \tag{6.14}$$

Eq. 6.12 is written in the assumption of the quasi-elastic limit but may, also be generalized for other electronic configurations of the final state. In the following section, we will discuss the evaluation of RIXS amplitudes using the off-diagonal exciton Green's functions.

6.4 Off-diagonal Green's function

The off-diagonal in vibrational space elements of the Green's function breaks the condition of the conservation of the number of particles. During the scattering of an exciton from time t' to t there is a non-zero probability to create some number of phonons which will remain in the system at the moment of the annihilation of the exciton.

For simplicity we will consider one phonon mode and wave-vector, and afterwards we will generalize it for an arbitrary numbers of modes. The final state phonon wave function $|n_\nu\rangle = \frac{(b^+_\nu)^{n_\nu}}{\sqrt{n_\nu!}} |0\rangle$ is related to the ground state (no phonons and no excitons) wave-function $|0\rangle$ with a bosonic normalization factor. Rewriting Eq. 6.13 in time domain we have

$$i\Lambda^{(n_\nu)}_{\xi_1,\xi_2}(t,t') = \frac{1}{\sqrt{n_\nu!}} \langle 0| \, b^{n_\nu}_\nu(t) a_{\xi_1}(t) S(t,t') a^+_{\xi_2}(t') \, |0\rangle \ . \tag{6.15}$$

The phonon annihilation operators $b_\nu(t)$ make the equation different from the one which we used for diagonal in vibrational space Green's function (see XAS Chapter) 5.10. After expanding the S-matrix presence of such operators gives rise to a non-closed

type of diagrams. The S-matrix as defined before by the exciton-phonon interaction is

$$S(t,t') = Te^{-i\int_{t'}^{t} dt_1 V(t_1)} \ . \tag{6.16}$$

The time-dependent interaction term in the Hamiltonian is ($V = H - H_0$)

$$V(t) = \sum_{\xi_1,\xi_2,\nu} M^{\nu}_{\xi_2\xi_1} a^{+}_{\xi_2}(t) a_{\xi_1}(t) B_{\nu}(t) \ . \tag{6.17}$$

Here and after index $\nu = \lambda, q$ represents the mode and the wave-vector of the phonon. Here, as well as in previous chapters, we will focus on the linear electron-phonon coupling and then shortly discuss contribution form the higher-order terms.

6.5 No-recoil limit

As we saw without an exciton-phonon interaction the full Green's function is diagonal in both electronic and vibrational spaces (Eq. 6.14). First we will consider the localized excitation which interacts with the local vibrational mode. This can significantly simplify the structure of the resulting Green's function, making it diagonal in the excitonic but still non-diagonal in vibrational space. The exciton-phonon interaction term in this limit is

$$V = \sum_{\lambda,\xi} M^{\lambda}_{\xi\xi} a^{+}_{\xi} a_{\xi} B_{\lambda} \ . \tag{6.18}$$

We denote final state phonon mode as λ' and for simplicity we drop this index in the notation for the off-diagonal Green's function leaving only n as a superscript denoting the number of phonons in the final state. The expansion of the S-matrix leads to the following time-ordered series in exciton-phonon interactions ($t' = 0$)

$$\Lambda^{(n)}(\xi,\xi,t) = -i\sum_{m=0}^{\infty} \frac{(-i)^{2m}}{(2m)!} \int_0^t dt_1 \cdots \int_0^t dt_{2m} \left\langle 0 \right| T(b_{\lambda'}(t))^n a_{\xi}(t) V(t_{2m}) \cdots V(t_1) a^{+}_{\xi}(0) \left| 0 \right\rangle \ . \tag{6.19}$$

here and after we implicitly suggest consideration of only connected diagrams [12] in the S-matrix expansions. We will first consider the results for $n = 0, 1$ and then

write down the generic solution of these series for an arbitrary number of final state phonons. The term with zero real (final state) phonons can be written formally as

$$\Lambda^{(0)}(\xi,\xi,t) = -i\sum_{m=0}^{\infty}\frac{(-i)^{2m}}{(2m)!}\int_0^t dt_1\cdots\int_0^t dt_{2m}\,\langle 0|\,Ta_\xi(t)V(t_{2m})\cdots V(t_1)a_\xi^+(0)\,|0\rangle \ . \tag{6.20}$$

Since H^0 commutes with the number operator $a_\xi^+ a_\xi$ and all exciton lines have the same index ξ, we may factor out the bare exciton Green's function $iL_\xi(t) = \langle 0|\,Ta_\xi(t)a_\xi^+(0)\,|0\rangle$ from this series [12, 74, 75] leaving

$$\Lambda^{(0)}(\xi,\xi,t) = L_\xi(t)\sum_{m=0}^{\infty}\frac{(-i)^{2m}M_{\xi\xi}^{\lambda_1}\cdots M_{\xi\xi}^{\lambda_{2m}}}{(2m)!}$$

$$\times\sum_{\lambda_1\ldots\lambda_{2m}}\int_0^t dt_1\cdots\int_0^t dt_{2m}\,\langle 0|\,TB_{\lambda_{2m}}(t_{2m})\cdots B_{\lambda_1}(t_1)\,|0\rangle \ . \tag{6.21}$$

After pairing all phonon operators into phonon Green's function the series can be summed up giving an exponential generating function $\exp[C_\xi(t)]$ which involves only interactions with virtual phonons [75]. We thus obtain

$$\Lambda^{(0)}(\xi,\xi,t) = L_\xi(t)e^{C(t)} \ , \tag{6.22}$$

where the $C_\xi(t)$ is the second order cumulant introduced in the previous section. And imaginary part of $\Lambda^{(0)}(\xi,\xi,t)$ is proportional to the spectral function of an exciton ξ.

For the case of one real (final state) phonon (n=1), two types of phonon Green's function will be present in the expansion Eq. 6.20 after pairing all phonon operators. One is related to the propagation of virtual phonons, and the other describes the real phonon. Using the same argument as before, we factor the bare exciton propagator out of the series

$$\begin{aligned}\Lambda^{(1)}(\xi,\xi,\lambda',t) &= L_\xi(t)\sum_{m=0}^{\infty}\frac{(-i)^{2m}M_{\xi\xi}^{\lambda_1}\cdots M_{\xi\xi}^{\lambda_{2m}}}{(2m+1)!}\\ &\sum_{\lambda_1\ldots\lambda_{2m+1}}(\ 2m\ +1)\int_0^t dt_{2m+1}M_\xi^{\lambda'}\,\langle 0|\,TB_{\lambda_{2m+1}}(t_{2m+1})b_{\lambda'}(t)\,|0\rangle\,\delta_{\lambda'\lambda_{2m+1}}\\ &\times\int_0^t dt_1\cdots\int_0^t dt_{2m}\,\langle 0|\,TB_{\lambda_{2m}}(t_{2m})\cdots B_{\lambda_1}(t_1)\,|0\rangle \ .\end{aligned} \tag{6.23}$$

The main difference between $\Lambda^{(1)}$ and $\Lambda^{(0)}$ is the presence of the first integral, with integration variable t_{2m+1}. This integral contains the real phonon with one vertex and a single time integration variable and may be condensed to the expression

$$Y(\xi, \lambda', t) = iM_{\xi}^{\lambda'} \int_0^t D_{\lambda'}^{>}(t-\tau)d\tau \ . \tag{6.24}$$

Since this Y factor does not involve virtual phonons it may be considered separately. It appears $2m{+}1$ times in the $(2m{+}1)$-th term in the expansion of Eq. 6.23 and combines with $\frac{1}{(2m+1)!}$ to give a final factor of $\frac{1}{(2m)!}$. If we factor this term out of the sum, the remaining terms are the same as the $\Lambda^{(0)}$ contribution for the virtual phonon dressed exciton propagator. This gives

$$\Lambda^{(1)}(\xi, \xi, \lambda', t) = \Lambda^{(0)}(\xi, \xi, t) Y(\xi, \lambda', t) \ . \tag{6.25}$$

Extending this result to an arbitrary number of final state phonons we have

$$\Lambda^{(n)}(\xi, \xi, \lambda', t) = \Lambda^{(0)}(\xi, \xi, t) \frac{[Y(\xi, \lambda', t)]^n}{\sqrt{n!}} \ . \tag{6.26}$$

The factor $\frac{1}{\sqrt{n!}}$ comes from the normalization of the final-state vibrational wave-function. Thus the off-diagonal elements of exciton Green's function can be expressed as the product of the diagonal contributions and the phonon vertex. The Eq.6.26 gives an exact solution in this limit. The non-local character of the phonon excitations also can be included within such approximation and leads to the same answer (Eq. 6.26),

$$\forall \boldsymbol{q} : \ M^{\nu}_{\boldsymbol{k}_\xi, \boldsymbol{k}_\xi + q} = M^{\nu}_{\boldsymbol{k}_\xi, \boldsymbol{k}_\xi}; \ \epsilon_{\boldsymbol{k}_\xi + \boldsymbol{q}} = \epsilon_{\boldsymbol{k}_\xi} \ . \tag{6.27}$$

The physical meaning of this limit can be viewed as flat, (dispersionless) excitonic bands. Thus if one can neglect the exciton intra-band scattering, the resulting coupling constant as well as exciton energy will stay the same through all the momentum space.

6.6 Numerical results

For numerical demonstration, we again chose the O K-edge of the acetone molecule which involves the coupling of a single localized exciton to the C=O bond stretching

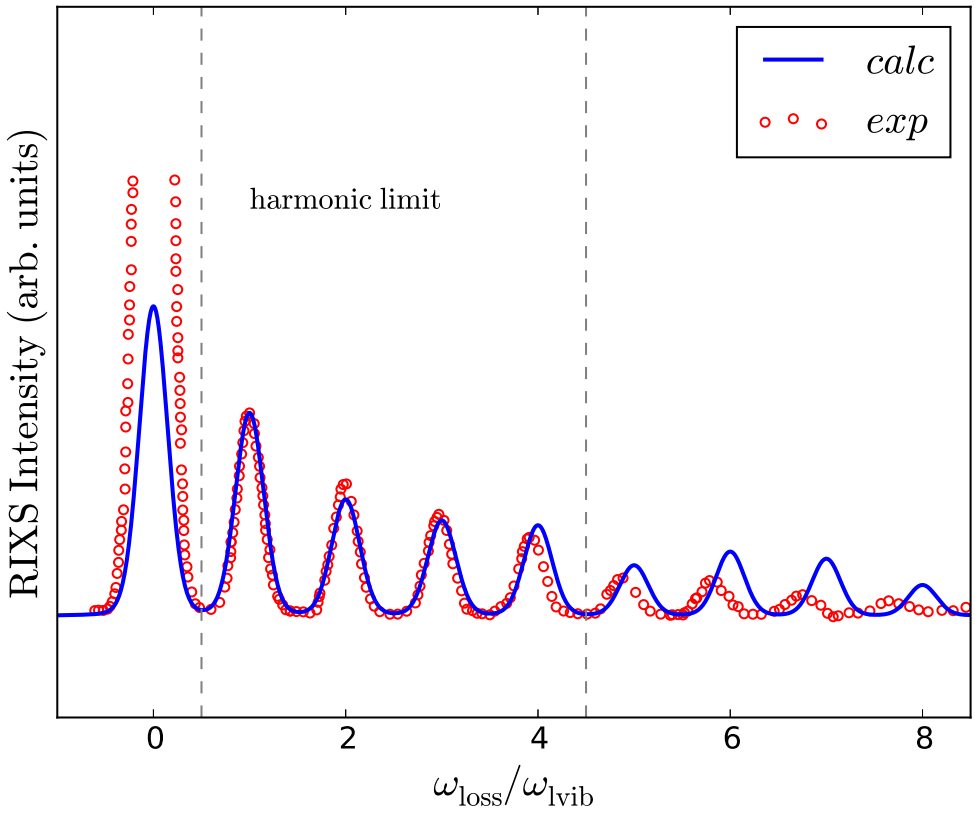

Figure 6.2: Comparison of the RIXS spectra calculated within the Green's function formalism for acetone (blue line) with experiment (red dots) The differences in the elastic line intensities arise from the Thomson scattering and other sample dependent effects. The small difference in peak position and intensities of the higher energy satellites arises from the neglected anharmonicity of the potential energy curve.

mode. There are two different unoccupied π orbitals in the acetone molecule. However, due to the character of the stretching mode, the exciton-vibrational coupling less likely leads to scattering of an exciton. From experimental observation other vibrational modes are negligible [52, 58]. According to 6.26 and 6.28 the RIXS cross-section can be written as

$$\sigma(\omega_i, \omega_{loss})|_\xi = -\frac{1}{\pi} \sum_n |d^o_\xi|^2 |d^i_\xi|^2 |\Lambda^{(n)}_\xi(\omega_i, \lambda)|^2 \mathrm{Im} D^n_\lambda(\omega_{loss}) \ , \tag{6.28}$$

where the excitonic state is $\xi = 1s^1\pi^*$ and the vibrational mode λ represents the C-O stretching mode. It is clear that the electron-photon matrix elements d^o_ξ d^o_ξ are only

a scaling factors and for simplicity can be omitted. The non-diagonal exciton Green's function $\Lambda_{\xi}^{(n)}$ in vibrational space is in fact diagonal in the electronic space.

It consists of the diagonal in vibrational space Green's function $\Lambda^{(0)}(t)$ and the explicit interaction with real (final) states phonons $Y(t)$ according to 6.26. The $\Lambda^{(0)}(t) = L_{\xi}(t)e^{C(t)}$ was calculated using the cumulant form defined in the previous Chapter 5 for the acetone molecule. The exciton-phonon coupling constant $M = 0.35\,eV$ was obtained from frozen phonon BSE calculations and the phonon frequency $\omega_{ex} = 0.15\ eV$ from the excited state potential energy surface.

The part of the off-diagonal Green's function which reflects interaction with real state phonon $Y(t)$ we calculated using 6.24. For phonon modes in periodic crystals it is reasonable to assume a single vibrational frequency for both the ground and the core-excited states. This will be less accurate for local vibrational modes in molecules. However, evaluating the Franck-Condon overlap integrals for a model of acetone we found that the different curvatures of the ground and core-excited PES should lead only minor corrections to the shape of the RIXS spectrum for the present case. Consequently, we used the excited state frequency for the calculation of the RIXS amplitude 6.29 and ground state frequency for the calculation of final state non-thermal equilibrium Green's function (see 6.30) calculated from the ground state potential energy surface and DFPT ($\omega = 0.214\ eV$). The lifetime of the intermediate state also has to be included in the calculation of the exciton non-diagonal Green's function

$$\Lambda^{(n)}(t) = \Lambda^{0}(t)\frac{Y^{n}(t)}{\sqrt{n!}}e^{-(\Gamma_m/\hbar)t}\ . \tag{6.29}$$

The inverse intermediate state lifetime Γ_m is also consistent with the XAS calculations for acetone. The final spectrum was calculated using the non-equilibrium phonon Green's functions and the RIXS amplitudes. The phonon Green's function was modelled as

$$D_{\lambda}^{n}(\omega) = -i\int_{0}^{\infty} dt e^{-in\omega_{\lambda}t}e^{i\omega t}e^{-(\gamma_{ph}/\hbar)t}\ , \tag{6.30}$$

where γ_{ph} is a small positive constant which represents the phonon lifetime in the ground state, and it was taken $0.04\ eV$. Additional Gaussian broadening was added to the final spectrum, given as in Fig. 6.5 to account for the experimental resolution. The resulting

spectra, as well as the experimental data from the work of [52], are presented in Fiq. 6.5. While the overall agreement with experiment is favorable, small differences in the intensities and peak positions at higher oscillator numbers can be attributed to the neglection of anharmonic contributions [52]. The difference in the elastic line intensity is the consequence of the Thompson scattering [58] and other sample dependent effects. These preclude the quantitative use of the elastic line and we use normalization of calculated and experimental spectrum using intensity of the first phonon.

The calculation of the RIXS amplitude was done in time domain (Eq. 6.29), and then it was Fourier transformed. For the calculation of RIXS, one can use a single point Fourier transformation of non-diagonal Green's function since only the amplitude at incoming energy is required. This reduces the size of the problem from $N_t \times N_t$ to N_t, which is the number of time steps. The latter is, in fact, a convergence parameter and decreases with increase of Γ_m. The incoming photon energy dependent RIXS amplitude $|\Lambda^{(n)}(\omega_i)|$ is shown in Fig. 6.4. The variation of the incoming energy from the resonance leads to noticeable changes in the intensity of the phonon satellites.

6.7 Discussion

Despite of the success of the Green's function approach in the no-recoil limit the recoil effects might be important for the general consideration of the solids. Thus we discuss two possible ways of the generalization of the obtained results.

Vertex function The results obtained in the previous section (Eq. 6.26) may be considered from the diagrammatic perspective as corrections to the exciton-phonon scattering vertex. Here we will discuss the cumulant representation of such vertex correction which in the no-recoil reproduces the results of the previous section but has more freedom for an extension.

For clarity we will focus on the one phonon contribution. Formally the series Eq. 6.23 can be seen as the moments expansion for vertex with one real phonon and two exciton lines. Keeping for now the no-recoil limit the lowest non-zero term can be

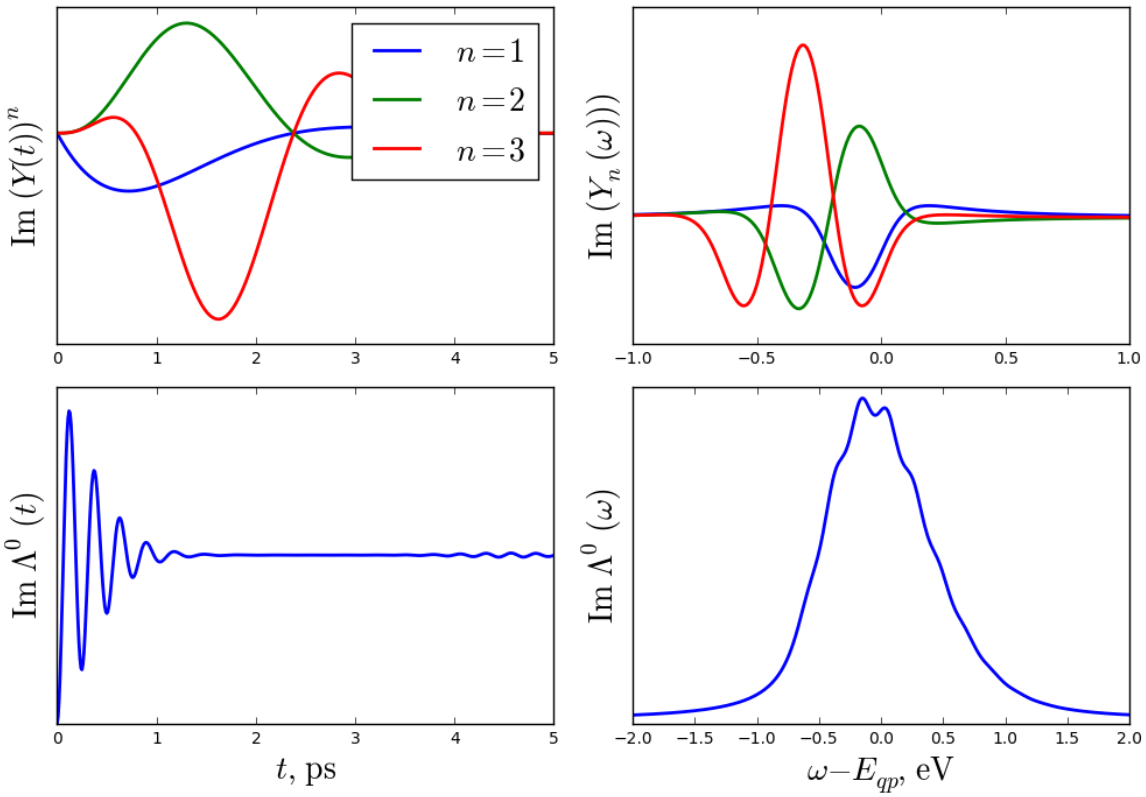

Figure 6.3: Calculation of $\Lambda^0(t)$ and $Y^n(t)$. The imaginary part of Λ^0 in the frequency space gives a regular spectral function. The imaginary part of function $Y_n(\omega)$ contains however negative parts which model the phase of the interaction. The resulting RIXS amplitude $|\Lambda^{(n)}(\omega)|^2$ is a convolution of these two functions for specific n. The boarding on the right side panel and damping on the left comes from the finite lifetime.

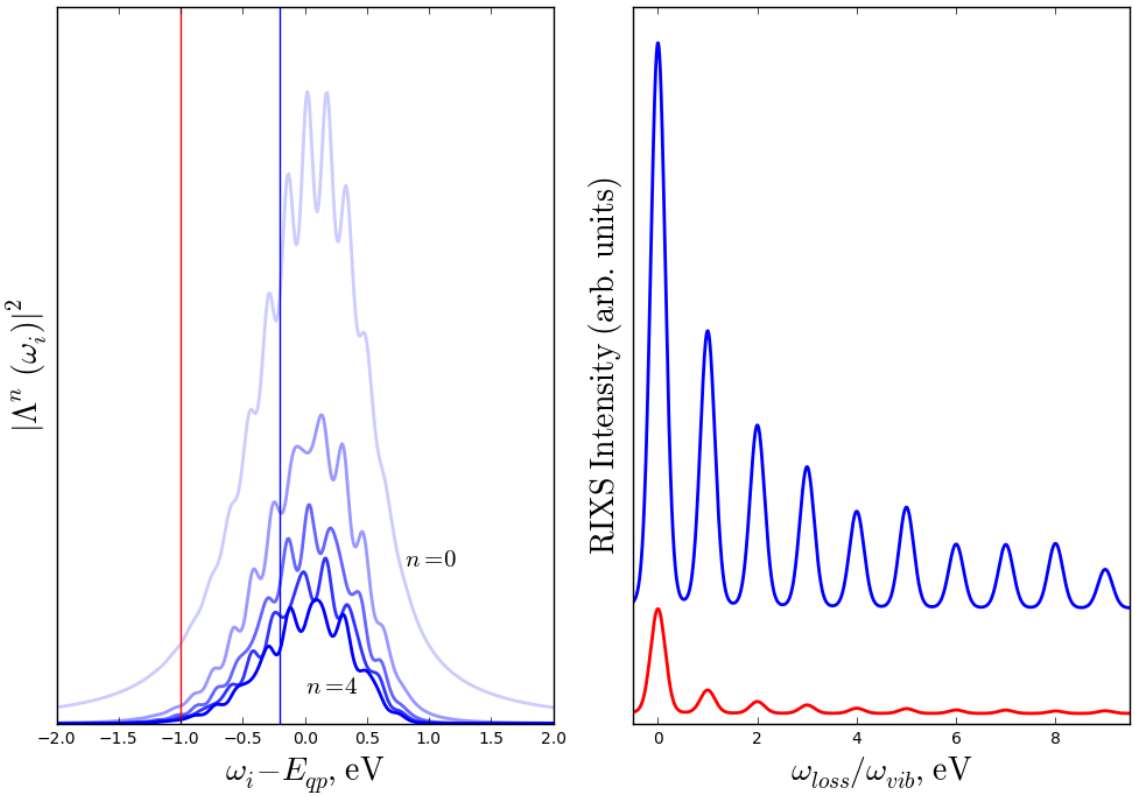

Figure 6.4: Influence of the detuning effect on the RIXS spectra. The left panel, shows RIXS amplitude for different number of real phonons $n = 0 - 4$. The right panel shows the resulting RIXS spectra for incoming energy in and out of the resonance. The finite lifetime tends to smooth the structure of the RIXS amplitude and decrease effects of the detuning. Although for a long core-hole lifetime even small detuning ($\Delta\omega_i \sim \omega_{vib}$ becomes important aspect in the formation of the phonon peak ratios.

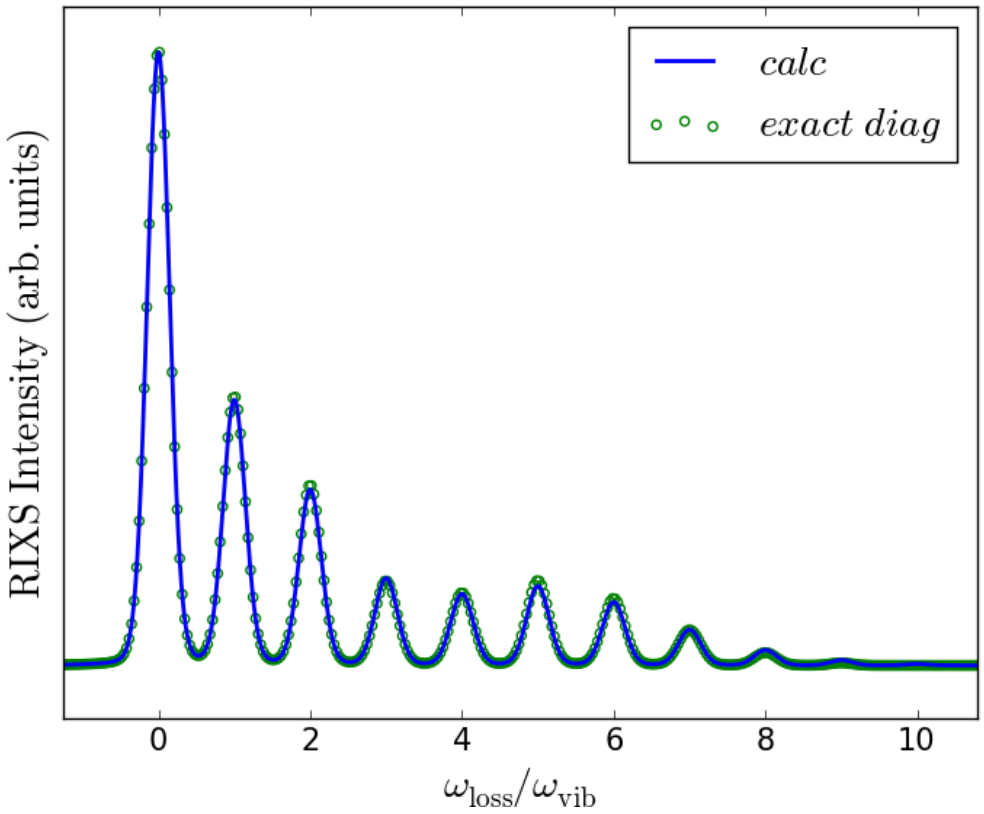

Figure 6.5: Comparison of the RIXS cross-sections calculated using the exact diagonalization techniques and the Green's function method.

written as (here we use short notations $t_1 = 1$ and $f(\bar{t}) = \int_0^t d\tau f(\tau)$)

$$\Gamma_0^{(1)}(\xi, \nu', 1, 2, 3) = -iM^{\nu}_{\xi\xi} L_\xi(1, \bar{4}) D^{>}_{\nu'}(2, \bar{4}) L_\xi(\bar{4}, 3) \ . \tag{6.31}$$

The superscript $\Gamma^{(1)}$ means that there is one final state phonon. This is a lowest order three-point vertex. Assuming that $1 = 2 = t, 3 = t'$ according to notations from the previous section, it is reduced to $L_\xi(t) Y_\xi(\nu, t)$. The higher order terms have the same irreducible structure as well as the further interactions with the virtual phonons (see Fig. 6.6 with the set of diagrams included in the second order vertex correction)

$$\Gamma^{(1)}(\xi, \nu', 1, 2, 3) = \sum_n \Gamma_{2n+1}(\xi, \nu', 1, 2, 3) \ . \tag{6.32}$$

Then using an exponential ansatz for the generating function of such series the resulting real phonon vertex can be presented as

$$\Gamma^{(1)}(\xi, \nu', 1, 2, 3) = \Gamma_0(\xi, \nu', 1, 2, 3) exp(\sum_n F_n(\xi, \nu', 1, 2, 3)) \ . \tag{6.33}$$

The expression for W_n can be found equating all terms in Eqs. 6.32 and 6.33 with the same order in exciton-phonon coupling as it was done for the cumulant expnasion of the Green's function [12, 101]. The truncation gives series $\sum_n F_n(\xi, \nu', 1, 2, 3)$ at the lowest order, Eq. 6.33 gives the exponential form of vertex correction in the third order of exciton-phonon coupling

$$\Gamma^{(1)}(\xi, \nu', 1, 2, 3) = \Gamma_0(\xi, \nu', 1, 2, 3) exp[(\Gamma_0(1, 2, 3))^{-1} \Gamma_3(1, 2, 3)] \ . \tag{6.34}$$

The third order term in the expansion 6.32 has the second order in the coupling with virtual phonons and first in coupling with real phonon and consists of three terms (Fig. 6.6)

$$\Gamma_3(123) = \frac{1}{3}[\Gamma_{3a}(123) + \Gamma_{3b}(123) + \Gamma_{3c}(123)] \ , \tag{6.35}$$

where

$$\begin{aligned}
\Gamma_{3a}(\xi,\nu',1,2,3) &= M^{\nu'}_{\xi\xi} L_\xi(2\bar{6})\Sigma_\xi(\bar{6}\bar{5})L_\xi(\bar{5}\bar{4})D_{\nu'}(3\bar{4})L_\xi(\bar{4}1) \qquad (6.36)\\
\Gamma_{3b}(\xi,\nu',1,2,3) &= M^{\nu'}_{\xi\xi} L_\xi(2\bar{6})\Sigma_\xi(\bar{5}\bar{4})L_\xi(\bar{6}\bar{5})D_{\nu'}(3\bar{6})L_\xi(\bar{4}1)\\
\Gamma_{3c}(\xi,\nu',1,2,3) &= M^{\nu'}_{\xi\xi} \sum_\nu |M^{\nu}_{\xi\xi}|^2 L_\xi(2\bar{6})L_\xi(\bar{6}\bar{5})D_{\nu}(\bar{6}\bar{4})L_\xi(\bar{5}\bar{4})D_{\nu'}(3\bar{5})L_\xi(\bar{4}1).
\end{aligned}$$

Here Σ denotes just a bubble exciton-phonon diagram in analogy to the FM self-energy. One can see that in the limit of the non-dispersive exciton bands (which is true for no-recoil limit) the integration over internal variables for exciton lines cancels out : $L_\xi(1\bar{2})L_\xi(\bar{2}3) = L_\xi(13)$ and all time integrals in the Eq. 6.36 equally contribute to Eq. 6.35 which reduces to Eq. 6.26 (for $1 = t' = 0,\ 2 = 3 = t$)

$$\Gamma^{(1)}(\xi,\nu,t) = L_\xi(t)Y_{\xi,\nu}(t)e^{C_\xi(t)} = \Lambda^{(1)}(\xi,\nu,t)\ . \qquad (6.37)$$

Thus the exponential form of the vertex correction 6.34 leads to correct results in the limit of non-dispersive excitonic band. This is sufficient as a motivation search to the approximate solution of the dispersive case in the same form. The lowest order expression 6.35 can be written without an assumption of the no-recoil limit. The disadvantage of such treatment, however, is a rapid scaling of the number of irreducible terms in the lowest order cumulant with the number of real phonons. For one real phonon, there are three terms for two real phonons there are six and so on. However, computationally such complication can be overcome using parallel performance.

Finite momentum Transfer Limit To account for recoil in the exciton-phonon scattering process the exciton Green's function must be off-diagonal in both vibrational and excitonic subspaces. Formally we can rewrite the Eq. 6.20 as

$$\Lambda^{(n)}(\xi',\xi,t) = -i\sum_{m=0}^{\infty}\frac{(-i)^{2m}}{(2m)!}\int_0^t dt_1\cdots\int_0^t dt_{2m}\,\langle 0|\,T(b_{\nu'}(t))^n a_{\xi'}(t)V(t_{2m})\cdots V(t_1)a^+_\xi(0)\,|0\rangle\ . \qquad (6.38)$$

The interaction potential has the general form of the linear electron-phonon coupling. Using the cumulant expansion of the vertex function one can write down an exciton

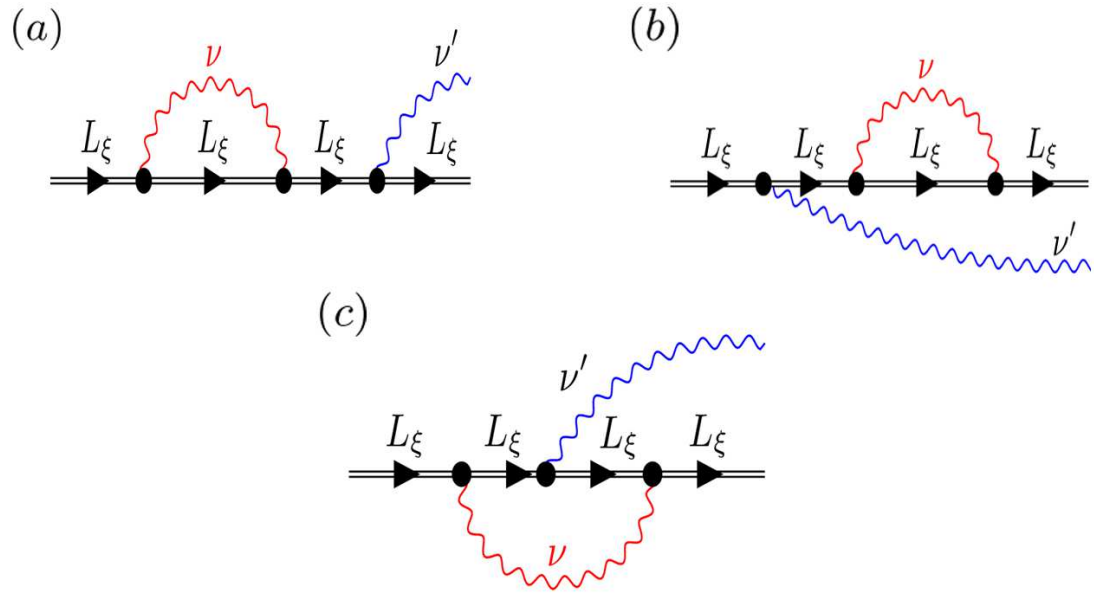

Figure 6.6: Low order diagrams for exciton-phonon interactions during the RIXS process. Black lines are bare exciton propagators, red oscillating curves represent virtual phonons while blue oscillating curves are used for real phonons.

Green's function for n, number of real phonons as

$$\Lambda^{(n)}(\xi,\xi,\nu',t) = \Gamma_0^{(n)}(\xi,\xi',\nu',t)exp(F_{2n+1}(\xi',\xi,\nu,',t)) \ , \tag{6.39}$$

where $\Gamma_0^{(n)}(\xi,\xi',\nu',t)$ is a lowest $(n+2)$ point exciton-phonon vertex and the lowest non-zero cumulant $F_{2n+1}(\xi',\xi,\nu,',t)$ for such configuration can be written by analogy to F_3 from Eq. 6.34. In principle for solids where the dispersion of the excitation plays a key role the phonon contribution to RIXS is often limited by few peaks for each mode [4, 5]. Thus the off-diagonal Green's function can be estimated for just a few real (final state) phonons. However, such approximation still has to be tested regarding limitations and convergences for model studies.

As an alternative approach we suggest a more straightforward way of approximating the exciton-phonon off-diagonal Green's function. The RIXS amplitudes $\Lambda^{(n)}$ can be represented by the diagrams in Fig. 6.7. The basic element of the diagrams is Λ_ξ, which gives the full contribution in the $n = 0$ case where the final state contains no phonons. This is the same as the XAS phonon-dressed exciton propagator given by

Eq.5.13 in Chapter 5 (see also Fig. 5.2). In context of RIXS we refer to this term as the exciton propagator dressed by virtual (intermediate state) phonons. This term includes the contributions of virtual phonons to infinite order.

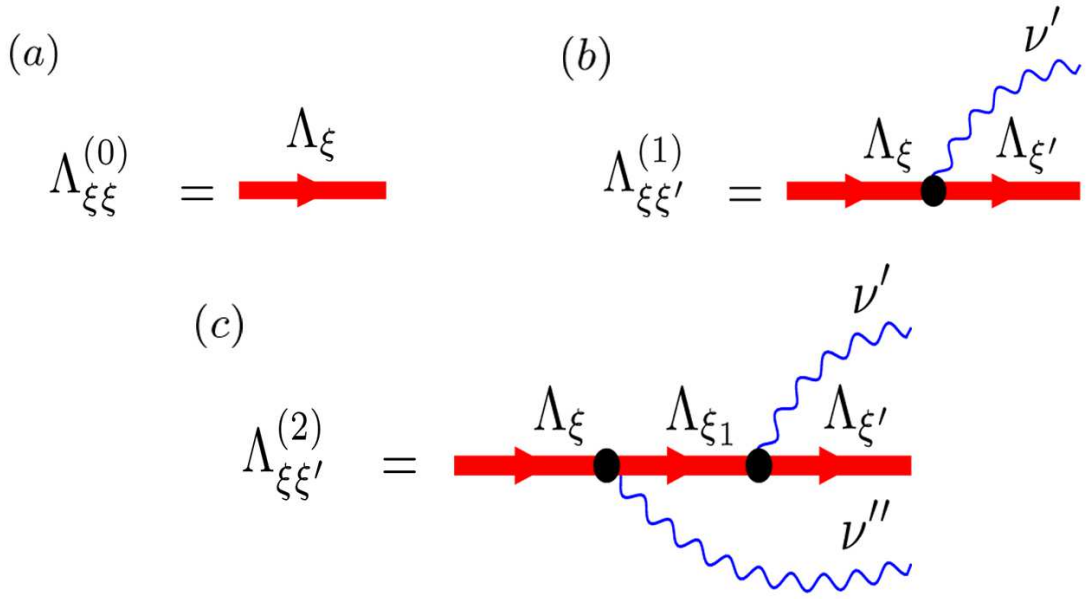

Figure 6.7: Diagrams for the RIXS amplitudes for (a) zero, (b) one and (c) two real (final-state) phonons. Heavy red lines indicate phonon-dressed exciton propagators and blue oscillating curves represent final-state phonons.

When the final-state contains a non-zero number of phonons, the RIXS amplitudes may be written down following usual diagrammatic rules using $M^{\nu'}_{\xi\xi'}$ for a vertex Λ_ξ for an exciton line and $D^{>}_{\nu'}$ for a phonon propagator. The term with one real (final-state) phonon (Fig. 6.7b) is

$$\Lambda^{(1)}(\xi,\xi',\nu',t) = iM^{\nu'}_{\xi\xi'}\Lambda_\xi(t-\bar{\tau})D^{>}_{\nu'}(t-\bar{\tau})\Lambda_{\xi'}(\tilde{\tau}) \ , \tag{6.40}$$

where internal time integration is implied by the shorthand notation. The phonon Green's function $iD^{>}_{\nu'}(t-\tau) = \langle 0|\, Tb_{\nu'}(t)b^{+}_{\nu'}(\tau)\,|0\rangle$ is a causal one (half of the full phonon Green's function) and corresponds to the propagation of a real phonon which is created at time τ and destroyed at time $t > \tau$. For two real phonons (Fig. 6.7c), we

have

$$\begin{aligned}\Lambda^{(2)}(\xi,\xi',\nu',\nu'',t) &= i^2\sum_{\xi_1} M^{\nu''}_{\xi\xi_1}\Lambda_{\xi}(t-\tilde{\tau}_2)D^{>}_{\nu''}(t-\tilde{\tau}_2) \\ &\times \Lambda_{\xi_1}(\tilde{\tau}_2-\tilde{\tau}_1)M^{\nu'}_{\xi_1\xi'}D^{>}_{\nu'}(t-\tilde{\tau}_1)\Lambda_{\xi'}(\tilde{\tau}_1)\,. \end{aligned} \tag{6.41}$$

One can build the higher terms $\Lambda^{(n)}$ contributing any number of real phonons to the RIXS final state by analogy. This approximation contains an infinite number of specific types of diagrams but neglects others. The missing type of the contribution involves vertex correction to the exciton-phonon scattering process (in the lowest order see diagram (*c*) in Fig. 6.6). However such evaluation accounts the vertex correction of the virtual phonon. The numerical evaluation of these terms for a periodic crystal is feasible, though cumbersome. We studied such approximation as the lowest correction to the basic exciton-phonon scattering process. It closely reproduced the intensity of the full calculations in the no-recoil limit for different coupling constant (see Fig. 6.8).

Weak coupling In the limit of weak coupling one can consider only the lowest order diagrams. For example, Devereaux *et al*. [2] recently calculated the RIXS cross-section for a small cluster model of CuO in the limit of no virtual phonons and one final-state phonon.

In an effort to quantify the region of applicability of this weak coupling limit, we compare model calculations of the 1-phonon contribution to RIXS $\sigma^{(1)}$ as a function of coupling strength *i*) when all virtual phonons are neglected, *ii*) when virtual phonons are included to infinite order without vertex corrections, and *iii*) when virtual phonons are included to infinite order with vertex corrections.

These results are presented in Fig. 6.8. The yellow line gives the intensity of the first phonon peak when virtual phonons are neglected. The red and blue lines correspond to the inclusion of all virtual phonons, without or with vertex corrections, respectively. The solid lines are evaluated using a ratio Γ_M/ω_{ph} of the intermediate-state lifetime to phonon frequency appropriate for the Cu L-edge of a 2D cuprate, while the dashed lines use a value consistent with the O K-edge.

We confirm that the weak coupling approximation is reasonable for coupling strengths less than about 1. However, this depends on the ratio of the core-hole lifetime and the

phonon frequency. Due to the longer core-hole lifetime of the O 1s level, the curves for the O K-edge including virtual phonons deviate from the weak coupling approximation earlier than those for the Cu L-edge. For the O K-edge the values of $\sigma^{(1)}$ including virtual phonons already differ by a factor of 2 from the weak coupling approximation by $g = 1$.

The deviation of the results including with all virtual phonons (red and blue curves) from the zero virtual phonon values (yellow line) indicates that the calculated $\sigma^{(1)}$ contribution is over-estimated since the 2-phonon contribution ($\sigma^{(2)}$) becomes non-negligible and takes spectral weight from $\sigma^{(1)}$. If the coupling strength varies throughout the Brillouin zone the correction to the one phonon intensity will also vary in momentum space, likely making it important to go beyond the weak coupling limit.

For periodic systems with several active phonon modes at different frequencies it can be difficult to distinguish the second harmonic of low frequency modes from the first harmonic of higher frequency modes. This makes it difficult to experimentally identify weak coupling cases. This partly explains why quantitative experimental studies of electron-phonon coupling by RIXS are still limited. However, we note that some of these measurements report intermediate or even strong coupling values [5, 27, 67, 96]. For reference, in Fig. 6.8 we use vertical dashed lines to indicate experimentally obtained coupling parameters for TiO_2 and the quasi-1D Li_2CuO_2.

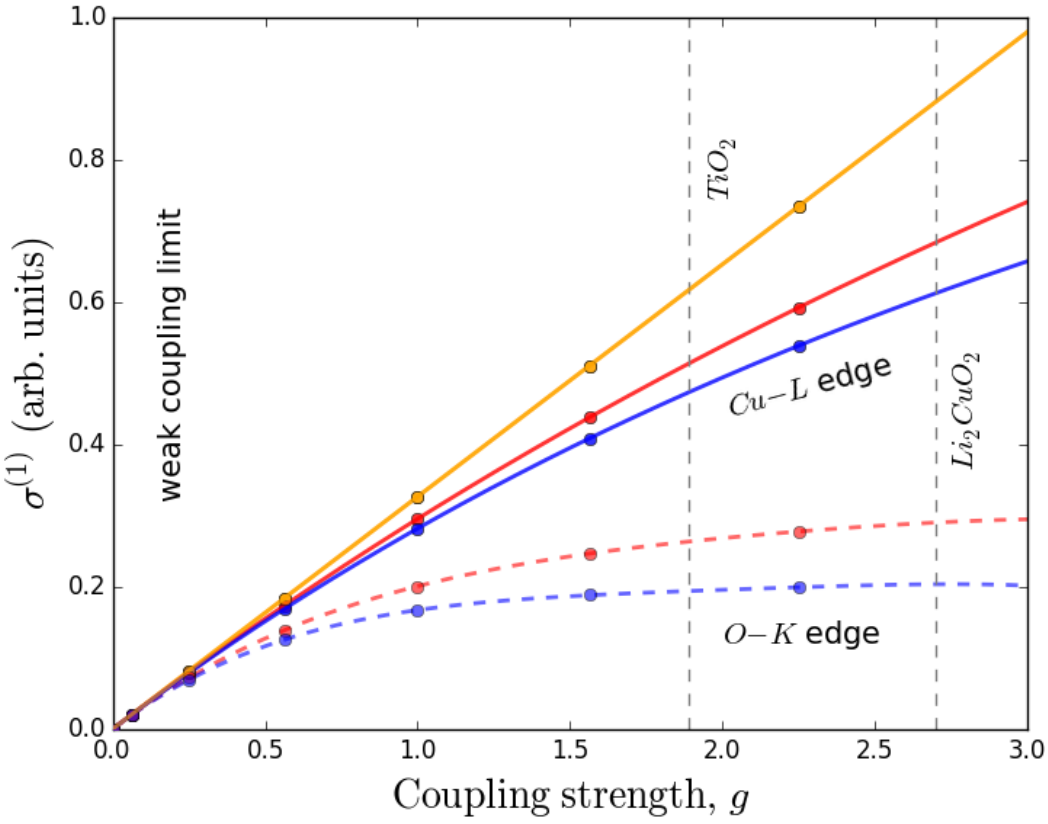

Figure 6.8: Intensity of the first phonon peak with respect to the coupling strength. Calculations were performed for a single phonon mode in the no-recoil limit using different approximations: yellow line - lowest order contribution (no virtual phonons); red curves - virtual phonons, but no vertex corrections (Eq. 6.40); blue curves - virtual phonons including vertex corrections (Eq. 6.25). Dashed and solid lines correspond to different core-hole lifetimes. The ratio Γ_M/ω_{vib} was set to 2 (dashed lines) and 6 (solid lines) as typical values for O K- and Cu L-edges, respectively. All curves were consistently normalized to the value of the lowest order contribution (yellow line). Vertical dashed lines indicate values of the coupling strength measured by RIXS for TiO_2 [5] and Li_2CuO_2 [67].

6.8 Conclusion

In this section the problem of the phonon contribution to RIXS with the Green's function formalism. First, we discussed the idea of presenting phonon in RIXS as a convolution of two spectral functions related to the XAS and XES process. Then the Kramers-Heisenberg cross-section was presented in terms of off-diagonal Green's function in the excitonic basis and final state non-thermal phonon Green's function. While keeping explicit summation over the final state we implicitly account for the virtual phonon contribution.

We discussed the expansion of the non-diagonal exciton Green's function in presence of the exciton-phonon interaction. The expression for the non-diagonal exciton Green's function was obtained in the no-recoil limit, where the non-depressive exciton (or localized exciton) couples to the phonon degrees of freedom. We tested formalism on the acetone molecule, where the experimental RIXS spectra show rich vibrational contribution. Using developed formalism and parameter-free calculation we reproduced the vibrational contribution in the harmonic limit successfully.

We discussed possibles ways of the extensions of the formalism for periodic materials where the scattering of an exciton is important. Suggested approach based on the diagrammatic construction of the non-diagonal Green's funciton elements overcome current limitation of the weak coupling limit RIXS calculations [2].

Chapter 7

Conclusions

Contents

7.1 Outlook

The objective of this project was to develop a rigorous approach to account for the phonon contribution in RIXS and to relate the measured quantity to the electron-phonon coupling constant. The work consists of four parts: (I) model *ab-initio* based study of the phonon contribution to RIXS; (II) core-hole-phonon interactions and the phonon contribution to XPS; (III) coupling of neutral excitations (excitons) to phonons and the phonon contribution to XAS; (IV) Green's function approach to the phonon contribution to RIXS.

We studied the phonon contribution to the RIXS loss spectrum from the qualitative, quantitative and formal perspectives. Contrary to common assertion, we found that RIXS is not a direct probe of electron-phonon coupling, even when measured at the Cu L_3-edge. Both excitonic binding effects and direct core-hole-phonon interactions cause considerable deviations from the electron-phonon interpretation. We found, however, that an exciton-phonon coupling description is able to quantitatively explain previous experimental data for acetone. We expect that the exciton-phonon description of the RIXS interaction will hold in general. This result significantly impacts the use of RIXS to quantify electron-phonon coupling strengths in cuprates and other materials. This creates motivation for further development of a rigorous approach that will be suitable for crystalline materials.

The core-hole phonon interaction was not included in previous studies of the phonon contribution to RIXS [2–4]. To demonstrate the importance of the role played by the core-hole, we started with a description of the phonon contributions to X-ray photoemission.The experimental X-ray photoemission spectra [99] at the shallow Si $2p$ level (around 100 eV) of silicon tetra-halides show obvious phonon sidebands, clearly signaling the ability of the core-hole to excite vibrations. We combined the cumulant ansatz for the core-hole Green's function with real-space MD calculations of the system response and coupling strength. The developed approach allowed us to successfully reproduce experimental data for the small molecules SiF_4 and SiH_4. Moreover, this approach can be directly scaled to crystalline materials. Furthermore, this approach is also capable of capturing any anharmonic response of the lattice.

The next step of our studies was the development of an efficient formalism to treat

the coupling between neutral electronic excitations and phonon degrees of freedom. For RIXS this process plays an essential role in the formation of the intermediate state. The complication comes from the presence of both electron-phonon and electron-electron interaction. The latter tends to mix the independent particle state and form an exciton bond state. Using an argument of the different time scales of the interactions we described first the electron-electron interaction on the level of the BSE and then dressed the resulting exciton propagator within the framework of the cumulant with the exciton-phonon interactions. This procedure leads to significant simplification of the interacting two-particle problem. However, it involves the calculation of the excited state coupling to phonons. The approach was tested on the K-edge XAS spectra for the N_2 and acetone molecules.

The model calculation of the RIXS phonon contribution using an exciton-phonon coupling constant showed quantitative agreement with the experimental data for acetone. This motivated us to develop a many-body Green's function description of the phonon contribution to RIXS within an excitonic representation. We employed a cumulant expansion for the exciton Green's function in conjunction with a Fan-Migdal type exciton self-energy. This methodology provided an accurate reproduction of the phonon satellite structure observed experimentally in the X-ray absorption spectrum of acetone. It also successfully reproduced the phonon excitation series measured by RIXS. The Green's function formulation is advantageous compared to wavefunction-based calculations that require enormous summations of all possible RIXS intermediate states. Our methodology includes only an explicit summation over the RIXS final states which are limited to the lowest few phonon oscillator levels in practice.

We demonstrated our formalism on acetone due to the availability of high quality and unambiguous experimental data. However, this methodolgy is extendible to periodic crystals. Periodic systems present additional numerical challenges associated with sampling phonon coupling strengths throughout the Brillouin zone. Although computationally demanding, such sampling is still possible within the framework of first-principles calculations [70].

7.2 Perspectives

As a perspective of this project the following steps should be done.

First, the application of the formalism developed herein to crystalline materials would be of interest for the RIXS field in general. However, it requires calculating phonon frequncies and exciton-phonon coupling strengths throughout the Brillouin zone. The frozen phonon approach used in this work will become too computationally expensive when applied to periodic systems. As we suggested at the end of Chapter 5 the calculation of exciton-phonon coupling values can be done analogously to density functional perturbation theory, which would allow application to a broader set of compounds.

Furthermore, beyond the understanding and quantitative results for the exciton-phonon coupling from RIXS developed in this thesis, one has to solve the inverse problem to disentangle the values of the electron-phonon coupling constants from the exciton-phonon coupling values. This, however, requires knowledge of the core-hole-phonon coupling which was defined in Chapter 4. Model Hamiltonian calculations can also be used to clarify this point.

At the same time, the methodology can be applied to other bosonic modes, such as magnons. Nevertheless, no other bosons appear to couple as strongly as phonons. Thus they do not show multiple harmonics in RIXS, and the weak coupling limit should be sufficient for studying such excitation.

Appendices

Appendix A

Density functional theory

Density functional theory in the last couple of decades became a powerful technique to obtain ground state properties for both solids and molecules. From one side due to the Hohenberg and Kohn theorem [115] and on the other side due to the progress in computational development. The statements which are in the origin of the DFT are general, but in practice there several limitations which rise needs for correction and instantaneous developments of new approach within the DFT basis [116]. As it is clear from the name of the techniques that the key point is the density of the system

$$n(\boldsymbol{r}) = \int\int \psi(\boldsymbol{r}_1, ..\boldsymbol{r}_n)\psi^*(\boldsymbol{r}_1, .., \boldsymbol{r}_n)d\boldsymbol{r}_1..d\boldsymbol{r}_n \ . \tag{A.1}$$

Any observable is defined by the expectation values of the corresponding operator and thus to get any kind of information of the system (and especially about the ground state energy) the bottleneck problem is a solution of the many-body Schrödinger equation. The great simplification of the problem comes with the understanding [115] that there is one to one correspondence between the ground state density of the system and the ground state wave-function. This makes any observable a functional of the ground state density n_0. And since $\psi[n_0]$ are the ground state wave-function, they have to minimize the energy

$$E_{GS} = \min_{n \to n_0} \langle \psi[n] | \, H \, | \psi[n] \rangle = \langle \psi[n] | \, T + U + V \, | \psi[n] \rangle \ . \tag{A.2}$$

Here electron kinetic T and interaction U are unique and the system depending part is the hidden in V (in the BO approximation $V$is commonly the nuclei potential). Thus

the ground state density has to minimize also the following terms

$$E_{GS} = \min_{n \to n_0} (F[n] + V[n]) \ , \tag{A.3}$$

where the system dependend functional $V[n]$ can be written as $V[n] = \int n(r)v(r)dr$. If one knows the external potential he can find the ground state density and the vice verse. One has to admit the uniqcnees of the solution in the non-degenerate case. On the other side if the density is not the ground state density the expectation value on the right side of Eq. A.2 will be equal or bigger then the ground state one. This was also proven by Hohenberg and Kohn [115]. Finally the concept is

$$n(\boldsymbol{r}) <=> \psi(\boldsymbol{r}, .., \boldsymbol{r}_n) <=> v_{ext}(\boldsymbol{r}) \ . \tag{A.4}$$

The ground state density defines the many-body wave-functions and from the later one can find the external potential. However, it does not give a precise receipt on how to do it on practice. The main difficulties related to the non-local character of the density functionals. The first particle approach which was formulated a long time before the HK theorems by Thomas and Fermi [117, 118]. This approximation which indeed treats explicit dependence of terms in Eq. A.2 on electronic density, although it neglects entirely correlations and exchange terms which are non-local and appear from the kinetic term T. The modern DFT approach based on the Kohn-Sham ansatz [119]. The idea is to employ an auxiliary system of non-interacting electrons to get the initial guess for density and exchange-correlation potential and then solve realistic problem self-consistently. This makes DFT techniques an effective single-particle approach. The ansatz, however, works well with many solids and molecules but fails to some strong correlation effects (e.g., the Mott-insulator state in the copper-based, etc. [116]). The Hamiltonian of the auxiliary system is simple and consists of the kinetic term and effective potential

$$H_{KS} = \frac{1}{2}\nabla^2 + V_{eff}(\boldsymbol{r}) \tag{A.5}$$

The solutions of such Hamiltonian for N_{ks} particles defines density function and the population of the ψ_i orbitals, which are called Kohn-Sham orbitals. The kinetic term explicitly is

$$T_{ks} = -\sum_{i}^{N_{ks}} \frac{1}{2}|\nabla\psi_i|^2 = T_{ks}[n] \ . \tag{A.6}$$

On the other side, the expression for effective potential is less defined. Writing explicitly Hartree term for an electron-electron interaction as well as the external (system-dependent) potential, all exchange and correlation terms effectively introduced as $E_{xc}[n]$. Finally the ground state energy of the auxiliary system

$$E_{KS}[n] = T_s[n] + \int drV_{ext}(\boldsymbol{r})n(r) + \frac{1}{2}\int drdr'\frac{n(\boldsymbol{r})n(\boldsymbol{r'})}{|\boldsymbol{r}-\boldsymbol{r'}|} + E_{xs}[n] \ . \tag{A.7}$$

Equating such effective ground state energy to the ground state of the fully interacting system the exchange-correlation part then is

$$E_{xs}[n] = \langle T\rangle - T_s[n] + \langle V_{int}\rangle - E_H[n] \ . \tag{A.8}$$

The difference between interacting and non-interacting particles kinetic terms defines correlation contribution and the exchange term is known as a Fock term. The last can be written explicitly in terms of single orbitals. In other words, the KS equations is an attempt to reformulated the many-body interacting problem in terms of the non-interacting part and active exchange-correlation part which can be approximated to be local or semi-local. Under the assumption that the exact exchange-correlation potential is a known solution of N Eq. A.5 leads to the exact ground state energy and density of the interacting system. There several approaches to defining exchange-correlation part and the semi-local form is

$$E_{xc}[n] = \int drn(\boldsymbol{r})\epsilon_{xc}([n], \boldsymbol{r}) \ , \tag{A.9}$$

where $\epsilon([n], \boldsymbol{r})$ energy density depends on the electronic density at the point r . This the similar to Dirac term in the TF model the first guess for an exchange-correlation functional is the local density approximation (LDA). In this case ϵ_{xc} assumed to be identical to one of the homogeneous electron gas with the same density, for which the exchange-correlations terms are local. Moreover, the generalization accounting for spin degrees of freedom leads to the local spin density approximation where the exchange and correlation terms are defined as functions of spin up and spin down densities. On top of the local description, the further improvements come from the gradients of the

density, the generalized gradient approximation (GGA) reads

$$E_{xc}^{(GGA)}[n] = \int drn(\boldsymbol{r})\epsilon_x^{hom}([n], \boldsymbol{r})F_{xc}(n, |\nabla n|, |\nabla n|^2, ..) \ , \tag{A.10}$$

The expansion of the XC terms in terms of the density gradients has to be corrected (generalized) to avoid divergence and non-physical behavior for higher orders. The GGA is a most commonly used form of the exchange-correlation functional [120] and also can be written for the spin-polarized case. In case of strong orbital localization of electrons, as it happens for many of transition metal oxides, mean-field DFT (LDA/GGA) calculations tends significantly underestimate on-site electron-electron interaction. One of the possible ways to improve the situation is to apply extra coulomb potential U selectively for few orbitals. This approximation leads to the shift of the localized orbitals with respect to others and correct properties, such as band gaps. This approach is known as LDA+U and has the similar origin to the Hubbard U [121]. The most precise form of the E_{xc} comes from the mixing of different type of the exchange-correlation functional. The so-called hybrid functional is in fact mixture of the LDA/GGA functionals and pure Hartree-Fock exchange functional of the orbitals. The motivation comes from adiabatic continuation from non-interacting to interacting system [122]. Since non-interacting solution has to driven by functional in a pure LDA picture but on the other end, the fully interacting system obeys the HF exchange useful, taking an average answer those functionals are weighted in different ways. One suggested by Perdew and Ernzerhof, and Burke is

$$E_{xc} = E_{xc}^{LDA} + \frac{1}{4}(E_{xc}^{HF} - E_{xc}^{GGA/LDA}) \ , \tag{A.11}$$

it was tested on a large number of system and find to be satisfactory [123].

The eigenvalues of the KS Hamiltonian in principle does not correspond to the real excitation energies (energy of removal or addition of one electron but), although the can be used as starting point to get excitation energies using a perturbation expansion for an excited wave-function and eigenstates.

Pseudo-potential formalism

One of the great simplification in the framework of KS DFT, achieved by using the pseudo-potential formalism. The core-electrons are strongly localized and mainly does not involved in the molecular bonds, in contrast to valence electrons. Such a difference in the behavior also reflects in the form of the wave-functions. The idea of the pseudo-potentials is to describe the valence electrons using the smooth wave-functions and hide core-electron by modifying the total scattering potential of the nuclear. Formally this can be achieved by the orthogonalized plane-wave (OPW) method [116]

$$\psi_{lm}(\boldsymbol{r}) = \tilde{\psi_{lm}}(\boldsymbol{r}) + \sum_j B_{jlm} u_{jlm}(\boldsymbol{r}) \ , \tag{A.12}$$

where initial wave-function ψ_{lm} decomposed in the smooth part ($\tilde{\psi_{lm}}$) which is made to be orthogonal to u_{jlm}. The u_{jlm} can be chosen optimally for the specific problem, but are always chosen to be a core atomic states. Since the wave-function ψ_{lm} has to obey the effective KS Hamiltonian with an effective potential V, the corresponding Hamiltonian for pseudo-wave-function includes an extra part in the effective potential

$$V_p = V + V_{\boldsymbol{R}} \ . \tag{A.13}$$

The effective potential, in fact, is smoother then the original one, but also has to be non-local because of $V_R\tilde{\psi}^v(\boldsymbol{r}) = \sum_j (\epsilon_i^v - \epsilon_j^c) \langle \psi_j^c | \psi_i^v \rangle \psi^c(\boldsymbol{r})$. Although using an the fact of to preserve scattering properties potential does not has to be unique we can choose the effective part to be smooth and weak, which leads to rapid convergence in momentum space. Thus one can reduce the initial all electron problem to the valence electron problem in the effective ionic potential, which can approximate from the full HF calculation of a single atom. In general, the solution of the pseudo-Hamiltonian has to be considered as a generalized eigenvalue problem, since the pseudo-wave-function are not orthonormal. The further generalization leads the ultra-soft pseudo-potential approach, which priorities the smoothness of the pseudo-wave-function. On the other side, one can choose the pseudo-wave-function to be normalized as a solution of the

Hamiltonian with a potential model build to reproduce valence all electron properties

$$V^{nc} = \sum_{lm} |Y_{lm}\rangle \, V_{lm}(\boldsymbol{r}) \, \langle Y_{lm}| \ . \tag{A.14}$$

here Y_{lm} are the spherical harmonics defined by the angular momentum and spin. This formulation implies semi-local potential (local regarding the radial part but non-local regarding angular quantum number). So the resulting functions preserve conditions $\langle \psi_i^{nc}| \, |\psi_j^{nc}\rangle = \delta_{ij}$ but looses in smoothness, compare to ultra-soft ones. Also initial OPW method now days is reformulated within the projected augmented waves approach [124].

Appendix B

Density functional perturbation theory

One of the main assumptions in DFT was BO approximation. The electron-nuclear potential we considered as an external to the electronic system, which has to be minimized. This picture, however, neglect mutual interactions between electron subsystem and subsystem of ions. Such interactions are essential for the various type of phenomena in the solid states from electronic transitions to electron and spin transport properties [6–11]. Notably, exchange of phonons produces the attractive interaction between electrons that binds Cooper pairs in conventional BCS superconductors [19]. As observed in photoemission and inverse photoemission, phonons renormalize quasiparticle energies and spectral weights and bestow them with lifetimes [18, 38, 39]. The many-body wave-function using a solution for interacting electrons and fixed nuclear as a parameter leads to the generalization of the Hamiltonian Eq. A.4

$$[\sum_{\alpha} \frac{1}{2M_{\alpha}} \boldsymbol{\nabla}^2_{\boldsymbol{R}_{\alpha}} + E(\boldsymbol{R})]\Psi(\boldsymbol{R}) = \tilde{E}\Psi(\boldsymbol{R}) \ , \tag{B.1}$$

here the energy $E(\boldsymbol{R})$ is a solution of the many-body Hamiltonian $H(\boldsymbol{R})$ Eq. B.1 which depends on position of the nuclei $\boldsymbol{R} = \{\boldsymbol{R}_{\alpha}\}$, thus BO potential energy surface. The first term represent the kinetic term of the nuclear with mass M_{α}. The general way of proceeding the electron-lattice interacting problem, is an expansion of the $H(\boldsymbol{r}, \boldsymbol{R}) = T(\boldsymbol{r}) + V_{KS}(\boldsymbol{r}, \boldsymbol{R})$ and consequently $V_{KS}(\boldsymbol{R})$ interacting potential, which depends on

the nuclear position in terms of atomic position displacements $\boldsymbol{Q}_\alpha = \boldsymbol{R}_\alpha - \boldsymbol{R}^0_\alpha$. The the first and the second gradients of the potential energy surface $E(\boldsymbol{R})$ defines an electron-phonon couplings terms and inter-atomic forces, and force constants (second derivatives) from the Hellmann-Fyanman theorem

$$\boldsymbol{F}_\alpha = \langle \Psi | \frac{\partial H(\boldsymbol{R})}{\partial \boldsymbol{Q}_\alpha} | \Psi \rangle = \frac{\partial E(\boldsymbol{R})}{\partial \boldsymbol{Q}_\alpha}$$

$$U_{\alpha,\beta} = \frac{\partial \boldsymbol{F}_\alpha(R)}{\partial \boldsymbol{Q}_\beta} = \frac{\partial^2 E(\boldsymbol{R})}{\partial \boldsymbol{Q}_\beta \partial \boldsymbol{Q}_\alpha} \ . \tag{B.2}$$

The phonon eigenstates and eigenvalues in harmonic limit can also be related to the inter-atomic forces constants at the equilibrium position (since the first derivatives vanish) [125]. Differentiating the equation of motion for the atomic displacement operator, where getting a condition for the normal mode frequencies. The electron-phonon interaction matrix elements and properties of the phonon, therefore, can obtained using a derivative of the ground-state solutions with respect to atomic displacements. In the following section, we will see how it works in practice for within the DFT framework and in details consider the electron-phonon interaction in first and the second order.

Phonons

In the harmonic approximation, the Hamiltonian for nuclei at the equilibrium positions can be written using second-order derivatives of the BO potential energies [126]. We introduce following notations $\boldsymbol{Q}_{p\alpha}$ is the displacement vector for atom with coordinates $\boldsymbol{R}_{p\alpha} = \boldsymbol{R}_p + \boldsymbol{\tau}_\alpha$. Index p defines the position of the unitcell in the solid and α defines the position of the atom inside the unitcell.

$$H_n = \sum_{\alpha,\beta} U_{\alpha\beta,p,p'} \boldsymbol{Q}_{\alpha p} \cdot \boldsymbol{Q}_{\beta p'} - \sum_{\alpha,p} \frac{1}{2M_\alpha} \boldsymbol{\nabla}^2_{\alpha p} \ . \tag{B.3}$$

here we omitted constant contribution from unperturbed potential $V(\boldsymbol{R}^0)$. It implicitly stated that the matrix elements defined by ground state many-body electronic wavefunctions and thus depends on the electronic density. The Hamiltonian B.3 becomes

diagonal using the second quantized form of the atomic displacements operator

$$\mathbf{Q}_{\alpha p} = i \sum_{\boldsymbol{q},\lambda} \sqrt{\frac{\hbar}{2N_q M_\alpha \omega_\lambda(\boldsymbol{q})}} \boldsymbol{\xi}^{\alpha}_{\boldsymbol{q},\lambda} (b_{\boldsymbol{q},\lambda} + b^{+}_{-\boldsymbol{q},\lambda}) e^{i\boldsymbol{q}\cdot\boldsymbol{R}_p}, \tag{B.4}$$

Here creation and annihilation operators b, b^+ respect bosonic commutation relations $[b_q, b^+_{q'}] = \delta_{q,q'}$. The polarization vector $\boldsymbol{\xi}_{\lambda,\boldsymbol{q}}$ and $\omega_\lambda(\boldsymbol{q})$ are respectively normalized eigenfunctions and eigenvectors of

$$\sum_{\alpha} D^{dm}_{\alpha beta}(\boldsymbol{q}) \boldsymbol{\xi}^{\alpha}_{\lambda,\boldsymbol{q}} = \omega_\lambda(\boldsymbol{q}) \boldsymbol{\xi}^{\beta}_{\lambda,\boldsymbol{q}} \tag{B.5}$$

where the dynamical matrix is

$$D^{dm}(q)_{\alpha,beta} = \sum_{p} \frac{1}{\sqrt{M_\alpha M_\beta}} U_{\alpha\beta p0} e^{i\boldsymbol{q}\cdot\boldsymbol{R}_p} \tag{B.6}$$

Finally the phonon Hamiltonian reads

$$H = \sum_{\lambda,\boldsymbol{q}} \omega_\lambda(\boldsymbol{q}) (b^{+}_{\boldsymbol{q},\lambda} b_{\boldsymbol{q},\lambda} + 1/2) \tag{B.7}$$

The force constants and dynamical matrix it self can then be find in terms of the first order derivatives of the electron ground state density and KS potential [11].

Electron-phonon interaction

To eliminate the electron-phonon interaction we will expand the ground-state KS potential $V_{KS}(\boldsymbol{r}, \boldsymbol{R}_\alpha)$ in terms of the atomic displacements similar to Eq. 1.2 (here index l represent Cartesian coordinate)

$$V_{KS}(\boldsymbol{r}, \boldsymbol{R}) = \sum_{\alpha} V_{KS}(\boldsymbol{r}, \boldsymbol{R}^0_{p\alpha}) + \sum_{p,\alpha,l} \frac{\partial V_{KS}(\boldsymbol{r}, \boldsymbol{R}^0_{p\alpha l})}{\partial Q_{p\alpha,l}} Q_{p\alpha,l} + \sum_{p,p',\alpha,\beta,l,m} \frac{1}{2} \frac{\partial^2 V_{KS}(\boldsymbol{r}, \boldsymbol{R}^0_{p\alpha l})}{\partial Q_{p\alpha l} \partial Q_{p'\beta m}} Q_{p\alpha l} Q_{p'\beta m} + \dots . \tag{B.8}$$

The atomic displacements can be rewritten using normal modes coordinates and respective phonon operators Eq. B.4. The first order term then is

$$V_{KS}^{(1)}(\boldsymbol{r},\boldsymbol{R}^0)=\sum_{p,\alpha,l}\frac{\partial V_{KS}(\boldsymbol{r},R^0_{p\alpha l})}{\partial Q_{p\alpha l}}Q_{p\alpha l}=\sum_{\boldsymbol{q},\lambda}\Delta_{\lambda,\boldsymbol{q}}V_{KS}(b_{\boldsymbol{q}\lambda}+b^+_{-\boldsymbol{q}\lambda})\ , \tag{B.9}$$

where $\Delta_{\lambda,\boldsymbol{q}}V_{KS}=\Delta_{\boldsymbol{q},\lambda}v_{ks}e^{i\boldsymbol{q}\boldsymbol{r}}$ And recalling the electron-phonon terms in the Hamiltonian Eq. 1.3 $H_{eph}=H^{(1)}_{eph}+H^{(2)}_{eph}$

$$H^{(1)}_{eph}=\sum_{n',n,q,\lambda}M^{(1)}_{n,n'k,q}c^+_{n'k+q}c_{nk}(b^+_{-q,\lambda}+b_{q,\lambda})\ , \tag{B.10}$$

$$H^{(2)}_{eph}=\sum_{n,n'q,q',\lambda,\lambda'}M^{(2)}_{n,n'k,q,q',\lambda,\lambda'}c^+_{n'k+q+q'}c_{nk}(b^+_{-q,\lambda}+b_{q,\lambda})(b^+_{-q',\lambda'}+b_{q',\lambda'})\ . \tag{B.11}$$

The electron-phonon coupling of the first and the second order has energy units and consist of the electron-phonon matrix elements and phonon normal amplitudes

$$M^{(1)}_{n,\boldsymbol{k},\boldsymbol{q},\lambda}=\sqrt{\frac{\hbar}{2N\mu\omega_\lambda(\boldsymbol{q})}}\left\langle\psi_{n'\boldsymbol{k}+\boldsymbol{q}}\right|\Delta_{\boldsymbol{q},\lambda}v_{KS}\left|\psi_{nk}\right\rangle\ , \tag{B.12}$$

$$M^{(2)}_{n,n'\boldsymbol{k},\boldsymbol{q},\boldsymbol{q'},\lambda,\lambda'}=\frac{\hbar}{2N\mu\sqrt{\omega_{\lambda'}(\boldsymbol{q'})\omega_\lambda(\boldsymbol{q})}}\left\langle\psi_{\boldsymbol{n'}\boldsymbol{k}+\boldsymbol{q}+\boldsymbol{q'}}\right|\Delta_{\boldsymbol{q'},\lambda'}\Delta_{\boldsymbol{q},\lambda}v_{KS}\left|\psi_{n\boldsymbol{k}}\right\rangle\ , \tag{B.13}$$

Thus the calculation of the dispersive electron-phonon coupling constants entirely rely on the variation of KS potential

$$\Delta_{q,\lambda}V_{KS}=\sum_{\alpha,l}\boldsymbol{\xi}^{\alpha,l}_{\boldsymbol{q},\lambda}\sum_p e^{-i\boldsymbol{q}(\boldsymbol{r}-\boldsymbol{R_p})}\frac{\partial V_{KS}}{\partial Q_{\alpha,l}}|_{\boldsymbol{r}=\boldsymbol{R}_p}\ , \tag{B.14}$$

Frozen-phonon calculation The most intuitive way of calculating the electron-phonon matrix elements is to take numerical derivatives with respect to displacements along the phonon eigenvectors

$$\Delta_{q,\lambda}V_{KS}(\boldsymbol{r},\boldsymbol{R})=\lim_{Q_{\boldsymbol{q},\lambda}\to 0}\frac{V_{KS}(\boldsymbol{r},R^0+\boldsymbol{Q}_{\boldsymbol{q},\lambda})-V_{KS}(\boldsymbol{r},\boldsymbol{R}^0)}{Q_{\boldsymbol{q},\lambda}}\ . \tag{B.15}$$

This involve at least two shots of full self-consistent calculations for $V_{KS}(\boldsymbol{r},\boldsymbol{R}^0+Q_{q,\lambda})$ and $V_{KS}(\boldsymbol{r},\boldsymbol{R}^0)$, within a supercell which sufficiently big to model phonon mode with

vector $\boldsymbol{q}$. The obvious limitation of such approach is a dramatic increase of computational time with $q \to 0$.

DFPT To overcome supercell limitations one can explicitly find a derivatives of the density dependent terms in the KS potential within the unitcell [11, 126].

$$V_{KS}(\boldsymbol{r}, \boldsymbol{R}) = \frac{Z_r e^2}{|\boldsymbol{R} - \boldsymbol{r}|} + \int d\boldsymbol{r'} \frac{n(\boldsymbol{r'}, \boldsymbol{r})}{|\boldsymbol{r} - \boldsymbol{r'}|} + V_{xs}(\boldsymbol{r}, \boldsymbol{r}) + \sum_{\boldsymbol{r'}} V_{nn}(\boldsymbol{r}, \boldsymbol{r'}) \ , \tag{B.16}$$

The nuclear-nuclear interaction is just un-screened Coulomb interaction, and it can be evaluated analytically [126] and was omitted here. The exchange-correlation potential is the functional derivative of the exchange functional with respect to electronic density: $V_{xc} = \frac{\delta E_{xc}[n(r,r)]}{\delta n(r,r)}$ and the rest two terms are the Hartree term and electron-nuclear interaction. The general idea is to find a correction to the solution of the Hamiltonian around the equilibrium atomic positions using perturbation theory. The parameter of an expansion is the atomic displacements $\boldsymbol{Q}_{p\alpha l} = \boldsymbol{R}_{p\alpha l} - \boldsymbol{R}^0_{p\alpha l}$. The key point is that the variation of the potential with respect to $Q_{p\alpha m}$ leads to the variation of the density.

The variation of the electron-nuclear interaction in the momentum space does not depend on the variation of the electronic density and in thus just gives

$$\partial_{p,\alpha \boldsymbol{q}} V_{en} = -i(\boldsymbol{q} + \boldsymbol{G}) V_{en}(\boldsymbol{q} + \boldsymbol{G}) e^{-i(\boldsymbol{q}+\boldsymbol{G})\cdot \boldsymbol{R}_p} \ . \tag{B.17}$$

however, one has to be careful since in the pseudopotential implementation electron-nuclear potential will be non-local. The Hartree part reads

$$\partial_{p,\alpha \boldsymbol{q}} V_H(\boldsymbol{G}) \sim V_H(\boldsymbol{q} + \boldsymbol{G}) \partial_{p,\alpha \boldsymbol{q}} n(\boldsymbol{G}) \ , \tag{B.18}$$

as well as the exchange-correlation term

$$\partial_{p,\alpha \boldsymbol{q}} V_{xc}(\boldsymbol{G}) \sim \sum_{\boldsymbol{G'}} f_{xc}(\boldsymbol{q} + \boldsymbol{G}, \boldsymbol{q} + \boldsymbol{G'}) \partial_{p,\alpha \boldsymbol{q}} n(\boldsymbol{G'}) \ , \tag{B.19}$$

where f_{xc} is the second order functional derivative of the exchange-correlation functional with respect to electronic density with $Q = 0$. Thus the calculation of the electron-phonon coupling mainly relies on the calculation of the electronic density variation. The later can be calculated within DFPT considering an induced change in the electronic

wave-function up to the first order. It can be calculated using Sternhaimer equation [126] for arbitrary $\boldsymbol{q}$.

$$(H^{KS}_{\boldsymbol{k}+\boldsymbol{q}} - \epsilon_{n\boldsymbol{k}})\Delta\psi_{n\boldsymbol{k}} = -\partial_{p\alpha\boldsymbol{q}} V_{KS}\psi_{n\boldsymbol{k}} \ . \tag{B.20}$$

The solutions of the B.21 defines the density variation as (for spin unpolarized system)

$$\partial_{p,\alpha\boldsymbol{q}} n(\boldsymbol{q})(\boldsymbol{r}) = 2\sum_{n,\boldsymbol{k}} \psi^*_{n,\boldsymbol{k}}\Delta\psi_{n\boldsymbol{k}} \ . \tag{B.21}$$

One can start with unscreened electron-nuclear interaction and the added screening including Hartree and exchange-correlation terms self-consistently. Then the second order matrix-elements and the phonon frequencies and dynamical can be found in a similar spirit by taking higher derivatives of potential.

Appendix C

Green's functions: non-thermal phonon population

For the case of X-ray emission spectroscopy one core-level hole is present in the initial state, which can be then filled by the outer electron. The processes have the inverse character to XAS however since interaction with phonons is now present in the initial state the cumulant contains an extra type of diagram which leads to the sign change of the exponential factor in Eq. 3.33 ($e^{-i\omega t} - i\omega t - 1$), which then gives rise to satellites on the other side of zero-phonon line (symmetrical to XAS) [75].

However for the most cases emission problem first conjugate to absorption of the photon. Since the lifetime of the excited state typically less then characteristic phonon time $\tau \sim 1/\omega_D$, the phonon system often doesn't have time to relax and adjust to the presence of the electronic excitation [127, 128] the initial population of the phonon levels for emission process will be driven by the previous XAS process. Thus, to obtain XES vibrational contribution it is important to understand how the spectral function modifies in the present of non-thermal phonon population of the initial state. The results of this appendix, however, limited to the no-recoil limit.

If initial state contains N_0 phonons both spectral function for emission and absorption have to be modified in the same way ($A_\xi^{N_0}(\omega) = \frac{1}{\pi}\int dt e^{-i\omega t} G_\xi^{N_0}(t)$):

$$G_\xi^{N_0}(t) = f_{N_0}(t) G_\xi^0(t) e^{C_\xi(t)} \ , \tag{C.1}$$

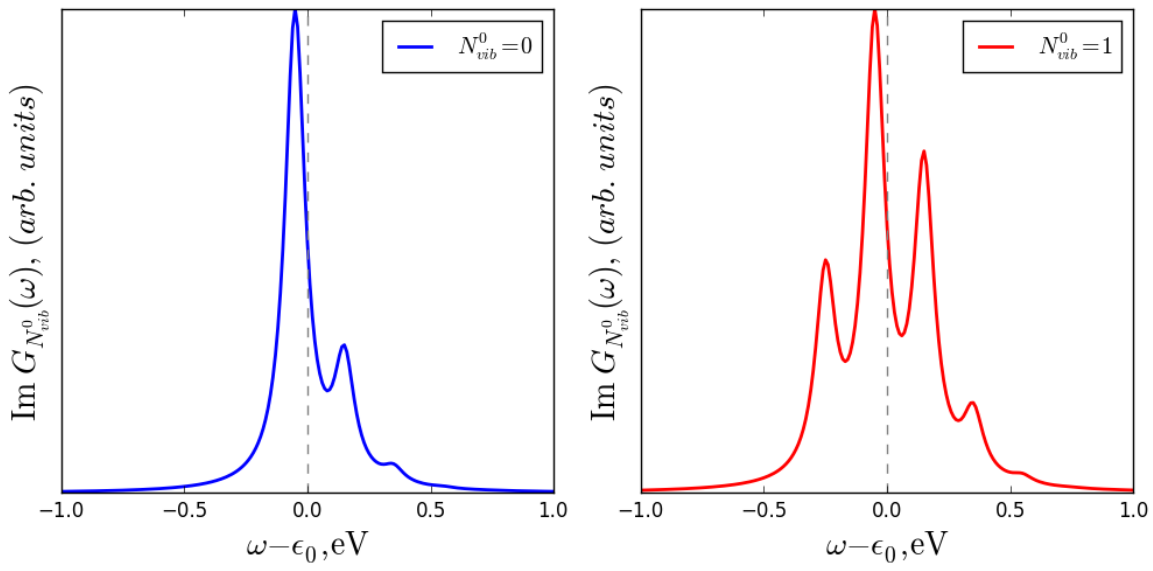

Figure C.1: Spectral function of the electron Green's function calculated in the presence of the non-thermal population of the initial phonon state. Left panel shows the spectral function for zero initial state phonons ($N^0_{vib} = 0$)) and right panel shows the spectral function for one initial state phonon ($N^0_{vib} = 1$)) case.

where

$$f_{N_0}(t) = \sum_{\nu} \sum_{k}^{N_0} \frac{(-1)^k}{k!} N_0 k |Y_\nu(t)|^{2k} D_\nu^{N_0-k}(t) \ . \tag{C.2}$$

Time-dependent factor $f_{N_0}(t)$ represent interaction of an exciton with phonons which are already present in the initial state. Here D_ν represent phonon Green's function in the zero-temperature limit of the wave vector q and mode λ ($\nu = q, \lambda$)) and one phonon vertex is $Y_\xi(\nu, t) = M^\nu_\xi \int_0^t d\tau D_\nu(\tau)$. This results obtained from the diagrammatic evaluation of the electron Green's function with non-equilibrium phonon population in the initial state. In the language of Franck-Condon factors, Im$G^{n0}_\xi(\omega)$ represent the probability of transition between n_0 level of the initial oscillator to any level of the final state oscillator.

And non-zero temperature limit simply can be obtained taking into account temperature population of the initial vibrational levels $G(t, \beta) = \sum_{n,\nu} e^{\beta\omega_\nu n} G^n(t)$, where β is the inverse temperature.

Appendix D

Lang-Firsov transformation

The Lang-Firsov canonical transformation [129] was first introduced to partially diagonalize the Hamiltonian with the first order electron-phonon interaction. Terms which include a scattering of an electron ($c^+_{k+q}c_k$) are remains in the transformed Hamiltonian. Thus, even if it is helpful to use such transformation for many electron-phonon problems, the exact solution might be obtained if interaction with phonon does not change the electronic state (e.g., Holstein type of Hamiltonian).

$$H = \epsilon_e c_i^+ c_i + \omega_\lambda (b_\lambda^+ b_\lambda + 1/2) + M c_i^+ c_i (b_\lambda^+ + b_\lambda) \ . \tag{D.1}$$

Using the generating function of the canonical transformation $S = (M_i^\lambda/\omega_\lambda) c_i^+ c_i (b_\lambda^+ - b_\lambda)$ we have:

$$\tilde{H} = e^S H e^{-S} \ . \tag{D.2}$$

And new annihilation electronic and phonon operators (c_i and b_i) in the old basis are

$$\tilde{c_i} = c_i + (M_i^\lambda/\omega_\lambda)[c_i^+ c_i (b_\lambda^+ - b_\lambda), c_i] + ..$$

$$= c_i + (M_i^\lambda/\omega_\lambda)(b_\lambda^+ - b)[n_i, c_i] + \frac{1}{2!}(M_i^\lambda/\omega_\lambda)^2 (b_\lambda^+ - b_\lambda)^2 [n_i, [n_i, c_i]]... = c_i e^{-\frac{M_i^\lambda}{\omega_\lambda}(b_\lambda^+ - b_\lambda)}$$

$$\tilde{b_\lambda} = b_\lambda + (M_i^\lambda/\omega_\lambda)[c_i^+ c_i (b_\lambda^+ - b_\lambda), b_\lambda] + .. = b_\lambda + (M_i^\lambda/\omega_\lambda) c_i^+ c_i [b_\lambda^+, b_\lambda] + 0 = b_\lambda - (M_i^\lambda/\omega_\lambda) c_i^+ c_i \ . \tag{D.3}$$

And similar for creation operators

$$\tilde{c_i}^+ = c_i^= e^{\frac{M_i^\lambda}{\omega_\lambda}(b_\lambda^+ - b_\lambda)};\ \tilde{b}_\lambda^+ = b_\lambda^+ - (M_i^\lambda/\omega_\lambda)c_i^+ c_i\ . \tag{D.4}$$

The resulting Hamiltonian $\tilde{H}$ can be seen as a displaced harmonic oscillator with respect to original one $H_{vib} = \omega_0(b_\lambda^+ b_\lambda + 1/2)$. This can be shown rewriting vibrational part of $\tilde{H}_{vib}$ in terms of momentum and coordinate operators

$$H'_{vib} = \frac{m\omega_0^2}{2}(x-\alpha)^2 + \frac{3m\omega_0^2}{2}\alpha^2 + \frac{p^2}{2m}\ , \tag{D.5}$$

where $\alpha = \sqrt{\frac{M\hbar}{2m\omega_0^3}}$. Here the position $x_{eq} = 0$ correspond to the minimum of the non-interacting harmonic oscillator. The coupling constant M than leads to the shift of the minimum of the potential energy with respect to $x_{eq} = \alpha$ and vertical shift in energy $\Delta E = \frac{3m\omega_0^2}{2}\alpha^2$.

Going then to exciton-phonon problem one should in principle correct the results taking into account different statistic of the interacting particles. The excitons satisfie para-bosonic statistics [64]. However in the low exciton density limit which is the case for light-driven excitations , it is reasonable to treat them as bosons and thus $[a_\xi^+, a_{\xi'}] \sim \delta_{\xi,\xi'}$ [65, 109]. Applying the same form of the transformation to the interacting boson-boson problem we have ($S = \frac{M_\xi^\lambda}{\omega_\lambda} a_\xi^+ a_\xi (b_\lambda^+ - b_\lambda)$). Transformed phonon operators in both cases are the same:

$$\tilde{b} = b - \frac{M_\xi^\lambda}{\omega_\lambda} a_\xi^+ a_\xi;\ (\tilde{b}^+ = b_\lambda^+ - \frac{M_\xi^\lambda}{\omega_\lambda} a_\xi^+ a_\xi)\ . \tag{D.6}$$

While exciton and electron operators differ by the sign in the exponential factor

$$\tilde{a_\xi} = a_\xi e^{\frac{M_\xi^\lambda}{\omega_\lambda}(b_\lambda^+ - b_\lambda)} (\tilde{a_\xi}^+ = a_\xi^+ e^{-\frac{M_{\xi\lambda}}{\omega_\lambda}(b_\lambda^+ - b_\lambda)})\ . \tag{D.7}$$

However, since a_ξ appears only in the pair with complex conjugate (a_ξ^+) exponential factor is canceled. Thus interacting exciton-phonon Hamiltonian can be diagonalized by this transformation and small change does not affect the analytical form of the Franck-Condon factors in Eq. 2.6.

Appendix E

Two-partcile cumulant expansion

This appendix dedicated to the electron-phonon interaction in the context of the two-particle Green's function. However, here we neglected the contribution from the electron-electron interaction. The two particle interacting Hamiltonian with a linear electron-phonon term has the following form

$$H = H_0 + \sum_{\nu_1,\beta_1,\beta_2} M^{\nu_1}_{\beta_1,\beta_2} c^+_{\beta_2} c_{\beta_2} B_{\nu_1} + \sum_{\nu_2} M^{\nu_2}_{\alpha_1,\alpha_2} c^+_{\alpha_2} c_{\alpha_1} B_{\nu_1} \ . \tag{E.1}$$

Here the β,α are represent excited electron and hole momentum and band index $\{n, \mathbf{k}\}$ respectively. And similar the index $\nu = \{\mathbf{q}, \lambda\}$ defines the phonon wave-vector $\mathbf{q}$ and the mode λ. The electron-hole Coulomb interactions are omitted in this model. The non-interacting part of the Hamiltonian is just a sum of single particle parts $H_0 = h_e + h_h$. Although both h_e and h_h may contain quasi-particle correction form electron-electron interaction in the solids. The two particles four points Green's function in time domain $(1 = t_1)$

$$iL_{\alpha\alpha',\beta\beta'}(1,1',2,2') = \frac{\langle 0| \, T c^+_{\alpha'}(2') c'_{\beta}(2) S(2,2',1',1) c^+_{\beta}(1) c^+_{\alpha}(1') \, |0\rangle}{\langle 0| \, S \, |0\rangle} \ . \tag{E.2}$$

The expansion of the S-matrix leads to the series in the interacting potential V. The normalization factor $\langle 0| \, S \, |0\rangle$ cancels contribution form the disconnected diagrams. As-

suming that $1 = 1',\ 2 = 2'$ for the expansion of the Green's function we have

$$L(1,2) = \sum_n \frac{(-i)^n}{n!} W_n(1,2) \ , \tag{E.3}$$

here W_n is n-th order of moment of electron-phonon interaction and contains all different terms of n-th order which appears after application of the Wick's theorem. On the other hand the two particle Green's function (correlation function) can be written in a cumulant form

$$L(1,2) = L_0(1,2) exp[\sum_m C_m(1,2)] \ , \tag{E.4}$$

Then one can find any order of cumulant in terms of moments L_n [78, 101, 107]. The first non-zero term in Eq. E.3 which includes electron-phonon interaction is

$$W_2(1,2) = -\left\langle 0\right| c_{\beta'}(2) c^+_{\alpha'}(2) V(\bar{3}) V(\bar{4}) c_\beta(1) c^+_\alpha(1) \left|0\right\rangle_c \ , \tag{E.5}$$

and after applying the Wick's theorem it turns into 4 for different combinations of the non-interacting Green's functions.

$$W_{2a}(1,2) = -G_\beta(1,2)\delta_{\beta\beta'} \sum_{\alpha_1,\nu} M^\nu_{\alpha,\alpha_1} M^\nu_{\alpha_1,\alpha'} G_\alpha(1,\bar{3}) G_{\alpha_1}(\bar{3},\bar{4}) D_\nu(\bar{3},\bar{4}) G_\alpha(\bar{3},2) \ , \tag{E.6}$$

$$W_{2b}(1,2) = -G_\alpha(1,2)\delta_{\alpha\alpha'} \sum_{\beta_1,\nu} M^\nu_{\beta,\beta_1} M^\nu_{\beta_1,\beta'} G_\beta(1,\bar{2}) G_{\beta_1}(\bar{3},\bar{4}) D_\nu(\bar{3},\bar{4}) G_\beta(\bar{4},2) \ , \tag{E.7}$$

$$W_{2c}(1,2) = -\sum_\nu M^\nu_{\alpha,\alpha'} M^\nu_{\beta,\beta'} G_\alpha(1,\bar{3}) G_{\alpha'}(\bar{3},2) D_\nu(\bar{3},\bar{4}) G_\beta(1,\bar{4}) G_{\beta'}(\bar{4},2) \ , \tag{E.8}$$

$$W_{2d}(1,2) = -\sum_\nu M^\nu_{\alpha,\alpha'} M^\nu_{\beta,\beta'} G_\alpha(1,\bar{4}) G_{\alpha'}(\bar{4},2) D_\nu(\bar{4},\bar{3}) G_\beta(1,\bar{3}) G_{\beta'}(\bar{3},2) \ , \tag{E.9}$$

The lowest cumulant (the second order cumulant in electron-phonon interaction) has simple relation the terms written above $W_{2a} + W_{2b} + W_{2c} + W_{2d} = L^0 C_2$. Thus the cumulant $C \sim C_2$ (truncating the cumulant series after the second order) has the following from (here we used notation for the FM self-energy ($\Sigma^{FM}_{\alpha,\alpha'}$) and lowest phonon exchange term $\Xi^{xph}_{\alpha,\beta,\alpha'\beta'} = i\sum_\nu M^\nu_{\alpha,\alpha'} M^\nu_{\beta,\beta'}[D_\nu(1,2) + D_\nu(3,4)]$)

$$C_{\alpha,\alpha}(1,2) = (-i)^2 [G_\alpha(1,2)]^{-1} G_\alpha(1,\bar{3}) \Sigma^{FM}_{\alpha,\alpha'}(\bar{3},\bar{4}) G_{\alpha'}(\bar{4},2) \ , \tag{E.10}$$

$$C_{\beta,\beta}(1,2) = (-i)^2[G_\beta(1,2)]^{-1}G_\beta(1,\bar{3})\Sigma^{FM}_{\beta,\beta'}(\bar{3},\bar{4})G_{\beta'}(\bar{4},2)\ , \tag{E.11}$$

$$C^\gamma(1,2) = (-i)^2[G_\alpha(1,2)G_\beta(1,2)]^{-1}G_\alpha(1,\bar{3})G_\beta(1,\bar{4})\Xi^{xph}_{\alpha,\beta,\alpha'\beta'}(\bar{3},\bar{4},\bar{5},\bar{6})G_\alpha(\bar{5},2)G_\beta(\bar{6},2) \tag{E.12}$$

And resulting two particles Green's function is

$$L_{\alpha\alpha'\beta\beta'}(1,2) = G_\alpha(1,2)G_\beta(1,2)e^{C_{\alpha'\alpha}(1,2)+C_{\beta'\beta}(1,2)+C^\gamma_{\alpha'\alpha,\beta\beta'}(1,2)}\ . \tag{E.13}$$

First two terms of the cumulants are one-particle kernels for the electron-phonon and core-hole-phonon contribution. However, the last one contains the phonon exchange term and is responsible for the interference effects in the resulting two-particle spectral function. A similar expression was obtained for plasmon contribution in X-ray absorption problem [87].

Appendix F

Time-dependent perturbation theory

Interaction presentation

There are three standard views on time evaluation in quantum mechanics. In the Schrödinger picture, the wave-function cares all information of the time evaluation of the system $\psi(t)$. The wavefunction should obey the differential equation

$$i\frac{d\psi(t)}{dt} = H\psi(t) \ . \tag{F.1}$$

In contrast to this presentation and Eq. F.1 one can describe the system using the equation of motion

$$i\frac{dO(t)}{dt} = [H(t), O(t)] \ , \tag{F.2}$$

and time evolution of the operators itself (Heisenberg picture). So this is enough if the solution of the stationary Hamiltonian ($H\psi = \epsilon\psi$) is known. However, in many cases, there is a part of the Hamiltonian which easily can be solved H_0, and the rest ($V = H - H_0$) normally contains interaction. Then splitting initial problem into two parts, let the operator propagate in time according to the solution of H_0 : $O_I(t) = e^{iH_0t}Oe^{-iH_0t}$ and the wavefunction will contains the information about the time evolution under the interacting potential $\psi_I(t) = e^{-iHt}e^{iH_0t}\psi(0)$ (subscript I denote the interaction

representation). These three representations are lead to the same expectation value of the observable. In the Schrödinger representation it is

$$\langle O(t)\rangle = \langle\psi(t)|\, O(0)\, |\psi(t)\rangle = \langle\psi|\, e^{iHt} O e^{-iHt}\, |\psi\rangle \ , \tag{F.3}$$

and according to the Heisenberg representation the expectation value is

$$\langle O(t)\rangle = \langle\psi(0)|\, O(t)\, |\psi(0)\rangle = \langle\psi|\, e^{iHt} O e^{-iHt}\, |\psi\rangle \ . \tag{F.4}$$

Finally, in the interaction representation we have

$$\begin{aligned}\langle O(t)\rangle = \langle\psi_I(t)|\, O_I(t)\, |\psi_I(t)\rangle &= \langle\psi|\, e^{iHt} e^{-iH_0 t} e^{iH_0 t} O(0) e^{-iH_0 t} e^{iH_0 t} e^{-iHt}\, |\psi\rangle \\ &= \langle\psi|\, e^{iHt} O e^{-iHt}\, |\psi\rangle \ . \end{aligned} \tag{F.5}$$

Time-evaluation operator

The time evolution which comes from the interacting part of the Hamiltonian is given by the time evolution operator of the from :$U(t) = e^{iH_0 t} e^{-iHt}$. The time derivative of the operator will be

$$\frac{dU(t)}{dt} = ie^{iH_0 t}(H_0 - H)e^{-iHt} = -ie^{iH_0 t} V e^{-iH_0} U(t) = -iV(t)U(t) \ . \tag{F.6}$$

Thus it can be defined self consistently as

$$U(t) = U(0) - i\int_0^t dt_1 V(t_1)U(t_1) \ , \tag{F.7}$$

or alternatively, applying chain rule n times, as a sum of n orders in the interaction potential

$$U(t) = 1 + \sum_{n=1}^{\infty}(-i)^n \int_0^t dt_1 .. \int_0^{t_{n-1}} dt_n V(t_1)..V(t_n) \ . \tag{F.8}$$

The integrals of the type: $\int_0^t dt_1 \int_0^{t_1} O(t_1)O(t_2)dt_2 = \frac{1}{2!}\int_0^t \int_0^t dt_1 dt_2 T[O(t_1)O(t_2)]$ might be rewritten using the time ordering operator T which orders operator with the smaller

time at the right:

$$T[O(t_1)O(t_2)] = \theta(t_1 - t_2)O(t_1)O(t_2) + \theta(t_2 - t_1)O(t_2)O(t_1) \tag{F.9}$$

And a prefactor $\frac{1}{2!}$ came form the double counting of the integral contribution in the last case. And Eq. F.8 become:

$$U(t) = 1 + \sum_{n=1}^{\infty} \frac{(-i)^n}{n!} \int_0^t dt_1 .. \int_0^t dt_n T V(t_1)..V(t_n) \ . \tag{F.10}$$

As a shorthand notation one can use the exponential generating function to denote the series in Eq. F.11:

$$U(t) = T e^{-i \int_0^t dt_1 V(t_1)} \ . \tag{F.11}$$

Similarly to account for propagation form t to arbitrary t' on can introduce the scattering matrix $S(t,t)$

$$S(t,t') = U(t')U^+(t) \ . \tag{F.12}$$

One can see that it as well satisfies the chain rule and lead to the generalization of the expansion Eq. F.11 changing integration limits form t to t'.

Time-dependent coefficients

The usual question which has to be addressed by the time-dependent theory is how the probability to find the system in one of the basis states evolve with time. If initially at time $t' = 0$ unperturbed system is in the state i, which describes by the stationary solution of the $H_0 \left|i\right\rangle = \epsilon_i \left|i\right\rangle$, the probability to find system in the state n after passing some time $(t - t')$ in perturbed regime, is $|\left\langle n\right| U(t) \left|i\right\rangle|^2$. The time-evolution is driven here by the time evolution operator. In the absence of the perturbation, this projection would be non-zero only if $n = i$, since each of basis states will be evolving in time as $e^{-i\epsilon_n t}$, but the mixing of them will be preserved. The state $\left\langle i\right|$ then has a time-dependent coefficient of an expansion in the initial basis

$$\left|i\right\rangle = \sum_n \left|n\right\rangle \left\langle n\right| U(t) \left|i\right\rangle = \sum_n c_{ni}(t) \left|n\right\rangle \ , \tag{F.13}$$

so the transition probability proportional to the square of these coefficients. We can treat this time-dependent process of state mixing in different order of approximations. Combining Eq. F.13 and expansion of time evolution operator Eq. F.11

$$c_{ni}(t) = c_{ni}^{(0)}(t) + c_{ni}^{(1)}(t) + c_{ni}^{(2)}(t) + \dots \ . \tag{F.14}$$

The approximate coefficients itself are (up to the second order)

$$c_{ni}^{(0)}(t) = \delta_{ni} \ ,$$

$$c_{ni}^{(1)}(t) = -i \int_0^t dt \, \langle n| \, V(t_1) \, |i\rangle \, dt_1$$

$$c_{ni}^{(2)}(t) = i^2 \int_0^t dt_1 \int_0^t dt_2 \frac{1}{2} \, \langle n| \, TV(t_1)V(t_2) \, |i\rangle \, dt_2 dt_1 \ . \tag{F.15}$$

Using them it's possible to calculate transition rate $\frac{d|c_{ni}(t)|^2}{dt}$ and in the application to light induced transition the differential cross-section. Noticing that $V(t) = e^{iH_0 t} V e^{-iH_0 t}$ the matrix element become $\langle n| \, V(t) \, |i\rangle = V_{ni} e^{-i\epsilon_{ni} t}$. Then if we will assume harmonic nature of a perturbation $V(t) = V(e^{-i\omega t} + e^{i\omega t})$ this give rise to two terms for first order coefficient

$$c_{ni}^{(1)}(t) = -i \int_0^t V_{ni} e^{i(\epsilon_{ni} - \omega)t_1} dt_1 - i \int_0^t V_{ni} e^{i(\epsilon_{ni} + \omega)t_1} dt_1 \ . \tag{F.16}$$

and four terms for second order

$$\begin{aligned} c_{ni}^{(2)}(t) = &- \int_0^t \int_0^t dt_1 dt_2 \sum_m V_{nm} V_{mi} e^{i(\epsilon_{mi} - \omega)t_1} e^{i(\epsilon_{nm} - \omega)t_2} \\ &- \int_0^t \int_0^t dt_1 dt_2 \sum_m V_{nm} V_{mi} e^{i(\epsilon_{mi} - \omega)t_1} e^{i(\epsilon_{nm} + \omega)t_2} \\ &- \int_0^t \int_0^t dt_1 dt_2 \sum_m V_{nm} V_{mi} e^{i(\epsilon_{mi} + \omega)t_1} e^{i(\epsilon_{nm} - \omega)t_2} \\ &- \int_0^t \int_0^t dt_1 dt_2 \sum_m V_{nm} V_{mi} e^{i(\epsilon_{mi} + \omega)t_1} e^{i(\epsilon_{nm} + \omega)t_2} \ . \end{aligned} \tag{F.17}$$

All these terms correspond to the combinations of absorption, emission or scattering processes.

Bibliography

[1] M. Le Tacon, A. Bosak, S. M. Souliou, G. Dellea, T. Loew, R. Heid, K. P. Bohnen, G. Ghiringhelli, M. Krisch, and B. Keimer. *Inelastic X-ray scattering in* $YBa_2Cu_3O_{6.6}$ *reveals giant phonon anomalies and elastic central peak due to charge-density-wave formation. Nature Physics*, 10(1):52, 2013.

[2] T. P. Devereaux, A. M. Shvaika, K. Wu, K. Wohlfeld, C. J. Jia, Y. Wang, B. Moritz, L. Chaix, W. S. Lee, Z. X. Shen, G. Ghiringhelli, and L. Braicovich. *Directly characterizing the relative strength and momentum dependence of electron-phonon coupling using resonant inelastic X-ray scattering. Phys. Rev. X*, 6(4):041019, 2016.

[3] L. J. P. Ament, M. van Veenendaal, T. P. Devereaux, J. P. Hill, and J. van den Brink. *Resonant Inelastic X-ray Scattering Studies of Elementary Excitations. Rev. Mod. Phys.*, 83(6):705–767, 2010.

[4] S. Johnston, C. Monney, V. Bisogni, K. J. Zhou, R. Kraus, G. Behr, V. N. Strocov, J. Málek, S. L. Drechsler, J. Geck, T. Schmitt, and J. Van Den Brink. *Electron-lattice interactions strongly renormalize the charge-transfer energy in the spin-chain cuprate* Li_2CuO_2. *Nat. Commun.*, 7:10563, 2016.

[5] S. Moser, S. Fatale, P. Krüger, H. Berger, P. Bugnon, A. Magrez, H. Niwa, J. Miyawaki, Y. Harada, and M. Grioni. *Electron-phonon coupling in the bulk of anatase* TiO_2 *measured by resonant inelastic X-ray spectroscopy. Phys. Rev. Lett.*, 115(9):096404, 2015.

[6] A.B. Migdal. *Interaction between electrons and lattice vibrations in a normal Metal. Sov. Phys. JETP*, 34(7):1438–1446, 1958.

[7] G. M. Eliashberg. *Interactions between electrons and lattice vibrations in a superconductor. Sov. Phys. JETP*, 11(38):966–976, 1960.

[8] A. J. Millis, B. I. Shraiman, and R. Mueller. *Dynamic Jahn-Teller effect and colossal magnetoresistance in* $La_{1-x}Sr_xMnO_3$. *Phys. Rev. Lett.*, 77:175–178, 1996.

[9] C. Grimaldi, E. Cappelluti, and F. Marsiglio. *Spin-hall conductivity in electron-phonon coupled systems. Phys. Rev. Lett.*, 97(6):066601, 2006.

[10] J. A. Pascual-Gutiérrez, J.Y. Murthy, and R. Viskanta. *Thermal conductivity and phonon transport properties of silicon using perturbation theory and the environment-dependent interatomic potential. J. Appl. Phys.*, 106(6):063532, 2009.

[11] F. Giustino. *Electron-phonon interactions from first principles. Rev. Mod. Phys.*, 89(1):015003, 2017.

[12] Mahan D. G. *Many-Particle Physics.* Plenum Press, New York, second edition, 1990.

[13] G. Grimvall. *The electron-phonon interaction in metals.* North-Holland publishing Company, Amsterdam, 1981.

[14] G. Grimvall. *The Electron-Phonon Interaction in Normal Metals. Physica Scripta*, 14(1-2):63, 1976.

[15] H. Y. Fan. *Temperature Dependence of the Energy Gap in Semiconductors. Phys. Rev.*, 82:900–905, 1951.

[16] P. B. Allen and V. Heine. *Theory of the temperature dependence of electronic band structures. Journal of Physics C*, 9(12):2305, 1976.

[17] G. Antonius, S. Poncé, P. Boulanger, M. Côté, and X. Gonze. *Many-Body Effects on the Zero-Point Renormalization of the Band Structure. Phys. Rev. Lett.*, 112:215501, 2014.

[18] F. Giustino, S. G. Louie, and M. L. Cohen. *Electron-phonon renormalization of the direct band gap of diamond. Phys. Rev. Lett.*, 105(26):265501, 2010.

[19] J. Bardeen, L. N. Cooper, and J. R. Schrieffer. *Theory of superconductivity. Phys. Rev.*, 108(5):1175–1204, 1957.

[20] W. L. McMillan. *Transition temperature of strong-coupled superconductors. Phys. Rev.*, 167:331–344, 1968.

[21] P. B. Allen and B. Mitrovic. *Theory of Superconducting T_c.* Solid State Physics, Vol. 37. Academic, New York, 1982.

[22] J. G. Bednorz and K. A. Müller. *Possible high-T_c superconductivity in the* $\mathrm{Ba-La-Cu-O}$ *system. Zeitschrift für Physik B Condensed Matter*, 64(2):189–193, 1986.

[23] E. Fradkin, S. A. Kivelson, and J. M. Tranquada. *Colloquium: Theory of intertwined orders in high temperature superconductors. Rev. Mod. Phys.*, 87:457–482, 2015.

[24] S. A. Kivelson, I. P. Bindloss, E. Fradkin, V. Oganesyan, J. M. Tranquada, A. Kapitulnik, and C. Howald. *How to detect fluctuating stripes in the high-temperature superconductors. Rev. Mod. Phys.*, 75:1201–1241, 2003.

[25] M. Le Tacon, G. Ghiringhelli, J. Chaloupka, M. Moretti Sala, V. Hinkov, M. W. Haverkort, M. Minola, M. Bakr, K. J. Zhou, S. Blanco-Canosa, C. Monney, Y. T. Song, G. L. Sun, C. T. Lin, G. M. De Luca, M. Salluzzo, G. Khaliullin, T. Schmitt, L. Braicovich, and B. Keimer. *Intense paramagnon excitations in a large family of high-temperature superconductors. Nature Physics*, 7(9):725–730, 2011.

[26] L. Braicovich, J. van den Brink, V. Bisogni, M. Moretti Sala, L. J. P. Ament, N. B. Brookes, G. M. De Luca, M. Salluzzo, T. Schmitt, V. N. Strocov, and G. Ghiringhelli. *Magnetic Excitations and Phase Separation in the Underdoped* $\mathrm{La_{2-x}Sr_xCuO_4}$ *Superconductor Measured by Resonant Inelastic X-Ray Scattering. Phys. Rev. Lett.*, 104:077002, 2010.

[27] A. Lanzara, P. V. Bogdanov, X. J. Zhou, S. A. Kellar, D. L. Feng, E. D. Lu, T. Yoshida, H. Eisaki, A. Fujimori, K. Kishio, J. I. Shimoyama, T. Noda, S. Uchida, Z. Hussain, and Z. X. Shen. *Evidence for ubiquitous strong electron-phonon coupling in high-temperature superconductors. Nature*, 412(6846):510, 2001.

[28] S. Y. Savrasov and O. K. Andersen. *Linear-Response Calculation of the Electron-Phonon Coupling in Doped CaCu*O_2. *Phys. Rev. Lett.*, 77:4430–4433, 1996.

[29] J. J. Lee, F. T. Schmitt, R. G. Moore, S. Johnston, Y. T. Cui, W. Li, M. Yi, Z. K. Liu, M. Hashimoto, Y. Zhang, D. H. Lu, T. P. Devereaux, D. H. Lee, and Z. X. Shen. *Interfacial mode coupling as the origin of the enhancement of* T_c *in* FeSe *films on* $SrTiO_3$. *Nature*, 515(7526):245–248, 2014.

[30] M. D. Johannes and I. I. Mazin. *Fermi surface nesting and the origin of charge density waves in metals. Phys. Rev. B*, 77:165135, 2008.

[31] N. Bulut and D. J. Scalapino. $d_{x^2-y^2}$ *symmetry and the pairing mechanism. Phys. Rev. B*, 54:14971–14973, 1996.

[32] L. Pintschovius. *Electron-phonon coupling effects explored by inelastic neutron scattering. Phys. Status Solidi*, 242(1):30–50, 2005.

[33] M. D'Astuto, P. K. Mang, P. Giura, A. Shukla, A. Mirone, M. Krisch, F. Sette, P. Ghigna, M. Braden, and M. Greven. *Electron-phonon interaction in N-doped Cuprates: an inelasatic X-ray scattering study. Int. J. Mod. Phys. B*, 17(6):484–492, 2003.

[34] A. Q. R. Baron, H. Uchiyama, S. Tsutsui, Y. Tanaka, D. Ishikawa, J. P. Sutter, S. Lee, S. Tajima, R. Heid, and K. P. Bohnen. *Phonon spectra in pure and carbon doped* MgB_2 *by inelastic X-ray scattering. Physica C: Superconductivity*, 456(1-2):83–91, 2007.

[35] C. Verdi, F. Caruso, and F. Giustino. *Origin of the crossover from polarons to Fermi liquids in transition metal oxides. Nature Communications*, 8:15769, 2017.

[36] A. Fujimori, K. Kobayashi, T. Mizokawa, K. Mamiya, A. Sekiyama, H. Eisaki, H. Takagi, S. Uchida, R. J. Cava, J. J. Krajewski, and W. F. Peck. *Photoemission and inverse-photoemission study of superconducting* YNi_2B_2C*: Effects of electron-electron and electron-phonon interactions. Phys. Rev. B*, 50:9660–9663, 1994.

[37] C. Zhang, Z. Liu, Z. Chen, Y. Xie, R. He, S. Tang, W. He, J.and Li, T. Jia, S. N. Rebec, E. Y. Ma, H. Yan, D. Hashimoto, M.and Lu, S. K. Mo, Y. Hikita, R. G. Moore, H. Y. Hwang, D. Lee, and Z. Shen. *Ubiquitous strong electron-phonon coupling at the interface of* FeSe/$SrTiO_3$. *Nat. Commun.*, 8:14468, 2017.

[38] M. Hengsberger, D. Purdie, P. Segovia, M. Garnier, and Y. Baer. *Photoemission study of a strongly coupled electron-phonon system. Phys. Rev. Lett.*, 83(3):592–595, 1999.

[39] G. M. Bancroft, H. W. Nesbitt, R. Ho, D. M. Shaw, J. S. Tse, and M. C. Biesinger. *Toward a comprehensive understanding of solid-state core-level XPS linewidths: Experimental and theoretical studies on the* Si 2p *and* O 1s *linewidths in silicates. Phys. Rev. B*, 80(7):075405, 2009.

[40] Ø. Fischer, M. Kugler, I. Maggio-Aprile, C. Berthod, and C. Renner. *Scanning tunneling spectroscopy of high-temperature superconductors. Rev. Mod. Phys.*, 79(1):353–419, 2007.

[41] J. R. Schrieffer, D. J. Scalapino, and J. W. Wilkins. *Effective Tunneling Density of States in Superconductors. Phys. Rev. Lett.*, 10(8):1263–1099, 1963.

[42] S. Tanaka, K. Mukai, and J. Yoshinobu. *Direct observation of the electron-phonon coupling between empty states in graphite via high-resolution electron energy-loss spectroscopy. Phys. Rev. B*, 95(16):165408, 2017.

[43] A. C. Ferrari. *Raman spectroscopy of graphene and graphite: Disorder, electron-phonon coupling, doping and nonadiabatic effects. Solid State Commun.*, 143(1-2):47–57, 2007.

[44] V. Perebeinos, J. Tersoff, and Ph. Avouris. *Effect of exciton-phonon coupling in the calculated optical absorption of carbon nanotubes. Phys. Rev. Lett.*, 94(2):027402, 2005.

[45] L. J. P. Ament, M. van Veenendaal, and J. van den Brink. *Determining the electron-phonon coupling strength from Resonant Inelastic X-ray Scattering at transition metal L-edges. EPL (Europhysics Letters)*, 95(2):27008, 2011.

[46] N.B. Brookes, F. Yakhou-Harris, K. Kummer, A. Fondacaro, J.C. Cezar, D. Betto, E. Velez-Fort, A. Amorese, G. Ghiringhelli, L. Braicovich, R. Barrett, G. Berruyer, F. Cianciosi, L. Eybert, P. Marion, P. van der Linden, and L. Zhang. *The beamline* ID32 *at the ESRF for soft X-ray high energy resolution resonant inelastic X-ray scattering and polarisation dependent X-ray absorption spectroscopy. Nuclear Instruments and Methods in Physics Research Section A:*

Accelerators, Spectrometers, Detectors and Associated Equipment, 903:175 – 192, 2018.

[47] Akio Kotani and Shik Shin. *Resonant inelastic x-ray scattering spectra for electrons in solids. Rev. Mod. Phys.*, 73:203–246, 2001.

[48] J.J. Sakurai. *Advanced Quantum Mechanics*. A-W series in advanced physics. Pearson Education, Incorporated, 1967.

[49] Kurt Gottfried and Tung-Mow Yan. *Quantum Mechanics : Fundamentals / K. Gottfried, T.M. Yan.* 01 2003.

[50] J. J. Kas, J. J. Rehr, J. A. Soininen, and P. Glatzel. *Real-space Green's function approach to resonant inelastic x-ray scattering. Phys. Rev. B*, 83:235114, 2011.

[51] H. A. Kramers and W. Heisenberg. *Über die Streuung von Strahlung durch Atome. Zeitschrift für Phys. A Hadron. Nucl.*, 31(1):681–708, 1925.

[52] S. Schreck, A. Pietzsch, B. Kennedy, C. Såthe, P. S. Miedema, S. Techert, V. N. Strocov, T. Schmitt, F. Hennies, J.-E. Rubensson, and A. Föhlisch. *Ground state potential energy surfaces around selected atoms from resonant inelastic X-ray scattering. Sci. Rep.*, 7(May 2015):20054, 2016.

[53] S. Fatale, S. Moser, J. Miyawaki, Y. Harada, and M. Grioni. *Hybridization and electron-phonon coupling in ferroelectric* $BaTiO_3$ *probed by resonant inelastic X-ray scattering. Phys. Rev. B*, 94(19):195131, 2016.

[54] S. Johnston, F. Vernay, B. Moritz, Z.-X. Shen, N. Nagaosa, J. Zaanen, and T. P. Devereaux. *Systematic study of electron-phonon coupling to oxygen modes across the cuprates. Phys. Rev. B*, 82:064513, 2010.

[55] R. C. Couto, Vinícius V. Cruz, E. Ertan, S. Eckert, M. Fondell, M. Dantz, B. Kennedy, T. Schmitt, A. Pietzsch, F. F. Guimarães, H. Ågren, F. Gel'mukhanov, M. Odelius, V. Kimberg, and A. Föhlisch. *Selective gating to vibrational modes through resonant X-ray scattering. Nat. Commun.*, 8:14165, 2017.

[56] E. Ertan, V. Kimberg, F. Gel'Mukhanov, F. Hennies, J. E. Rubensson, T. Schmitt, V. N. Strocov, K. Zhou, M. Iannuzzi, A. Föhlisch, M. Odelius, and

A. Pietzsch. *Theoretical simulations of oxygen K-edge resonant inelastic X-ray scattering of kaolinite. Phys. Rev. B*, 95(14):144301, 2017.

[57] V. Vaz da Cruz, E. Ertan, R. C. Couto, S. Eckert, M. Fondell, M. Dantz, B. Kennedy, T. Schmitt, A. Pietzsch, F. F. Guimarães, H. Ågren, F. Gel'mukhanov, M. Odelius, A. Föhlisch, and V. Kimberg. *A study of the water molecule using frequency control over nuclear dynamics in resonant X-ray scattering. Phys. Chem. Chem. Phys.*, 19:19573–19589, 2017.

[58] Y. P. Sun, F. Hennies, A. Pietzsch, B. Kennedy, T. Schmitt, V. N. Strocov, J. Andersson, M. Berglund, J. E. Rubensson, K. Aidas, F. Gel'Mukhanov, M. Odelius, and A. Föhlisch. *Intramolecular soft modes and intermolecular interactions in liquid acetone. Phys. Rev. B*, 84(13):132202, 2011.

[59] S. Ismail-Beigi and S. G. Louie. *Excited-State Forces within a First-Principles Green's Function Formalism. Phys. Rev. Lett.*, 90:076401, 2003.

[60] D. Prendergast and G. Galli. *X-Ray absorption spectra of water from first principles calculations . Phys. Rev. Lett.*, 96:215502, 2006.

[61] M. Rohlfing and S. Louie. *Excitonic effects and the optical absorption spectrum of hydrogenated Si clusters. Phys. Rev. Lett.*, 80(15):3320–3323, 1997.

[62] E. L. Shirley. *Ab initio inclusion of electron-hole attraction: Application to X-ray absorption and resonant inelastic X-ray scattering. Phys. Rev. Lett.*, 80(4):794–797, 1997.

[63] S. Tinte and E. L. Shirley. *Vibrational effects on* $SrTiO_3$ Ti *1s absorption spectra studied using first-principles methods. J. Phys. Condens. Matter*, 20(36):365221, 2008.

[64] L.V. Keldysh and A.N. Kozlov. *Collective properties of excitons in semiconductors. Sov. Phys. JETP*, 27(3):521, 1968.

[65] V.M. Agranovich and B.S. Toshich. *Collective properties of Frenkel excitons. Sov. Phys. JETP*, 26(1):104–112, 1968.

[66] P. Giannozzi, S. Baroni, N. Bonini, M. Calandra, R. Car, C. Cavazzoni, D. Ceresoli, G. L. Chiarotti, M. Cococcioni, I. Dabo, A. Dal Corso, et al. *QUANTUM ESPRESSO: a modular and open-source software project for quantum simulations of materials. Journal of Physics: Condensed Matter*, 21(39):395502, 2009.

[67] S. Johnston, C. Monney, V. Bisogni, K. J. Zhou, R. Kraus, G. Behr, V. N. Strocov, J. Málek, S. L. Drechsler, J. Geck, T. Schmitt, and J. Van Den Brink. *Electron-lattice interactions strongly renormalize the charge-transfer energy in the spin-chain cuprate* Li_2CuO_2. *Nat. Commun.*, 7:10563, 2016.

[68] Richard M. Martin, Lucia Reining, and David M. Ceperley. *RPA and beyond: the Bethe-Salpeter equation*, pages 345–388. Cambridge University Press, 2016.

[69] L. Hedin. On correlation effects in electron spectroscopies and the gw approximation. *Journal of Physics: Condensed Matter*, 11(42):489, 1999.

[70] J. P. Nery, Ph. B. Allen, G. Antonius, L. Reining, A. Miglio, and X. Gonze. *Quasiparticles and phonon satellites in spectral functions of semiconductors and insulators: Cumulants applied to the full first-principles theory and the Fröhlich polaron. Phys. Rev. B*, 97:115145, 2018.

[71] S. M. Story, J. J. Kas, F. D. Vila, M. J. Verstraete, and J. J. Rehr. *Cumulant expansion for phonon contributions to the electron spectral function. Phys. Rev. B*, 90(19):195135, 2014.

[72] L. Hedin. *Effects of recoil on shake-up spectra in metals. Phys. Scr.*, 21(3-4):477–480, 1980.

[73] A. A. Abrikosov , L. P. Gorkov and I. E. Dzyaloshinski. *Methods of Quantum Field Theory in Statistical Physics.* Dover New York, 1975.

[74] P. Nozières and C. T. De Dominicis. *Singularities in the X-ray absorption and emission of metals. III. One-body theory exact solution. Phys. Rev.*, 178(3):1097–1107, 1969.

[75] D. C. Langreth. *Singularities in the X-ray spectra of metals. Phys. Rev. B*, 1(2):471–477, 1970.

[76] M. Guzzo, G. Lani, F. Sottile, P. Romaniello, M. Gatti, J. J. Kas, J. J. Rehr, M. G. Silly, F. Sirotti, and L. Reining. *Valence electron photoemission spectrum of semiconductors: Ab initio description of multiple satellites. Phys. Rev. Lett.*, 107(16):166401, 2011.

[77] J. Lischner, D. Vigil-Fowler, and S. G. Louie. *Physical origin of satellites in photoemission of doped graphene: Ab initio GW plus cumulant study. Phys. Rev. Lett.*, 110(14):146801, 2013.

[78] J. J. Kas, J. J. Rehr, and L. Reining. *Cumulant expansion of the retarded one-electron Green function. Phys. Rev. B*, 90(8):085112, 2014.

[79] J.S. Zhou, J. J. Kas, L. Sponza, I. Reshetnyak, M. Guzzo, C. Giorgetti, M. Gatti, F. Sottile, J. J. Rehr, and L. Reining. *Dynamical effects in electron spectroscopy. J. Chem. Phys.*, 143(18):184109, 2015.

[80] F. Caruso and F. Giustino. *The GW plus cumulant method and plasmonic polarons: application to the homogeneous electron gas. Eur. Phys. J. B*, 89(11):238, 2016.

[81] F. Borgatti, J. A. Berger, D. Céolin, J. S. Zhou, J. J. Kas, M. Guzzo, C. F. McConville, F. Offi, G. Panaccione, A. Regoutz, D. J. Payne, J.-P. Rueff, O. Bierwagen, M. E. White, J. S. Speck, M. Gatti, and R. G. Egdell. *Revisiting the origin of satellites in core-level photoemission of transparent conducting oxides: The case of n-doped* SnO_2. *Phys. Rev. B*, 97:155102, 2018.

[82] F. Caruso, H. Lambert, and F. Giustino. *Band structures of plasmonic polarons. Phys. Rev. Lett.*, 114(14):146404, 2015.

[83] F. Aryasetiawan, L. Hedin, and K. Karlsson. *Multiple plasmon satellites in* Na *and* Al *spectral functions from ab initio cumulant expansion. Phys. Rev. Lett.*, 77(11):2268–2271, 1996.

[84] G. Onida. *Electronic excitations: density-functional versus many-body Green's function approaches. Rev. Mod. Phys.*, 74:601, 2002.

[85] M. Gatti and M. Guzzo. *Dynamical screening in correlated metals: Spectral properties of* $SrVO_3$ *in the GW approximation and beyond. Phys. Rev. B*, 87(15):155147, 2013.

[86] K. Nakamura, Y. Nohara, Y. Yosimoto, and Y. Nomura. *Ab initio GW plus cumulant calculation for isolated band systems: Application to organic conductor* $(TMTSF)_2PF_6$ *and transition-metal oxide* $SrVO_3$. *Phys. Rev. B*, 93(8):085124, 2016.

[87] J. J. Kas, F. D. Vila, J. J. Rehr, and S. A. Chambers. *Real-time cumulant approach for charge-transfer satellites in x-ray photoemission spectra. Phys. Rev. B*, 91(12):121112, 2015.

[88] J. J. Kas, J. J. Rehr, and J. B. Curtis. *Particle-hole cumulant approach for inelastic losses in X-ray spectra. Phys. Rev. B*, 94:035156, 2016.

[89] A. Gali, T. Demján, M. Vörös, G. Thiering, E. Cannuccia, and A. Marini. *Electron-vibration coupling induced renormalization in the photoemission spectrum of diamondoids. Nat. Commun.*, 7:11327, 2016.

[90] J. Vinson, J. J. Rehr, J. J. Kas, and E. L. Shirley. *Bethe-Salpeter equation calculations of core excitation spectra. Phys. Rev. B*, 83:115106, 2011.

[91] E. E. Salpeter and H. A. Bethe. *A relativistic equation for bound-state problems. Phys. Rev.*, 84(6):1232–1242, 1951.

[92] M. Grüning, A. Marini, and X. Gonze. *Exciton-Plasmon States in Nanoscale Materials: Breakdown of the Tamm-Dancoff Approximation. Nano Letters*, 9(8):2820–2824, 2009.

[93] I. Tamm. *Relativistic interaction of elementary particles. J. Phys.(USSR)*, 9:449, 1945.

[94] S. M. Dancoff. *Non-Adiabatic Meson Theory of Nuclear Forces. Phys. Rev.*, 78:382–385, 1950.

[95] S. Albrecht, L. Reining, R. Del Sole, and G. Onida. *Ab Initio Calculation of Excitonic Effects in the Optical Spectra of Semiconductors. Phys. Rev. Lett.*, 80:4510–4513, 1998.

[96] W. S. Lee, S. Johnston, B. Moritz, J. Lee, M. Yi, K. J. Zhou, T. Schmitt, L. Patthey, V. Strocov, K. Kudo, Y. Koike, J. Van Den Brink, T. P. Devereaux, and Z. X. Shen. *Role of lattice coupling in establishing electronic and magnetic*

properties in quasi-one-dimensional cuprates. Phys. Rev. Lett., 110(26):265502, 2013.

[97] H. Hertz. *Ueber einen Einfluss des ultravioletten Lichtes auf die electrische Entladung. Ann. Phys.*, 17(983), 1887.

[98] A. Einstein. *Zur Elektrodynamik bewegter Körper. Ann. Phys.*, 31(132), 1905.

[99] T. D. Thomas, C. Miron, K. Wiesner, P. Morin, T. X. Carroll, and L. J. Sæthre. *Anomalous natural linewidth in the 2p photoelectron spectrum of* SiF_4. *Phys. Rev. Lett.*, 89(22):223001, 2002.

[100] D. Dunn. *Electron–phonon interactions in an insulator. Canadian Journal of Physics*, 53(4):321–337, 1975.

[101] O. Gunnarsson, V. Meden, and K. Schonhammer. *Corrections to Migdal's theorem for spectral funtions: A cumulant treatment of the time dependent Green's function. Phys. Rev. B*, 50(15):10462, 1994.

[102] L. Campbell, L. Hedin, J. J. Rehr, and W. Bardyszewski. *Interference between extrinsic and intrinsic losses in X-ray absorption fine structure. Phys. Rev. B*, 65(6):064107, 2002.

[103] R. Sankari, M. Ehara, H. Nakatsuji, Y. Senba, K. Hosokawa, H. Yoshida, A. De Fanis, Y. Tamenori, S. Aksela, and K. Ueda. *Vibrationally resolved O 1s photoelectron spectrum of water. Chem. Phys. Lett.*, 380(5-6):647–653, 2003.

[104] F. de Groot, A. Kotani, Y. Tokura, and Sarma D. Kotliar, G. *Core Level Spectroscopy of Solids.* Boca Raton: CRC Press, 2008.

[105] J J Rehr. *Theoretical approaches to x-ray absorption fine structure. Rev. Mod. Phys.*, 72(3):621–654, 2000.

[106] P. Noziéres, J. Gavoret, and B. Roulet. *Singularities in the X-Ray Absorption and Emission of Metals. II. Self-Consistent Teatment of Divergences. Phys. Rev.*, 178(3):1084–1096, 1969.

[107] K.A. Mäder and S. Baroni. *Vibrational broadening of x-ray emission spectra: A first-principles study on diamond. Phys. Rev. B*, 55(15):9649–9658, 1997.

[108] K. Gilmore and E. L. Shirley. *Numerical quantification of the vibronic broadening of the* $SrTiO_3$ Ti *L-edge spectrum. Journal of Physics Condensed Matter*, 22(31):0–5, 2010.

[109] G. Antonius and S. G. Louie. *Theory of the exciton-phonon coupling. arXiv/1705.04245*, 2017.

[110] M. Z. Mayers, M. S. Hybertsen, and D. R. Reichman. *Description of quasiparticle and satellite properties via cumulant expansions of the retarded one-particle Green's function. Phys. Rev. B*, 94(8):1–6, 2016.

[111] K. Gilmore, J. Vinson, E. L. Shirley, D. Prendergast, C. D. Pemmaraju, J. J. Kas, F. D. Vila, and J. J. Rehr. *Efficient implementation of core-excitation Bethe-Salpeter equation calculations. Comput. Phys. Commun.*, 197:315901, 2015.

[112] C. Gougoussis, M. Calandra, A. P. Seitsonen, and F. Mauri. *First-principles calculations of X-ray absorption in a scheme based on ultrasoft pseudopotentials: From α-quartz to high-T_c compounds. Phys. Rev. B*, 80(7):075102, 2009.

[113] C. T. Chen, Y. Ma, and F. Sette. *K-shell photoabsorption of the* N_2 *molecule. Phys. Rev. A*, 40(11):6737–6740, 1989.

[114] R. Püttner, I. Dominguez, T. J. Morgan, C. Cisneros, R. F. Fink, E. Rotenberg, T. Warwick, M. Domke, G. Kaindl, and A. S. Schlachter. *Vibrationally resolved O* 1*s core-excitation spectra of CO and NO. Phys. Rev. A*, 59:3415–3423, May 1999.

[115] P. Hohenberg and W. Kohn. *Inhomogeneous electron gas. Phys. Rev.*, 136:B864–B871, 1964.

[116] R. M. Martin. *Density functional theory.* Cambridge University Press, 2004.

[117] L. H. Thomas. *The calculation of atomic fields. Mathematical Proceedings of the Cambridge Philosophical Society*, 23(5):542–548, 1927.

[118] E. Fermi. *Un Metodo Statistico per la Determinazione di alcune Prioprietà dell'Atomo. Rend. Accad. Naz. Lincei*, (6):602–607, 1927.

[119] W. Kohn and L. J. Sham. *Self-consistent equations including exchange and correlation effects. Phys. Rev.*, 140:A1133–A1138, 1965.

[120] J. P. Perdew, K. Burke, and M. Ernzerhof. *Generalized gradient approximation made simple. Phys. Rev. Lett.*, 77(18):3865–3868, 1996.

[121] V.I. Anisimov, F. Aryasetiawan, and A. I. Lichtenstein. *First-principles calculations of the electronic structure and spectra of strongly correlated systems: the LDA + U method. Journal of Physics: Condensed Matter*, 9(4):767, 1997.

[122] A. D. Becke. *A new mixing of Hartree–Fock and local density-functional theories. The Journal of Chemical Physics*, 98(2):1372–1377, 1993.

[123] M. Ernzerhof and G. E. Scuseria. *Assessment of the Perdew–Burke–Ernzerhof exchange-correlation functional. The Journal of Chemical Physics*, 110(11):5029–5036, 1999.

[124] P. E. Blöchl. *Projector augmented-wave method. Phys. Rev. B*, 50(24):17953–17979, 1994.

[125] R. P. Feynman. *Forces in molecules. Phys. Rev.*, 56(4):340–343, 1939.

[126] S. Baroni, S. de Gironcoli, A. Dal Corso, and P. Giannozzi. *Phonons and related crystal properties from density-functional perturbation theory. Rev. Mod. Phys.*, 73:515–562, 2001.

[127] G.D. Mahan. *Emission spectra and phonon relaxation. Phys. Rev. B*, 15(10), 1977.

[128] C. O. Almbladh. *Incomplete phonon relaxation in X-ray emission. Solid State Commun.*, 22(6):339–342, 1977.

[129] I. G. Lang and Y. A. Firsov. *Kinetic theory of semiconductors with low mobility. Sov. Phys. JETP*, 16(5):1301, 1963.